



Michigan Technological University  
*Create the Future* Digital Commons @ Michigan Tech

---

Dissertations, Master's Theses and Master's  
Reports - Open

Dissertations, Master's Theses and Master's  
Reports

---

2006

## Fluidic oscillator design for water removal enhancement in a PEM fuel cell

Sheng Han Tseng  
*Michigan Technological University*

Follow this and additional works at: <https://digitalcommons.mtu.edu/etds>



Part of the [Mechanical Engineering Commons](#)

Copyright 2006 Sheng Han Tseng

---

### Recommended Citation

Tseng, Sheng Han, "Fluidic oscillator design for water removal enhancement in a PEM fuel cell", Master's Thesis, Michigan Technological University, 2006.  
<https://doi.org/10.37099/mtu.dc.etds/415>

Follow this and additional works at: <https://digitalcommons.mtu.edu/etds>



Part of the [Mechanical Engineering Commons](#)

Fluidic Oscillator Design for Water Removal Enhancement in a  
PEM Fuel Cell

By

Sheng Han Tseng

A THESIS

Submitted in partial fulfillment of the requirements

for the degree of

Master of Science in Mechanical Engineering

MICHIGAN TECHNOLOGICAL UNIVERSITY

December, 2006



This thesis, “Fluidic Oscillator Design for Water Removal Enhancement in a PEM Fuel Cell” is hereby approved in partial fulfillment of the requirements of the Degree of Master of Science in Mechanical Engineering.

Department of Mechanical Engineering - Engineering Mechanics

Advisor: \_\_\_\_\_  
Professor Jeffrey S. Allen

Committee Member: \_\_\_\_\_  
Professor Song Lin Yang

Committee Member: \_\_\_\_\_  
Professor Amitabh Narain

Committee Member: \_\_\_\_\_  
Professor Jason Keith

Department Chair: \_\_\_\_\_  
Professor William W. Predebon

Date: \_\_\_\_\_



## ABSTRACT

Fluidic Oscillator Design for Water Removal Enhancement in a PEM Fuel Cell

Sheng Han Tseng

Michigan Technological University, December, 2006

Advisor: Professor Jeffrey S. Allen

This research initiative was triggered by the problems of water management of Polymer Electrolyte Membrane Fuel Cell (PEMFC). In low temperature fuel cells such as PEMFC, some of the water produced after the chemical reaction remains in its liquid state. Excess water produced by the fuel cell must be removed from the system to avoid flooding of the gas diffusion layers (GDL). The GDL is responsible for the transport of reactant gas to the active sites and remove the water produced from the sites. If the GDL is flooded, the supply gas will not be able to reach the reactive sites and the fuel cell fails.

The choice of water removal method in this research is to exert a variable asymmetrical force on a liquid droplet. As the drop of liquid is subjected to an external vibrational force in the form of periodic wave, it will begin to oscillate. A fluidic oscillator is capable to produce a pulsating flow using simple balance of momentum fluxes between three impinging jets. By connecting the outputs of the oscillator to the gas channels of a fuel cell, a flow pulsation can be imposed on a water droplet formed within the gas channel during fuel cell operation. The lowest frequency produced by this design is approximately 202 Hz when a 20 inches feed-back port length was used and a supply pressure of 5 psig was introduced.

This information was found by setting up a fluidic network with appropriate data acquisition. The components include a fluidic amplifier, valves and fittings, flow meters, a pressure gage, NI-DAQ system, Siglab<sup>®</sup>, Matlab software and four PCB microphones. The operating environment of the water droplet was reviewed, speed of the sound pressure which travels down the square channel was precisely estimated, and measurement devices were carefully selected. Applicable alternative measurement devices and its application to pressure wave measurement was considered. Methods for experimental setup and possible approaches were recommended, with some discussion of potential problems with implementation of this technique. Some computational fluid dynamic was also performed as an approach to oscillator design.

## ACKNOWLEDGMENTS

I am deeply indebted to my advisor, Dr. Jeffrey Allen, for his constant support and guidance. Without his help, this work would not be possible. I would also like to thank my committee members for attending my defense. Professor Song Lin Yang, Professor Amitabh Narain and Professor Jason Keith. I am grateful for their patience and support. I would also like give a special thanks to Dr. Oner Arici who initiated my interest in alternative fuels and gave me a chance to prove myself in graduate school. Thanks to Dr. Blough and Professor Van Karson for your valuable suggestions during the analysis of my data obtained in the experiments.

I would like to thank the MnIT crew members who put up with the noisy experiments throughout the last two semesters. Joseph Hernandez, Russ Stacy, and Derek Fultz, with your jokes and supports these experiments were more than just frequencies. To my friends, with your presence the graduate study in Michigan Tech. became more than just an education, thank you for enriching my experience.

Finally I would like to thank my family members for their loving support and inspirations; you are the reason for me to pull through the 3 am coffee breaks and sleepless nights. Thank you for believing in me and I would like to dedicate this thesis to you.

## CONTENTS

<i>Abstract</i> . . . . .	i
<i>Acknowledgments</i> . . . . .	ii
<i>Table of Contents</i> . . . . .	iii
<i>List of Figures</i> . . . . .	v
<i>List of Tables</i> . . . . .	xi
1. <i>Introduction</i> . . . . .	1
1.1 Need for Fuel Cells . . . . .	1
1.2 What is a ‘Fuel Cell’? . . . . .	2
2. <i>Polymer Electrolyte Membrane Fuel Cell</i> . . . . .	6
2.1 Background . . . . .	6
2.2 Structure of PEMFC . . . . .	7
2.3 Water Management in PEM Fuel Cells . . . . .	18
2.4 Droplet Oscillation . . . . .	19
3. <i>Fluidic Amplifier</i> . . . . .	22
3.1 Introduction . . . . .	22
3.2 Types of Fluidic Amplifiers . . . . .	23
3.3 Comparison between Analog and Digital Amplifier . . . . .	28
4. <i>Vented and Non-Vented Analog Fluidic Amplifiers</i> . . . . .	30
4.1 Operating Principle . . . . .	30
5. <i>Experimental Setup and Results</i> . . . . .	35
5.1 Experiment 1: GE Oscillator Testing - Single Feed-back Port . . . . .	35
5.2 Single Exit Venting - With Varying Supply Flow Rates . . . . .	43
5.3 Experiment 2: GE Oscillator Testing - Both Exit Vented . . . . .	45
5.4 Experiment 3: Cascading of GE Oscillators . . . . .	50
5.5 Analog Fluidic Oscillator Design . . . . .	53
5.6 Experiment 4: Design 4 Testing . . . . .	60
5.7 Experiment 5: Cascading Study of Design 4 and GE Oscillators . . . . .	67
5.8 Experiment 6: Frequency Variation in Channel . . . . .	72
5.9 Summary . . . . .	83



---

6. Additional Work . . . . .	85
6.1 Fluent Simulation . . . . .	86
6.2 Simulation Results . . . . .	88
6.3 Changing Receiver Position . . . . .	91
6.4 Non-Vented Oscillator Design . . . . .	97
7. Conclusion . . . . .	99
References . . . . .	101
Appendix . . . . .	103
A. Types of Fuel Cells . . . . .	104
A.1 Advantages and Disadvantages of PEMFC . . . . .	112
B. Single Oscillator Testing, Single Feed-back Port Venting . . . . .	114
C. MatLab Code . . . . .	132
D. Control Volume Analysis . . . . .	135

## LIST OF FIGURES

1.1	General structure of fuel cell. . . . .	3
2.1	General components of PEMFC [4]. . . . .	7
2.2	Toray Carbon Paper 2050-A side A at 100X and the scale bar is 300 $\mu\text{m}$ . . . . .	12
2.3	Toray Carbon Paper 2050-A side A at 1000X and the scale bar is 30 $\mu\text{m}$ . . . . .	12
2.4	Toray Carbon Paper 2050-A side B at 100X and the scale bar is 30 $\mu\text{m}$ . . . . .	13
2.5	Toray Carbon Paper 2050-A side B at 700X and the scale bar is 30 $\mu\text{m}$ . . . . .	13
2.6	E-TEK GDL LT 1200-N side A at 40X and the scale bar is 800 $\mu\text{m}$ . . . . .	14
2.7	E-TEK GDL LT 1200-N side A at 200X and the scale bar is 100 $\mu\text{m}$ . . . . .	14
2.8	E-TEK GDL side B LT 1200-N at 40X and the scale bar is 100 $\mu\text{m}$ (microporous side). . . . .	15
2.9	E-TEK GDL LT 1200-N side B at 200X and the scale bar is 100 $\mu\text{m}$ (microporous side). . . . .	15
2.10	Sloshing motion of the water droplet where the dashed line indicate the shape of the water droplet when a periodic force was applied. . . . .	19
3.1	Schematic of an analog fluidic amplifier [13]. . . . .	24
3.2	Output differential pressure response to control differential of an analog amplifier [13]. . . . .	24
3.3	Momentum Interaction of two impinging jets [13]. . . . .	25
3.4	Schematic of a digital fluidic amplifier [13]. . . . .	27
3.5	Output differential pressure response to control differential of a digital amplifier [13]. . . . .	27
4.1	Schematic of a vented analog fluidic amplifier [13]. . . . .	31
4.2	Schematic of a non-vented analog fluidic amplifier [13]. . . . .	31
4.3	Schematic of a non-vented oscillator. . . . .	34
5.1	GE proportional amplifier [15]. . . . .	36
5.2	GE proportional amplifier dimentions [15]. . . . .	36
5.3	GE proportional amplifier gain curve [15]. . . . .	37
5.4	Experimental schematic of a fluidic oscillator construction (using one GE proportional amplifier) following the setup instruction provided by the manufacturer. . . . .	38
5.5	FFT results of the calibration process. . . . .	41

5.6	Experimental result showing the frequency produced when Line A was varied from 8 to 30 inches and Line B remained at 2 inches. . . . .	42
5.7	Experimental schematic of a GE fluidic oscillator setup with both output ports exposed to atmospheric. . . . .	43
5.8	NI-DAQ, Model SC-2345 [17]. . . . .	45
5.9	Frequency comparison between 16.5 and 18 inches feed-back length produced by the same oscillator. . . . .	46
5.10	Comparison of the frequency produced by the oscillators, one with both feed-back port oscillating and one with only one feed-back port oscillating. . . . .	49
5.11	Frequency observation with variable supply flow rate and variable feed-back length (both feed-back ports vented). . . . .	49
5.12	Experimental schematic of two GE fluidic oscillator setup in the cascading orientation. . . . .	52
5.13	Frequency comparison between Element 1 and Element 2. . . . .	52
5.14	C.M. Crane's Oscillator Design [18]. . . . .	58
5.15	Fluidic oscillator design (Design 1). . . . .	59
5.16	Fluidic oscillator design (Design 4). . . . .	61
5.17	Frequency produced by Design 4 when the feed-back length was varied between 4 to 20 inches and the supply pressure was varied between 5 to 15 psig (center vent closed). . . . .	62
5.18	Frequency produced by Design 4 when the feed-back length was varied between 4 to 20 inches and the supply pressure was varied between 5 to 15 psig (center vent opened). . . . .	64
5.19	Frequency comparison between center venting and non center venting for a feed-back length fixed at 4 inches. . . . .	65
5.20	Frequency comparison between center venting and non center venting for a feed-back length fixed at 6 inches. . . . .	65
5.21	Frequency comparison between center venting and non center venting for a feed-back length fixed at 8 inches. . . . .	66
5.22	Frequency comparison between center venting and non center venting for a feed-back length fixed at 17 inches. . . . .	66
5.23	Frequency comparison between center venting and non center venting for a feed-back length fixed at 20 inches. . . . .	67
5.24	A Cascading network using Design 4 to control two GE proportional amplifiers (Element 1 & 2). . . . .	68
5.25	Flow channels fabricated. Its main purpose is to mimic the actual PEMFC flow channels and also to study the effect of position on frequency variation in an air stream. . . . .	72
5.26	Schematic of the flow channels. . . . .	72
5.27	Frequency captured by PCB microphones (mounted at 'Position 1') at different channels when the supply pressure was allowed to vary from 1.5 to 3.0 psig and the supply flow rate into the GE amplifiers were allowed to change from 0 to 2 L/min. . . . .	74

5.28	Frequency captured by PCB microphones (mounted at ‘Position 2’) at different channels when the supply pressure was allowed to vary from 1.5 to 3.0 psig and the supply flow rate into the GE amplifiers were allowed to change from 0 to 2 L/min. . . . .	75
5.29	Frequency captured by PCB microphones (mounted at ‘Position 3’) at different channels when the supply pressure was allowed to vary from 1.5 to 3.0 psig and the supply flow rate into the GE amplifiers were allowed to change from 0 to 2 L/min. . . . .	76
5.30	Frequency captured by PCB microphones (mounted at ‘Position 4’) at different channels when the supply pressure was allowed to vary from 1.5 to 3.0 psig and the supply flow rate into the GE amplifiers were allowed to change from 0 to 2 L/min. . . . .	77
5.31	Signal wave captured by four different microphones at four different channels, 1.5 psig supply pressure was introduced into Design 4 and no flow was supplied to the GE amplifiers. . . . .	82
6.1	FLUENT result showing the oscillation of fluid jet in the oscillator towards the left feed-back port (short feed-back length). . . . .	89
6.2	FLUENT result showing the oscillation of fluid jet in the oscillator towards the right feed-back port (short feed-back length). . . . .	90
6.3	FLUENT result showing the oscillation of fluid jet in the oscillator towards the left feed-back port (long feed-back length). . . . .	90
6.4	FLUENT result showing the oscillation of fluid jet in the oscillator towards the right feed-back port (long feed-back length). . . . .	91
6.5	Velocity profile recorded by FLUENT, where the position axis indicate the location (in y-direction) of the interior in the left exit port. The maxima showed a velocity of approximately 76 m/s attained and the velocity at the wall (location 63 and 68) remained at 0 m/s. . . . .	92
6.6	Velocity profile recorded by FLUENT, where the position axis indicate the location (in y-direction) of the interior in the right exit port. The maxima showed a velocity of approximately 58 m/s attained and the velocity at the wall (location 50 and 55) remained at 0 m/s. . . . .	93
6.7	FLUENT result showing the direction of the jet deflection after the splitter position is modified (long feed-back port). . . . .	94
6.8	FLUENT result showing the direction of the jet deflection after the splitter position is modified (long feed-back port). . . . .	94
6.9	FLUENT result showing the direction of the jet deflection after the splitter position is modified (short feed-back port). . . . .	95
6.10	FLUENT result showing the direction of the jet deflection after the splitter position is modified (short feed-back port). . . . .	95
6.11	Velocity profile recorded by FLUENT, where the position axis indicate the location (in y-direction) of the interior in the left exit port. The maxima showed a velocity of approximately 80 m/s attained and the velocity at the wall (location 63 and 68) remained at 0 m/s. . . . .	96

6.12	Velocity profile recorded by FLUENT, where the position axis indicate the location (in y-direction) of the interior in the right exit port. The maxima showed a velocity of approximately 48 m/s attained and the velocity at the wall (location 50 and 55) remained at 0 m/s. . . . .	96
A.1	Operating schematic of PEMFC [3]. . . . .	105
A.2	Operating schematic of AFC [3]. . . . .	106
A.3	Operating schematic of PAFC [3]. . . . .	107
A.4	Operating schematic of MCFC [3]. . . . .	109
A.5	Operating schematic of SOFC [3]. . . . .	111
B.1	Experimental result showing the frequency response produced when Line A was set at 16 inches and Line B remained at 2 inches and the supply flow rate was set at 0.5 L/min. . . . .	115
B.2	Frequency of the wave form (generated at 0.5 L/min supply pressure) estimated using FFT codes. . . . .	115
B.3	Experimental result showing the frequency response produced when Line A was set at 16 inches and Line B remained at 2 inches and the supply flow rate was set at 1.0 L/min. . . . .	116
B.4	Frequency of the wave form (generated at 1.0 L/min supply pressure) estimated using FFT codes. . . . .	116
B.5	Experimental result showing the frequency response produced when Line A was set at 16 inches and Line B remained at 2 inches and the supply flow rate was set at 1.5 L/min. . . . .	117
B.6	Frequency of the wave form (generated at 1.5 L/min supply pressure) estimated using FFT codes. . . . .	117
B.7	Experimental result showing the frequency response produced when Line A was set at 16 inches and Line B remained at 2 inches and the supply flow rate was set at 2.0 L/min. . . . .	118
B.8	Frequency of the wave form (generated at 2.0 L/min supply pressure) estimated using FFT codes. . . . .	118
B.9	Experimental result showing the frequency response produced when Line A was set at 16 inches and Line B remained at 2 inches and the supply flow rate was set at 2.5 L/min. . . . .	119
B.10	Frequency of the wave form (generated at 2.5 L/min supply pressure) estimated using FFT codes. . . . .	119
B.11	Experimental result showing the frequency response produced when Line A was set at 16 inches and Line B remained at 2 inches and the supply flow rate was set at 3.0 L/min. . . . .	120
B.12	Frequency of the wave form (generated at 3.0 L/min supply pressure) estimated using FFT codes. . . . .	120
B.13	Experimental result showing the frequency response produced when Line A was set at 16 inches and Line B remained at 2 inches and the supply flow rate was set at 3.5 L/min. . . . .	121

B.14 Frequency of the wave form (generated at 3.5 L/min supply pressure) estimated using FFT codes. . . . .	121
B.15 Experimental result showing the frequency response produced when Line A was set at 16 inches and Line B remained at 2 inches and the supply flow rate was set at 4.0 L/min. . . . .	122
B.16 Frequency of the wave form (generated at 4.0 L/min supply pressure) estimated using FFT codes. . . . .	122
B.17 Frequency of the wave form (generated at 1.0 L/min supply pressure) estimated using FFT codes. The main frequency was calculated to be at 257.4885 Hz . . . . .	123
B.18 Experimental result showing the frequency response produced when Line A was set at 14.5 inches and Line B remained at 2 inches and the supply flow rate was set at 1.5 L/min. . . . .	123
B.19 Frequency of the wave form (generated at 1.5 L/min supply pressure) estimated using FFT codes. The main frequency was calculated to be at 274.7696 Hz . . . . .	124
B.20 Experimental result showing the frequency response produced when Line A was set at 14.5 inches and Line B remained at 2 inches and the supply flow rate was set at 2.0 L/min. . . . .	124
B.21 Frequency of the wave form (generated at 2.0 L/min supply pressure) estimated using FFT codes. The main frequency was calculated to be at 278.2258 Hz . . . . .	125
B.22 Experimental result showing the frequency response produced when Line A was set at 14.5 inches and Line B remained at 2 inches and the supply flow rate was set at 2.5 L/min. . . . .	125
B.23 Frequency of the wave form (generated at 2.5 L/min supply pressure) estimated using FFT codes. The main frequency was calculated to be at 285.1382 Hz . . . . .	126
B.24 Experimental result showing the frequency response produced when Line A was set at 14.5 inches and Line B remained at 2 inches and the supply flow rate was set at 3.0 L/min. . . . .	126
B.25 Frequency of the wave form (generated at 3.0 L/min supply pressure) estimated using FFT codes. The main frequency was calculated to be at 288.5945 Hz . . . . .	127
B.26 Experimental result showing the frequency response produced when Line A was set at 14.5 inches and Line B remained at 2 inches and the supply flow rate was set at 3.5 L/min. . . . .	127
B.27 Frequency of the wave form (generated at 3.5 L/min supply pressure) estimated using FFT codes. The main frequency was calculated to be at 292.0507 Hz . . . . .	128
B.28 Experimental result showing the frequency response produced when Line A was set at 14.5 inches and Line B remained at 2 inches and the supply flow rate was set at 4.0 L/min. . . . .	128

---

B.29	Frequency of the wave form (generated at 4.0 L/min supply pressure) estimated using FFT codes. The main frequency was calculated to be at 295.5069 Hz . . . . .	129
B.30	Experimental result showing the frequency response produced when Line A was set at 14.5 inches and Line B remained at 2 inches and the supply flow rate was set at 4.0 L/min. . . . .	129
B.31	Frequency of the wave form (generated at 4.0 L/min supply pressure) estimated using FFT codes. The main frequency was calculated to be at 298.9631 Hz . . . . .	130
B.32	Experimental result showing the frequency response produced when Line A was set at 14.5 inches and Line B remained at 2 inches and the supply flow rate was set at 4.0 L/min. . . . .	130
B.33	Frequency of the wave form (generated at 4.0 L/min supply pressure) estimated using FFT codes. The main frequency was calculated to be at 298.9631 Hz . . . . .	131
D.1	Free body diagram of the control volume analysis. . . . .	135

## LIST OF TABLES

5.1	Frequencies produced at different feed-back length suggested by the manufacturer [15]. . . . .	38
5.2	Comparison between the results obtained from the experiment and the manufacturer's recommended value. . . . .	42
5.3	Frequencies produced at different supply flow rate with feed-back length fixed at 16.5 inches (one feed-back port blocked). . . . .	46
5.4	Frequencies produced at different supply flow rate with feed-back length fixed at 18 inches (one feed-back port blocked). . . . .	47
5.5	Frequencies produced at different supply flow rate with feed-back length fixed at 18 inches with both ports exhausting. . . . .	47
5.6	Frequencies produced at different supply flow rate with feed-back length fixed at 20 inches with both ports exhausting. . . . .	48
5.7	Frequencies produced at different supply flow rate with feed-back length fixed at 22 inches with both ports exhausting. . . . .	48
5.8	Frequencies produced at different supply flow rate with feed-back length fixed at 32 inches with both ports exhausting. . . . .	48
5.9	Results of the cascading setup with 16 inches Element 1 feed-back port length. . . . .	52
5.10	Model optimal dimensions determined by experiment related to power nozzle width $w_S$ (Carne [18]). . . . .	58
5.11	Results of the frequency produced by Design 4 with varying supply pressure and feed-back length (center vent closed). . . . .	63
5.12	Results of the frequency produced by Design 4 with varying supply pressure and feed-back length (center vent opened to atmosphere). . . . .	64
5.13	Result of the frequency captured for cascading setup of Design 4 and GE proportional amplifiers with a feed-back length fixed at 20 inches, and no flow into the GE oscillators. . . . .	69
5.14	Result of the frequency captured for cascading setup of Design 4 and GE proportional amplifiers (feed-back length fixed at 20 inches, 0.5 L/min flow into the GE oscillators). . . . .	71
5.15	Result of the frequency captured for cascading setup of Design 4 and GE proportional amplifiers (feed-back length fixed at 20 inches, 1.0 L/min flow into the GE oscillators). . . . .	71
5.16	Result of the frequency captured for cascading setup of Design 4 and GE proportional amplifiers (feed-back length fixed at 20 inches, 1.5 L/min flow into the GE oscillators). . . . .	71



---

5.17	Frequency captured by PCB microphones (in Hz) mounted at 4 different positions on the top of 4 different channels. The supply pressure into Design 4 was fixed at 1.5 psig and the supply flow into the GE amplifiers was allowed to vary from 0 to 2.0 L/min . . . . .	78
5.18	Frequency captured by PCB microphones (in Hz) mounted at 4 different positions on the top of 4 different channels. The supply pressure into Design 4 was fixed at 2.0 psig and the supply flow into the GE amplifiers was allowed to vary from 0 to 2.0 L/min . . . . .	79
5.19	Frequency captured by PCB microphones (in Hz) mounted at 4 different positions on the top of 4 different channels. The supply pressure into Design 4 was fixed at 2.5 psig and the supply flow into the GE amplifiers was allowed to vary from 0 to 2.0 L/min . . . . .	80
5.20	Frequency captured by PCB microphones (in Hz) mounted at 4 different positions on the top of 4 different channels. The supply pressure into Design 4 was fixed at 3.0 psig and the supply flow into the GE amplifiers was allowed to vary from 0 to 2.0 L/min . . . . .	81

## 1. INTRODUCTION

In low temperature fuel cells such as the Polymer Electrolyte Membrane (PEM) fuel cells, liquid water is produced as a byproduct. At low gas flow rates, the water produced has a tendency to plug the reactant supply channels. When the channels are plugged, reactant supply to the catalyst sites is prohibited and results in fuel cell failure.

Ideally, water removal from the reactant supply channels would occur as soon as a water drop forms in the channel. One proposed method of removing a water drop is to oscillate the drop near its natural frequency in order to free it from the substrate. A variety of methods for oscillating the drop are available including mechanical vibrations, acoustic vibrations and flow pulsations. It is the latter method that is investigated in this thesis.

The first hypothesis of this research is that flow pulsation can be induced through the use of fluidic oscillators and that this approach is suitable for multiple parallel flow channels. The second hypothesis tested in this thesis is that commercial computation fluid dynamics software is applicable for modeling and optimization of fluidic oscillators.

### *1.1 Need for Fuel Cells*

Energy supply and demand plays an increasingly vital role in our national security and the economic output of our nation. Based on the data gathered by the U.S. Department of Energy, for the year of 2005, the average U.S. fossil fuel consumption has

reached to approximately 80 quadrillion Btu while its production was significantly lower at approximately 50 quadrillion Btu [1]. The price of crude oil is expected to increase from \$40.49 per barrel in 2004 to \$54.08 per barrel in 2025 (about \$21 per barrel higher than the projected 2025 price in 2005 energy report) and to \$56.97 per barrel in 2030 [1]. With this continual increase in oil prices the expected transportation, manufacturing, and raw material cost for our daily merchandise are expected to increase accordingly.

Alternative energy is a method of extracting energy from its natural source, such as light, wind, wave, flowing water, biological, and geothermal. Currently alternative energy only covers a minute sector in the overall energy production chart (8%) [1]. However this number is expected to grow as the public responds to increase in energy prices. According to the forecast predicted by the DOE, there should be at least a 20% increase in alternative energy production by the year of 2010 [1]. Among the possible candidates of alternative energy sources, a rapidly rising star that is receiving a tremendous amount of attention is the fuel cell.

Fuel cells have existed for over a century. Recent technological breakthroughs and improvements have brought this technology closer to wide spread implementation. Numerous fuel cell research and development efforts have reached the stage where both mobile and stationary power applications are nearing an acceptable cost for commercial markets. However, behind the popularity of fuel cells, the functionality and applications of fuel cell is still not very well known to the public.

## 1.2 What is a ‘Fuel Cell’?

A fuel cell is an electro-chemical energy conversion device which converts chemical energy to electrical energy. It functions in a similar fashion to a battery except that the life of the battery is governed by the amount of chemical reactants it contains while a fuel cell will continue to operate as long as fuel is supplied.

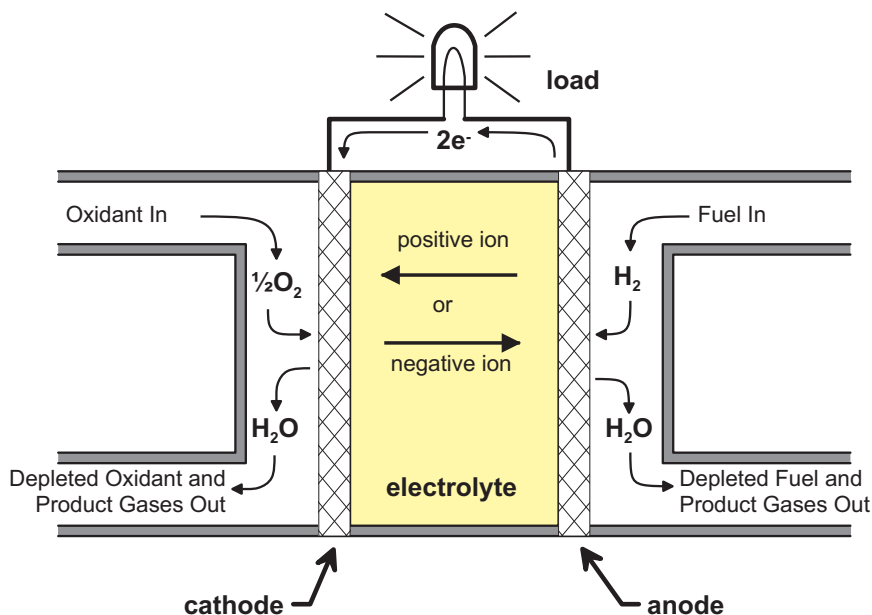


Fig. 1.1. General structure of fuel cell.

The basic physical structure of a fuel cell is shown on Figure 1.1. It consists of an centermost electrolyte layer in contact with an anode and cathode on either side. The electrolyte can be solid or liquid depending on the type of fuel cell but its principal function is the same, that is to conduct ions between the anode and the cathode.

The electrolyte also functions as an electron separator. During the oxidation and reduction process, the electron released must not be allowed to pass directly through the electrolyte. If the electrons pass directly through the electrolyte, a short circuit of the cell will occur and the fuel cell will fail.

The fuel supplied varies depending on the type of fuel cell. For low operating temperature cells, pure hydrogen and air is typically used. For higher operating temperature fuel cells, hydrocarbons ( $\text{C}_n\text{H}_n$ ) and other bio-fuels may be applicable because poisoning of platinum is not an issue for high operating temperature fuel cell. Gaseous hydrogen has become the fuel of choice for most applications because it has a high reactivity when suitable catalysts are used, and it is available from a wide vairyety of feed stocks.

Referring to Figure 1.1, hydrogen enters the fuel cell through the anode side (neg-

ative side), and oxygen enters through the cathode side (positive side). A catalyst<sup>1</sup> is typically used to facilitate the separation of the hydrogen gas into electrons and protons (hydrogen ions). The material of the catalyst changes as the operating temperature differs from one fuel cell to another. For acid electrolytes, hydrogen ions will pass through the electrolyte and combine with oxygen on the cathode side, producing water and heat in the process. The electrons, which cannot pass through the electrolyte, will be redirected from the anode to the cathode through an external load.

The electrodes are generally porous in nature for low operating temperature fuel cells. Using porous material as fuel cell electrodes has several advantages. First, for fuel cells that use platinum as catalyst, the porous nature of the electrode will increase the effective surface area for catalyst coating, thus decrease the overall thickness of the cell. Second, increase in porosity also provides the electrode with a larger surface area to volume ratio, achieving improved rates of reactions. The catalytic function of electrodes is more important in lower temperature fuel cells compared to higher operating temperature fuel cells because the reaction rates increase with temperature. Third, the electrode is responsible to conduct electrons away from or into the electrolyte once they are formed, therefore the electrode must be made from materials that have good electrical conductance and can be easily manufactured.

The above is a general description of a common electro-chemical structure of the fuel cell. Most of the fuel cells out in the market follow the basic trend of structure orientation, and the size and material of this structure will defer according to the scale of electricity and heat production during the chemical reaction of the fuels. Outside the electro-chemical structure one will usually find the gas supply channels which complete one cell stack. Depending on the requirement, the number of stacks may differ. The voltage is directly proportional to the number the cell stacks while the current produced is dependant on the surface area of the cell stack.

---

<sup>1</sup> A catalyst layer is generally found between the electrolyte and the electrodes to speed up the reduction and oxidation process of the fuels.

Appendix A provides an introduction of the classes or types of fuel cell that is in the market today, followed by a brief comment on some of the advantages and disadvantages each of the fuel cell family carries and some major differences between them.

## 2. POLYMER ELECTROLYTE MEMBRANE FUEL CELL

### *2.1 Background*

The focus of this research is on a particular low temperature fuel cell, the Polymer Electrolyte Membrane Fuel Cell (PEMFC). The PEM fuel cell was invented in the early 1960s by Willard Thomas Grubb and Lee Niedrach of General Electric and later was used in NASA's Gemini space program [2]. Despite their success in space programs, PEMFC were limited to space missions and other special applications because of expensive materials used. It was not until the late 1980s and early 1990s that fuel cells became a real option for wider applications. Several breakthroughs were achieved which made this possible, such as low platinum catalyst loading and thin film electrodes drove the cost of fuel cells down, making development of PEMFC systems more realistic [2].

The biggest advantage of low operating temperature nature of PEMFC is it allows the system to reach steady state operation from cold start in very short amount of time. Therefore it is ideal for powering automobiles and small backup generators. A PEMFC is capable of providing continual electrical energy supply from fuel at high levels of efficiency (40 ~ 50 %) and power density [2]. There are no moving parts in the structure of PEM fuel cell stack, therefore the maintenance effort is reduced to the minimum compared to traditional internal combustion engines. Currently the cost of single cell unit is still high, but with PEMFC's expanding research efforts and the advantages mentioned previously, potential for cheaper materials will begin to emerge and manufacturing costs will decrease [3].

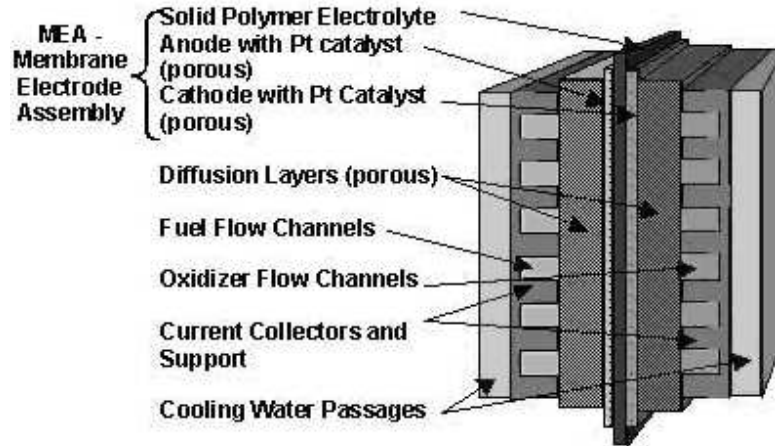


Fig. 2.1. General components of PEMFC [4].

## 2.2 Structure of PEMFC

A cell stack of PEMFC typically consists of four sections: The inner most polymer membrane, porous electrodes with catalyst layer embedded within, gas diffusion layers and finally the outer most bipolar plates. A schematic of the cell is shown in Figure 2.1.

The heart of PEMFC is the electrolyte. Its main function is to provide a conductive path for the protons to travel from the anode to the cathode while preventing electron and reactant gas crossover. It is a perfluorosulfonic acid polymer, typically Nafion 10®. Before the 1970s, the proton conducting membrane was usually made from polystyrene sulfonic acid used in the NASA Gemini Space Program. Du Pont's perfluorosulfonic acid membrane (otherwise known as Nafion®) is currently the most common electrolyte used. Although polystyrene sulfonic acid offered better water uptake, the Nafion® produces much better proton conductivity. Nafion® has a structure very similar to Teflon, except the end of the long carbon chain is replaced by a  $\text{CF}_2$  group which is connected to another  $\text{SO}_3\text{H}$  group, making Nafion® a super-acid. The improvement that this super-acid offers compared to the polystyrene sulfonic acid was that there was at least a two-fold increase in specific conductivity, and the more



of the  $\text{SO}_3\text{H}$  group, the higher the ionic conductivity [2]. Another advantage that the Nafion<sup>®</sup> offered is that the  $\text{CF}_2$  group is very stable when reacted with oxygen, where as in Teflon sometimes hydrogen peroxide was formed as by-product. Hydrogen peroxide's presence is unwelcome because of its corrosive nature, but the utilization of Nafion<sup>®</sup> was able to overcome this problem. The most significant improvement when Teflon was replaced with Nafion<sup>®</sup> was that the lifetime of the PEMFC was increased by at least four times [2].

The mechanical properties and geometries of Nafion<sup>®</sup> differ from one manufacturer to another, it is very similar to the sealing wrap commonly found in the supermarket except the thickness may vary from 50 to 175 microns (about 2 ~ 7 pages of normal paper) [2]. Being solid in nature, the electrolyte has the advantage of avoiding corrosion to the surrounding peripherals. The electrolyte also acts as a physical barrier to prevent the reactant gases from mixing. The ion conduction takes place via ionic groups (sulfonic acid group) within the polymer structure and it is highly dependant on the bound and free water associated with those groups. Therefore maximum ionic conductivity can only be achieved by maintaining the polymer membrane at maximum hydration. Upsetting the balance in water content could result in reduction in ionic conductivity, gas permeability and mechanical properties of the cell.

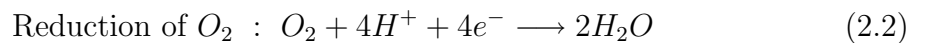
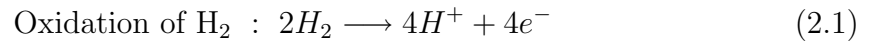
The PEMFC electrolyte is susceptible to ohmic overpotential, especially when the device is dealing with middle to high power density scales (from 0.3 ~ 1.0 A/cm<sup>2</sup>) [2]. One solution to this problem is to use a thinner electrolyte such as Nafion 112<sup>®</sup>. The typical thickness of Nafion 115<sup>®</sup> is about 127 micron meters while Nafion 112<sup>®</sup> has thickness about 50 micron meters, half of Nafion 115<sup>®</sup>. The result of using a thinner membrane is that the cell potential is dropped to about 0.75V at 1.0 A/cm<sup>2</sup>, which avoided the cell's overpotential problem at high current densities [2]. However the mechanical strength of the Nafion 112<sup>®</sup> is much less than Nafion 115<sup>®</sup> and small amount of reactant gas cross-over can occur. Under such condition the cell will very

likely to fail during long hour operation because the formation of hotspots on the surface of the membrane.

W.L. Gore and Associates were able to successfully overcome the problem of mechanical strength of Nafion 112® by using their Teflon supported Nafion membrane [5]. In their design, the Nafion 112® is supported by fine-mesh Teflon. As mentioned previously, if the thickness of the electrolyte is reduced the overpotential will be reduced accordingly, resulting in greater cell efficiency.

With all these promising results, there are still issues regarding to cost. A square meter of the Nafion 112®, costs approximately \$700 [2] because the fluorination step in the manufacturing process is very costly. This problem can only be improved if the demand of Nafion 112® is increased or the costly fluorination process is avoided.

During the operation of PEMFC, hydrogen enters the cell through the supply passages, reaches the anode and oxidizes into its protons and electrons with the help of platinum catalyst. The oxygen at the cathode will combine with the protons to form water and heat. The chemical reaction of this process is shown below:



Normally this process occurs very slowly at standard temperature and pressure. Therefore a catalyst is required to speed up the reaction. Typically in PEMFC platinum is used as the catalyst and it is required to have catalyst layer on both cathode and anode side to promote the oxidation and reduction process. The coating method of catalyst has improved tremendously over the years. The platinum loading has successfully decreased while the catalytic efficiency was able to be maintained at an optimum level.

The catalyst layer is porous in nature and it is made by carbon for electro-

conductivity. The porous characteristic serves two main purposes. First is to remove the excess water and provide passages for reactant gas to pass through and the second is to increase the surface area. The rate of oxidation and reduction is dictated by the amount of platinum loading, which associated with the utilization of maximum surface area to volume ratio of the platinum powder. Typically the platinum catalyst before installation will exist in its powder form and has an average diameter about 2 nanometers [6], with this advantage in diameter, an enormous total surface area will be accessible to the gas molecules. The large platinum surface area allows the electrode reactions to proceed at many areas simultaneously. The key to maximum electron flow is the area of dispersion of the platinum catalyst. The wider the dispersion, the higher the electron flow (more current). Therefore porosity of the carbon electrodes became an important criterion as it has direct relationship to catalyst loading.

#### *Gas Diffusion Layer with Micro-porous Layers*

The catalyst layer together with the polymer membrane made up the Membrane Electrode Assembly (MEA), a term which is commonly used in describing PEMFC structure. The MEA is sandwiched between two roughly 200  $\mu\text{m}$  thick carbon-fiber paper gas diffusion layers (GDL). The GDL functions as a current collector while serving two other main purposes. One is to transport excess water produced from the reaction sites to the bipolar plates where the water could be removed from the cell. The second is to transport reactant gases from the gas supply channel to the reaction sites. It is ideal for a fuel cell to operate at high current density to produce maximum power output and in order to achieve high current density during operation a high gas feed is required. So the GDL must be capable to effectively transport reactant gases with minimum restriction.

The GDL in PEMFC generally consists of two layers; the first layer is made of

a larger pore diameter carbon-based substrate, very similar to a carbon paper or carbon cloth. This layer is generally thicker and is designed to handle compression for maximum contact with the bi-polar plates. The second layer is a much thinner, much smaller pore diameter layer known as the microporous layer. This layer is made by carbon black powder and some hydrophobic materials and it is in intimate contact with the gas diffusion layer.

Typically the GDL is treated with a hydrophobic agent, usually polytetrafluoroethylene (PTFE), to make the structure non-wetting<sup>1</sup> so water droplets formed can be removed with minimum effort. However, “more” does not mean “better” in this case. If the non-wetting agent was excessively applied, the porosity of the GDL will decrease, resulting in low reactant gas transport. Experiments have been conducted and the optimum near-saturated operation was found to be between 15 to 20% wt [7]. Some Scanning Electron Microscopy (SEM) images were taken to gain a better insight to the structure of GDL, and the distribution of the porosities can be better understood.

The SEM images of GDLs produced by Toray and E-TEK were taken and are shown on Figure 2.2 to Figure 2.9. The working distance of the microscope was started at 39 mm since it is a typical ideal working distance to retrieve a good image. Changing the working distance will change the magnification and probe diameter, which may have a direct impact on the images’ resolution. Changing the working distance will also affect the convergence angle, which has a direct impact on the depth of field of the specimen.

An accelerating voltage of 20 keV was used and the condenser lens strength was adjusted automatically to compensate the imperfection of the image. Theoretically, at high accelerating voltage, the surface detail of the specimen will be low and the

---

<sup>1</sup> Wetting is a term used to describe the contact angle between the solid-liquid interface. Complete wetting (also referred to as spreading) is obtained at an angle of 0 degrees and complete non-wetting occurs at an angle of 180 degrees

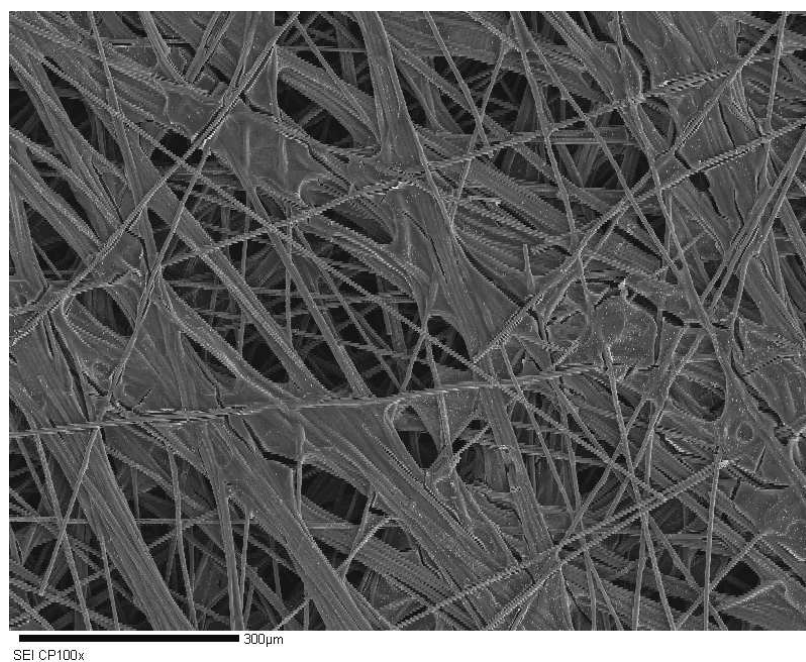


Fig. 2.2. Toray Carbon Paper 2050-A side A at 100X and the scale bar is 300  $\mu\text{m}$ .

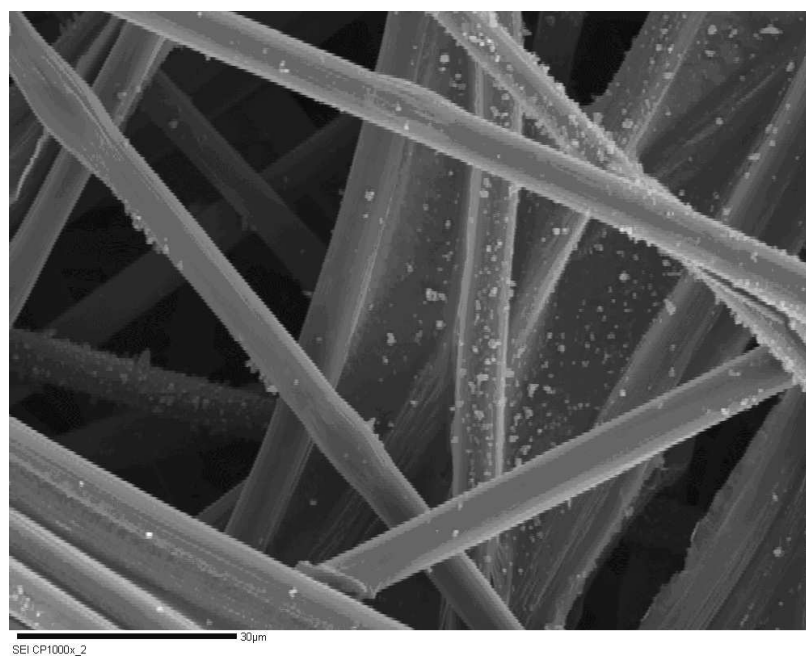


Fig. 2.3. Toray Carbon Paper 2050-A side A at 1000X and the scale bar is 30  $\mu\text{m}$ .

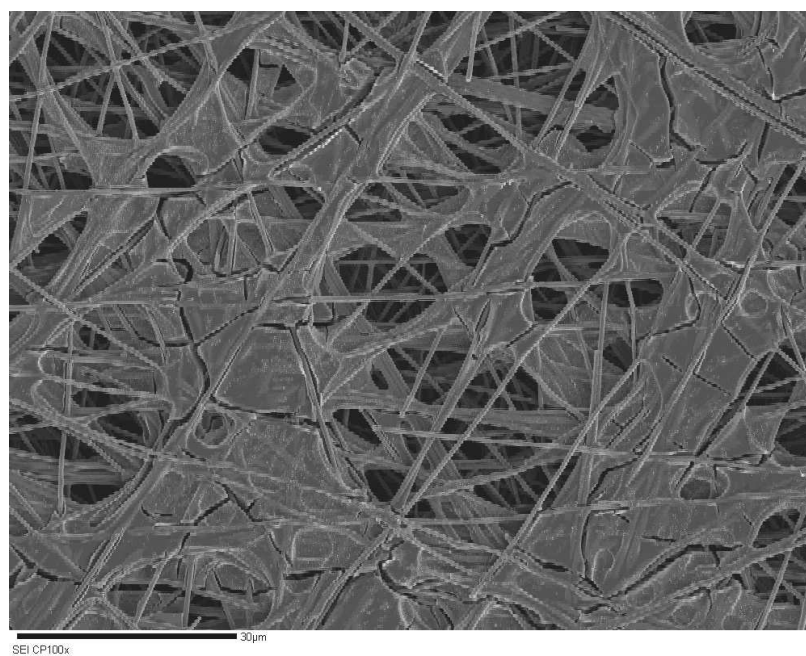


Fig. 2.4. Toray Carbon Paper 2050-A side B at 100X and the scale bar is 30  $\mu\text{m}$ .

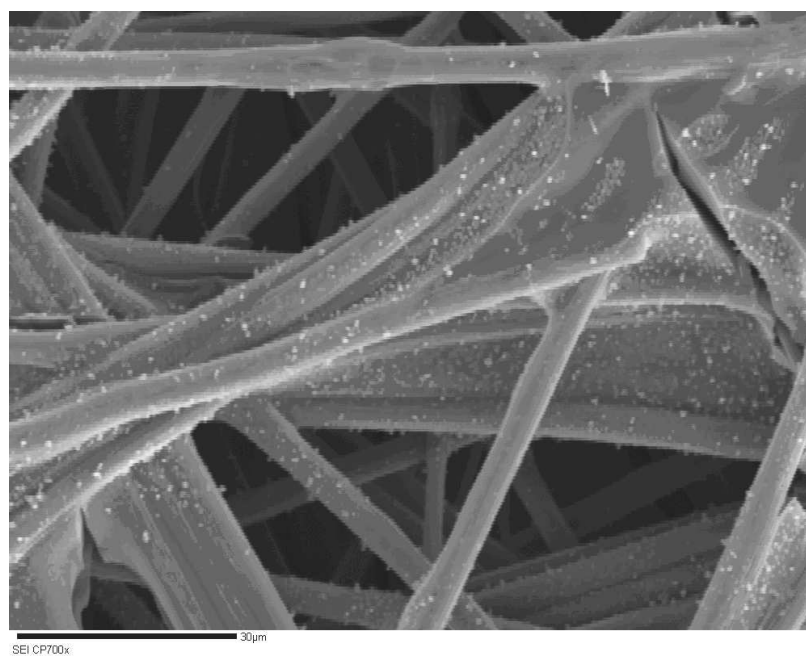


Fig. 2.5. Toray Carbon Paper 2050-A side B at 700X and the scale bar is 30  $\mu\text{m}$ .

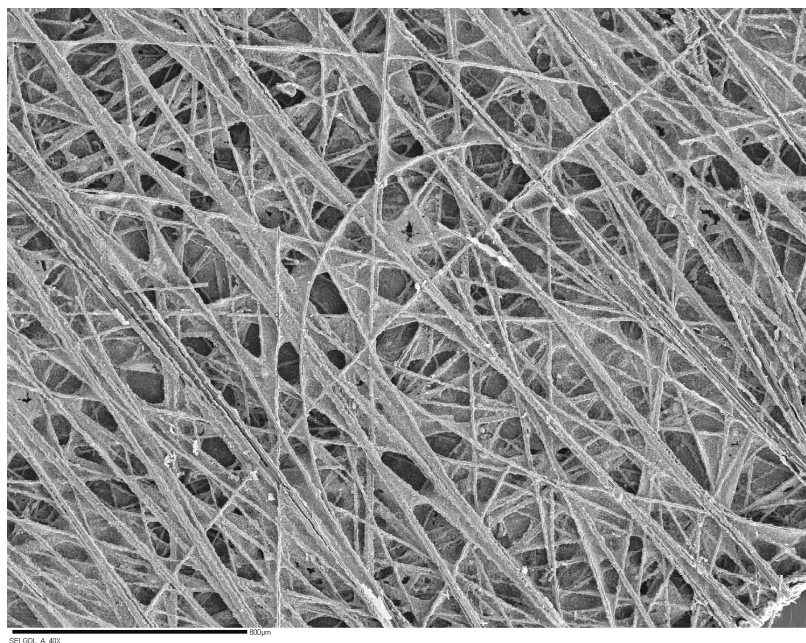


Fig. 2.6. E-TEK GDL LT 1200-N side A at 40X and the scale bar is 800  $\mu\text{m}$ .

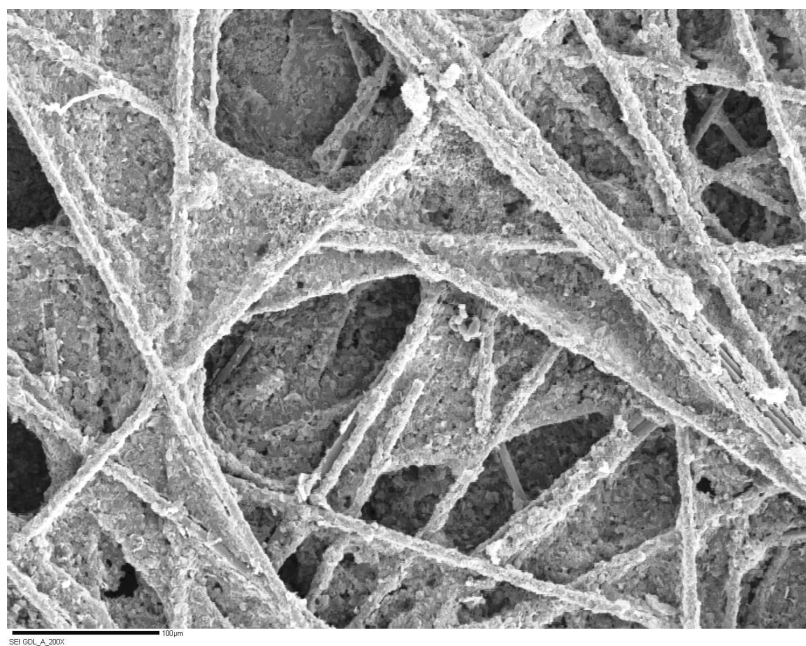


Fig. 2.7. E-TEK GDL LT 1200-N side A at 200X and the scale bar is 100  $\mu\text{m}$ .

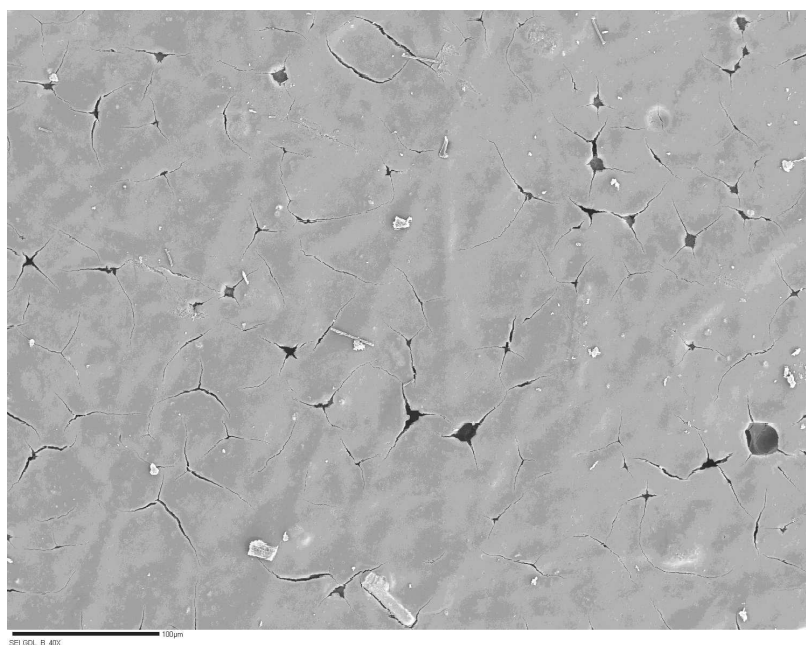


Fig. 2.8. E-TEK GDL side B LT 1200-N at 40X and the scale bar is 100  $\mu\text{m}$  (microporous side).

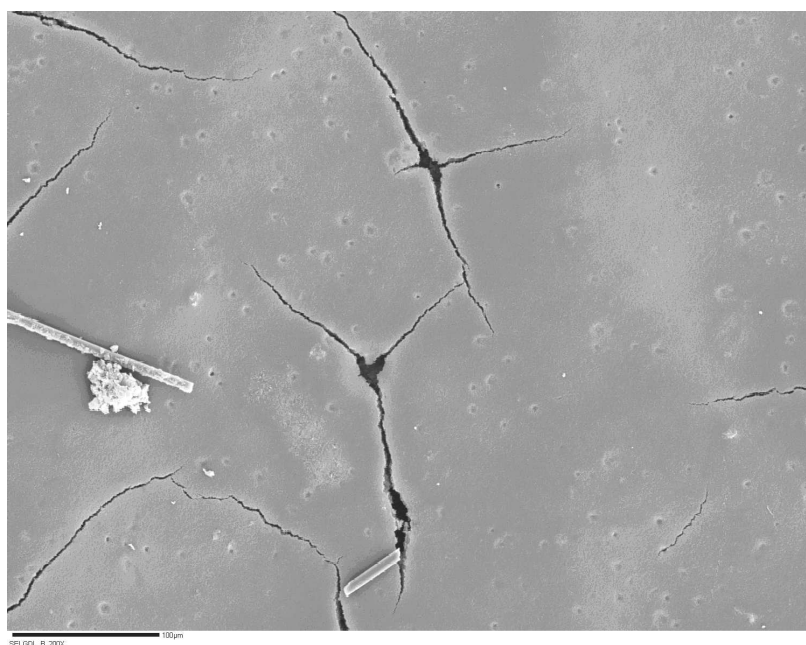


Fig. 2.9. E-TEK GDL LT 1200-N side B at 200X and the scale bar is 100  $\mu\text{m}$  (microporous side).



electron is able to penetrate the specimen further down in the z-direction (greater interaction volume) and reveal the information of the interior of the specimen. At low accelerating voltage ( $\leq 5\text{keV}$ ) the surface detail of the specimen will be better retrieved but the resolution may be poor. The performance of the electron optics at low accelerating voltage is always significantly worse than at higher energies, because the filament brightness is reduced so less current is available and the magnitude of the chromatic aberration effect increases.

The resolution of the image was controlled by the probe diameter. The smaller the probe diameter, the better the resolution; therefore to use a small probe diameter, a stronger condenser lens strength was used because a strong condenser lens will limit the amount of current to pass through it. A combination of high accelerating voltage and high condenser lens strength was used to obtain good quality and good resolution images. The aperture size was allowed to remain at 3 so that the convergence angle will not change since the effect of depth of field is not critical in this project. The magnification was increased to 100X (focus was adjusted at 1000X) and the first image of the Toray GDL (2050-A) was captured and shown in Figure 2.2. The second image of the same side of the Toray GDL was taken at 1000X and it is shown in Figure 2.3. The same setup procedures were repeated for side B of the Toray GDL and side A and B of the second specimen (E-TEK GDL, LT 1200-N), the images were captured and shown in Figure 2.4 to Figure 2.9 at different magnifications.

Observing the SEM sample of the GDL, the irregular carbon fiber network is clearly observable on Side A of the E-TEK GDL (Figure 2.6). When Side B of the same paper was put under the microscope, a very dissimilar surface topography was observed (Figure 2.8). This is a layer of Microporous layer, which is commonly used in PEMFC to improve water management. The typical thickness of microporous layer ranged from 10 to 100 micro-meters and it is usually placed between the catalyst layers and the GDL.

The most promising material for GDL is carbon fiber in non-woven papers and woven fabrics. These materials are chosen because of their high porosity (approximately 70%) and their outstanding electrical conductivity [8]. The porosity in the GDL provides a path for reactant gases to travel from the gas supply flow fields to the catalyst layers in both in-plane and through-plane orientation. It also provides flow passage for water removal from the reactant sites to the flow field channel. The paper consists of numerous carbon fiber networks (Figure 2.7) which allow electronic conductivity while acting as an efficient excess heat removal agent from the MEA to the bipolar plates where cooling channels are located. As mentioned previously, the electrolyte in the MEA is made of Nafion<sup>®</sup> which is essentially sealing-wrap like material, therefore, the GDL also provides mechanical support for the MEA in case the pressure difference between the electrodes and the gas flow fields gets too large.

### *Bipolar Plates*

The bipolar plate is the outer most structure of the PEMFC. The plates are made of a light-weight, strong, gas-impermeable, and electron-conducting material. In most of the PEMFC, graphite or metals are commonly used and composite plates are now being developed to further increase the strength and reduce the overall weight [2]. The main purpose of the bipolar plate is to serve as gas supply from the source to the reaction sites by a series of serpentine flow field network and also acts as a current collector. Flow fields are usually manufactured into both side of the plate to create a stack of cells. The power produced by the fuel cell stacks increases as the number of stack layers increases (similar to connecting batteries in series) and the current increases as the area of the fuel cell stack increases. The pattern of the flow field in the plate as well as the width and depth of the channels have a large impact on the effectiveness of the distribution of the reactant gases evenly across the active area of the membrane/electrode assembly. Flow field design also affects water supply to

the membrane and water removal from the cathode, therefore it must be carefully designed so it will not disrupt the overall supply of the reactant gases.

### 2.3 Water Management in PEM Fuel Cells

The major operational problem encountered by PEMFC is the issue of water management. Water transport issue is not only a function of operating condition (such as operating pressure, operating temperature, etc.) but also a function of characteristic of the structure and materials of the membranes layers and the electrode. The operating conditions of the cell varies depending on the type of application, but the commercial PEMFC is typically expected to be operating at atmospheric pressure and a steady state temperature of 80°C. Therefore most of the waste water produced will be in the liquid form. This excess water produced must be removed from the system because the performance is directly related to the water content within the fuel cell.

In the membrane electrode assembly (MEA), water is being produced as a byproduct at the cathode from the chemical reaction of the reactant gases, some of the water will be reused by the system for maintaining the hydration of the proton conducting membrane. The state of the art proton conducting membrane is made by Nafion<sup>®</sup>, which has excellent proton conductivity because of the high electro-negativity of the fluoride and sulfonic group attached at the end of the carbon chain [2]. During the process of proton exchange water is required to keep the proton and the sulfonic groups in their solvated form so the protons can ‘hop’ from one chain to another, since the ionic conductivity of the electrolyte is highest when it is fully hydrated. Experiments have showed that the hydration of the proton conducting membrane can be maintained by humidifying the reactant gases before entering the fuel cell [2]. However this technique requires an external humidifier and the overall size, weight and cost of the system will increase with such implementation.

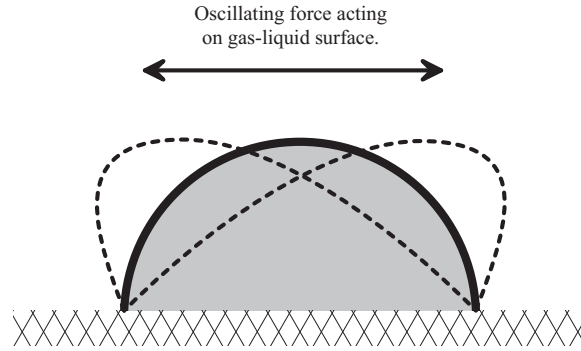


Fig. 2.10. Sloshing motion of the water droplet where the dashed line indicate the shape of the water droplet when a periodic force was applied.

In the porous gas diffusion electrodes the amount of water content has to be monitored carefully. If the excess water is not removed, the porous channels in the diffusion media will slowly plug up thus limiting the area through which reactant gases can flow, thereby retarding the overall performance of the fuel cell [8]. This research proposes a method of water removal by oscillating the water droplet formed in the gas supply channel at or near its natural frequency. By oscillating the fuel supply stream, an enhanced water removal can be achieved.

## 2.4 Droplet Oscillation

Several methods on the possible solution towards water management were mentioned in the previous section. Some of the techniques proposed in water management are: external humidification of the hydrogen gases, utilization of microporous layers to enhance the capillary force driven flow, implementation of integrated flow field design, and modification on the porosities of cell electrodes [2].

Oscillation of liquid drops is commonly used in areas such as liquid-liquid extraction, synthesis of ceramic powders, growing of pure crystals in low gravity, dynamic contact angle measurements, and measurement of dynamic surface tension [9]. When a drop of liquid is subjected to an external vibrational force in the form of periodic wave, it will begin to oscillate. When the frequency of the external vibrational force

approaches the resonance frequency of the liquid drop, the pressure balance (internal and external pressure) which holds the droplet in shape will be disturbed and the drop will tend to move from its original position on the surface. The frictional force at the three phase contact line and the bulk of the drop tends to hinder the fluid movement, thus a sloshing effect of the droplet will be observed as shown in Figure 2.10.

As the frequency of the external vibrational force approaches closer and closer to the resonance frequency of the droplet, the droplet may begin to shift across the substrate. Daniel et al. [10] observed that the liquid drop's motion reached a maximum velocity when the forcing frequency reaches the resonance mode of the drop oscillation. The drop oscillation is a strong function of the surface tension, density and the size of the liquid drop thus different droplet sizes will possess a difference resonance frequencies.

Moving fluid droplets has been an area of wide interest for over many years, it is a popular subject especially in the pharmaceutical field. It is useful for droplet mixing, thermal cycling and also enhancement of chemical reaction in micro scale devices. Several methods have been developed to maneuver a fluid droplet, methods such as surface energy gradient, thermal Marangoni flow, electrowetting, dielectrophoresis, and oscillation on asymmetric surfaces have demonstrated promising results in the past few years [10]. There are two types of imposing an asymmetrical force on the water droplet. The first is to oscillate the external environment which surrounds the fluid drop, and the second is to mechanically oscillate the substrate where this droplet rest on.

Daniel et al. [10] imposed an asymmetric force on a water droplet by mechanically vibrate the substrate which the water droplet rested on and presented a set of very interesting result. Based on Daniel's finding, the displacement of the water droplet (sessile) at a given forcing frequency and the direction and speed of the water droplet

is dependant upon the droplet size (nonlinearly). Three frequencies were used in their experiment together with a variety of droplet sizes, and their results have shown that with a droplet radius of approximately 0.7 mm and were subjected to a 100 Hz oscillation frequency, its displacement velocity peaks at 16 mm/s.

Moon and Kang [11] chose the second type of droplet oscillation method, which is the excitation of the environment which surround the water droplet. In their work a pendent drop with a diameter of approximately 2 mm was placed near a woofer and the motion of the water droplet is captured by a high speed camera. The oscillation of the water droplet was observed when the forcing frequency of the woofer was approximately at 58 Hz. Since this research is interested in a sessile drop orientation, based on the experimental result produced by Daniel et al. [10], a target frequency was identified.

### 3. FLUIDIC AMPLIFIER

#### *3.1 Introduction*

Fluidic oscillators were initially designed to enhance the performance of a wide range of fluidic systems. It is especially beneficial to smaller scale fluidic systems that have low fluid flow, such as automatic control in certain industrial applications, measurements in domestic gas storing, chemical or biological analysis, etc [12].

Fluidic oscillators belong to a family of fluidic amplifiers and there are a wide variety of fluidic amplifiers. The most apparent characteristic of fluidic amplifiers is that it has no moving parts and utilizes liquid or gas as working medium. Usually the fluid is accelerated either by passing through a nozzle or by an external compressor. The pressurized air stream is first introduced to the supply port of the amplifier which is then directed into an interaction region (see 3.2). If there is no pressure difference across the two control ports, the power jet passes directly through the interaction region, strikes the splitter and divides equally through the exit ports producing zero differential pressure. However, if a pressure difference exists across the control ports, the fluid jet stream will deflect before striking the splitter and causes more flow through one exit port than the other, producing an amplification of the control signal at the exit ports.

The main purpose in designing a fluidic oscillator is to effectively exert a variable asymmetrical force on a liquid droplet, causing the droplet to shift in position. By further investigating the operating principal of the fluidic amplifier, one may gain a better insight towards fluidic oscillator design.

### 3.2 Types of Fluidic Amplifiers

There are generally two families of fluidic amplifiers, one is the analog amplifier and the other is the digital amplifier. The main difference between an analog and a digital fluidic amplifier is that analog amplifiers are characterized by the continual modulation of the output from the changes of the control inputs while the output response of a digital fluidic amplifier will not be continuous with its control inputs. This concept will be further clarified in the following sections.

#### 3.2.1 Analog Amplifier

Figure 3.1 shows the schematic of an analog fluidic amplifier. There are two characteristics of the analog fluidic amplifier. First, the response of the output differential pressure to the control differential pressure of an analog fluidic amplifier must be linear (see 3.1), so the inherently non-linear fluid flow phenomenon must be avoided. Second, the momentum interaction between two or more fluid streams is the most dominant operating technique of an analog fluidic amplifier.

Pressure energy and change in momentum are two of the most important forces when stream of fluid jets are introduced into the amplifier. Initially the pressure within the interaction chamber of the amplifier is uniform due to the venting mechanism of the device to the ambient. As the pressurized jet is being introduced into the chamber, the uniform pressure distribution within the interaction volume rapidly equalizes and the behavior of the fluid stream is dictated by the balance of momentum. Therefore, depending on the type of application (the number of jets interacting in the opposing manner), the analog amplifier must be designed relative to the change in momentum between the interaction of jet streams.

Referring to Figure 3.3, two streams of jets (with velocities  $u_1$  and  $u_2$ ) are introduced into the interaction volume and the resultant jet,  $u_3$ , will travel in the direction illustrated above. The resultant momentum,  $J_R$  of the impeding jets can be estimated



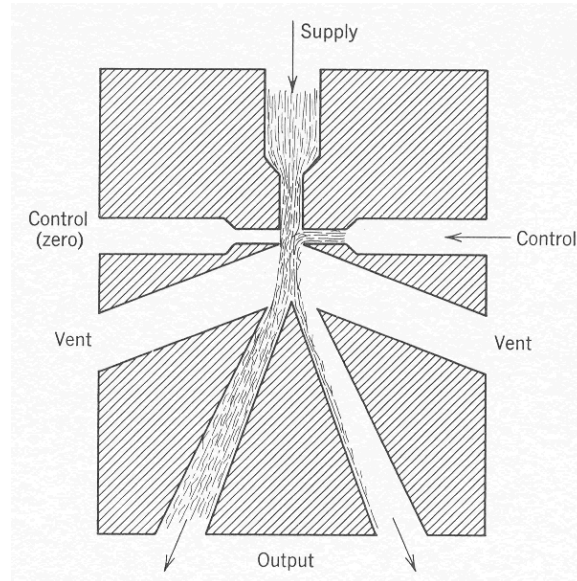


Fig. 3.1. Schematic of an analog fluidic amplifier [13].

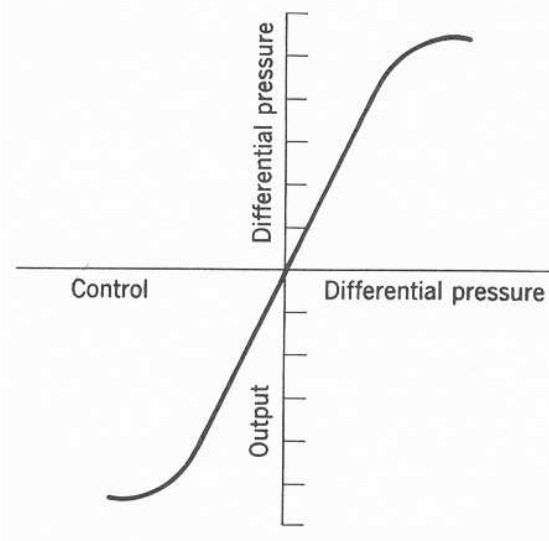


Fig. 3.2. Output differential pressure response to control differential of an analog amplifier [13].

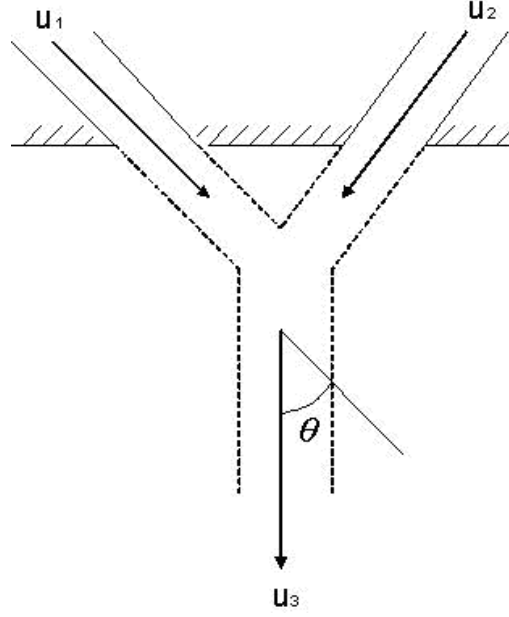


Fig. 3.3. Momentum Interaction of two impinging jets [13].

with the following relationships [14], where  $\rho$  is the density of the jet,  $A$  is the area of the cross-section of the channel, and  $u$  is the average velocity of the jet.

$$J_1 = \rho_1 A_1 u_1^2 \quad (3.1)$$

$$J_2 = \rho_2 A_2 u_2^2 \quad (3.2)$$

$$J_R = (J_1^2 + J_2^2)^{0.5} \quad (3.3)$$

If a pressure transducer is placed in the exact center at the downstream of the resultant jet, the pressure reading will be at maximum when  $J_1$  and  $J_2$  are equal. The pressure transducer signal will decrease if the flow through one of the channel is greater than the other and the resultant jet will deflect in a different direction (so the resultant angle is no longer equal to  $\theta$ ). The angle of deflection is directly proportional to the differential pressure and flows applied between the incoming impinging jets,  $J_1$  and  $J_2$ . The momentum interaction between the jet stream governs the functionality of the fluidic amplifiers. There are five major types of analog amplifiers,

1. Vented Jet-Interaction Amplifiers.
2. Closed Jet-Interaction Amplifiers.
3. Vortex Amplifiers.
4. Boundary-Layer-Control Amplifiers.
5. Impact Modulators.

Each of these amplifiers differs from the others depending on the type of momentum interaction of the operating jet stream.

### 3.2.2 *Digital Amplifier*

The digital fluidic amplifier functions by means of the attachment of a jet stream to the wall adjacent to the fluid flow. Figure 3.4 shows the general schematic of a digital fluidic amplifier. The pressure applied to the supply port generates a jet into the interaction region. Initially the pressure within the interaction region is uniform and the velocity of the fluid moving within the interaction volume is low. The high velocity fluid from the jet will mix with the low velocity fluid in the interaction volume and, as a result, the velocity of the input jet will decrease as it progress further into the interaction region. The fluid jet will exit through the exit ports in a similar fashion as the analog amplifier when there is no differential pressure exist across the control ports; some of the jet will exit through the left exit port and some of the jet will exit through the right exit port.

In the case of a differential pressure across the control ports, the fluid jet will produce an entrainment as the stream flows from the supply port through the interaction region. The entrainment will produce a low pressure region between the two walls in the interaction region and the fluid stream will be attracted towards the low pressure region. The location of the formation of this low pressure region is random,

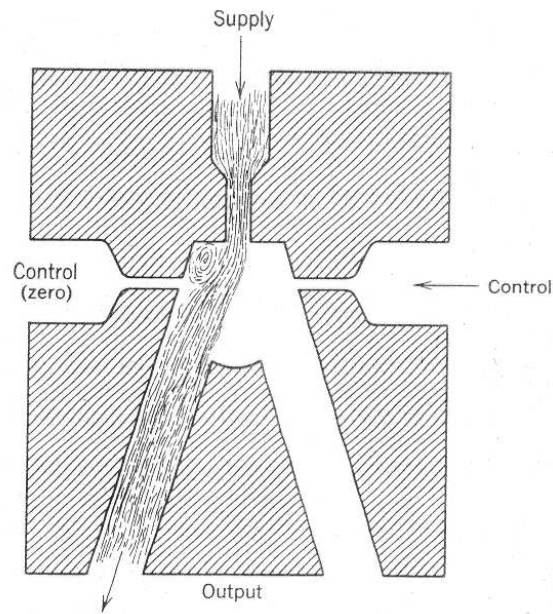


Fig. 3.4. Schematic of a digital fluidic amplifier [13].

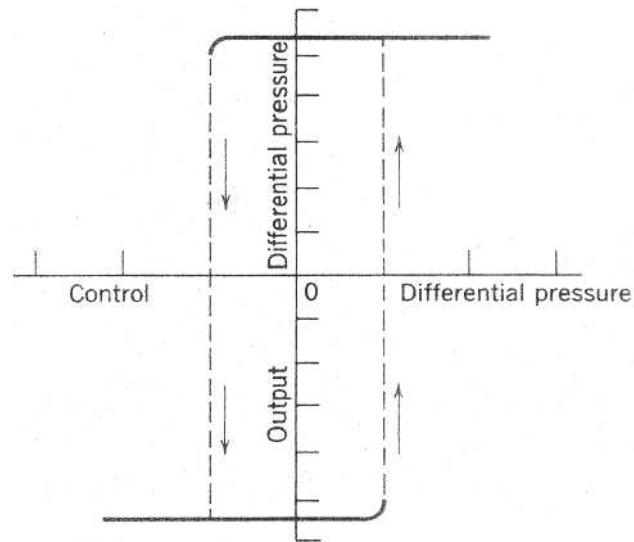


Fig. 3.5. Output differential pressure response to control differential of a digital amplifier [13].

sometimes near the left wall and sometimes near the right wall. The jet stream will move closer and closer towards the low pressure zone and finally it will attach to the wall. This phenomenon is commonly known as the Coanda effect.

Immediately after the jet stream attaches to the wall of its choice, the entrainment begins to produce another low pressure region on the opposite side of the wall, attracting the fluid to shift toward the new location. This behavior can be used to construct an ‘on-off’ switch in which the fluid will deflect opposite to the direction of the control port with higher supply pressure. There are generally four different types of digital fluidic amplifiers,

1. Wall Attachment Amplifier.
2. Turbulence Amplifier.
3. Axisymmetric Focused-Jet Amplifier.
4. Passive Logic Devices.

Digital fluidic amplifiers were not appropriate for this research because a continual modulation of the output by the changes of the control signal were necessary. Thus only a brief introduction of the digital fluidic amplifier has been presented since instantaneous signal output is not the topic of interest.

### *3.3 Comparison between Analog and Digital Amplifier*

Both the analog and digital fluidic amplifiers followed an identical operating principle. Both of these devices utilizes the balance of momentum between impinging jets which causes the deflection of jet streams. The most observable difference between the analog and the digital fluidic oscillators is the nature of their output response to the control signals. Figure 3.2 and Figure 3.5 shows the output differential curve versus the control differential pressure applied.

Note the difference between the output differential pressure behaviors with respect to the control differential pressure. In analog amplifiers, the output differential pressure is proportional to the control pressure supplied, while digital amplifiers have a rather consistent output differential pressure with little effect from supplied differential pressure. From Figure 3.5, one can clearly observe the effect of control differential pressure on the output of a digital amplifier. When the control differential pressure supplied reaches a maximum, the low pressure region produced by the entrainment of the fluid stream relocates to the opposite wall, resulting in a switch in the fluid stream; if the control pressure drops below this maximum (when the pressure difference is greater at the opposite side), the switching of the jet stream reoccurs and flips back to the original side.

The behavior of fluidic amplifier has a direct impact on the device selection for this research. An analog fluidic amplifier is the natural choice because the experiment required a continual variation in source signal, which implied that one must be able to increase and decrease the output signal by changing the differential pressure at the control ports. Therefore analog fluidic amplifier was selected as the controlling device and will be further analyzed.

## 4. VENTED AND NON-VENTED ANALOG FLUIDIC AMPLIFIERS

In the previous section, a total of five families of analog fluidic amplifier were identified, although they all followed the same operating principle, their field of application differs from one to another. Among these five candidates of analog fluidic amplifiers, the research further narrows down the focus to the vented and non-vented analog amplifiers. These analog amplifiers are selected due to the simplicity of structure and the nature of applications of this research.

Also in the previous section, the basic operating principle of vented analog fluidic oscillator was briefly described. The primary function of the venting mechanism of the analog amplifier is to reduce the loading effect of the amplifier so when the device is connected to a load (for example an actuator) the effect of the back pressure will not have a direct impact on the fluid jet interaction as it reflects into the interaction region and balanced out rapidly by the ambient pressure at the vents. Notice the difference in the geometry of the interaction volume between the vented and non-vented amplifiers (Figure 4.1 and Figure 4.2), the non-vented amplifier has a very different geometry compared to the vented jet-interaction amplifier.

### 4.1 *Operating Principle*

Due to the similarity of the two different types of analog jet-interaction amplifiers, their functionality and operating principle should be discussed separately so one can make a better judgment on the selection between the two analog jet-interaction am-

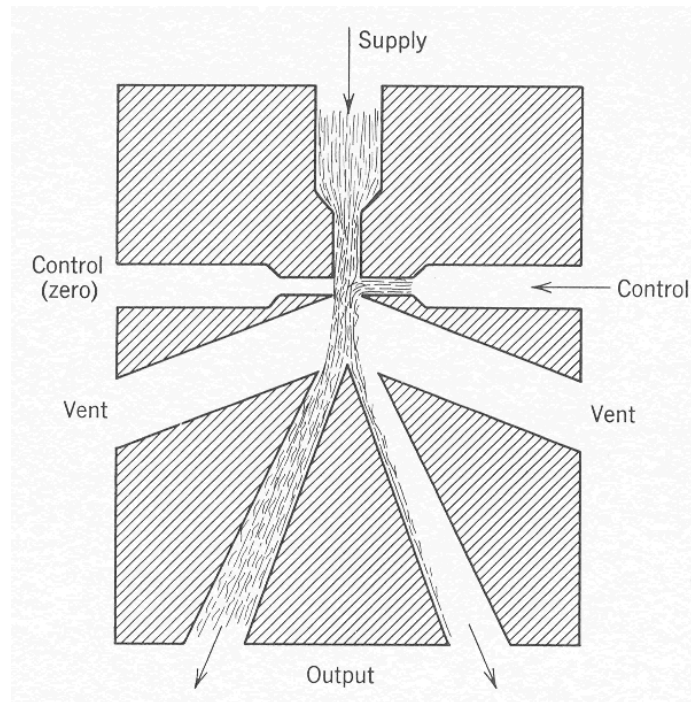


Fig. 4.1. Schematic of a vented analog fluidic amplifier [13].

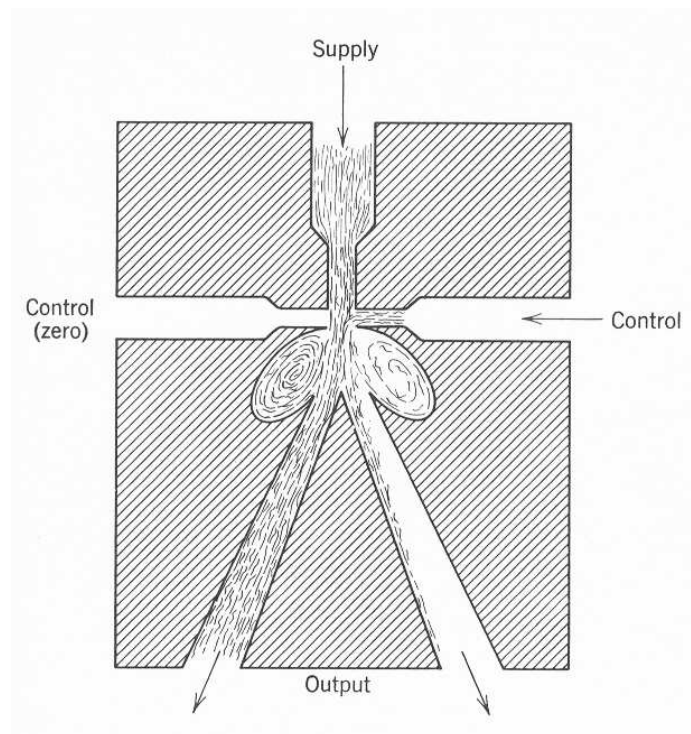


Fig. 4.2. Schematic of a non-vented analog fluidic amplifier [13].



plifiers.

#### 4.1.1 Vented Jet-Interaction Amplifier

The vented jet-interaction amplifier has the simplest configuration (Figure 4.1). A pressurized jet is applied to the inlet so that a high velocity fluid stream will pass through the supply port into the interaction region. Since the interaction region is vented, it will be maintained at an uniform pressure (same pressure as the ambient where the vent is exposed to). The high velocity, high pressure jet enters the interaction region and will be rapidly slowed down by the uniform pressure distribution within the interaction volume. The operating principle of the vented analog fluidic amplifier was previously described.

The vented jet-interaction amplifier will not experience any effect from the back pressure because the backpressure will be balanced out by the ambient pressure supplied from the vents. Therefore, if the ports are blocked due to external loading effect, the vent will provide an escape route for the incoming fluid jet and the deflection of supply jet will not be retarded.

There are several features of the vented jet-interaction amplifier when compared to other types of analog fluidic amplifiers:

1. High pressure gain.
2. Relative high frequency response (KHz)
3. Medium input and output impedance.
4. Medium noise to signal ratio.
5. Stable under most loads.

#### 4.1.2 Non-vented Amplifier

A basic schematic of the closed non-vented amplifier is shown in Figure 4.2. The operating principle of the non-vented amplifier is very similar with the vented jet-interaction amplifiers. The deflection of the power stream is proportional to the differential pressures applied at the control ports, therefore the differential output pressure is also proportional to the differential control pressure applied.

Since the non-vented amplifiers do not have vents, it does not have the ability to remove the back pressure produced at the exit ports. Therefore non-vented amplifiers are extremely sensitive to loading. When a load is applied at the exit ports (i.e., when the exit flow is restricted), the back pressure begins to build up at the exit ports and affect the pressure distribution at the interaction region, upsetting the pressure distribution of the whole device. If the restriction is high enough (when the exit ports are almost completely blocked) the difference in pressure between the inlet and the exit ports reduces to the minimum and the effect of the high velocity inlet jet becomes negligible, the amplifier then becomes ineffective.

The operating principles of the non-vented amplifier are very similar compared to the vented jet-interaction amplifier and it has identical advantages as the vented jet-interaction amplifier except that it is highly sensitive to loading. Judging from the application point of view, both vented and non-vented amplifiers are capable to fulfill the purpose of this research.

#### 4.1.3 Fluidic Oscillator

A fluidic oscillator is a device which utilizes the balance of momentum between three impinging jets, deflecting the main jet towards the region which a weaker force was introduced. It belongs to the family of fluidic amplifiers. Differing from fluidic amplifiers whose main purpose is to amplify the output signals, fluidic oscillators amplifies the feed-back signal as the signal travels back to the control ports.

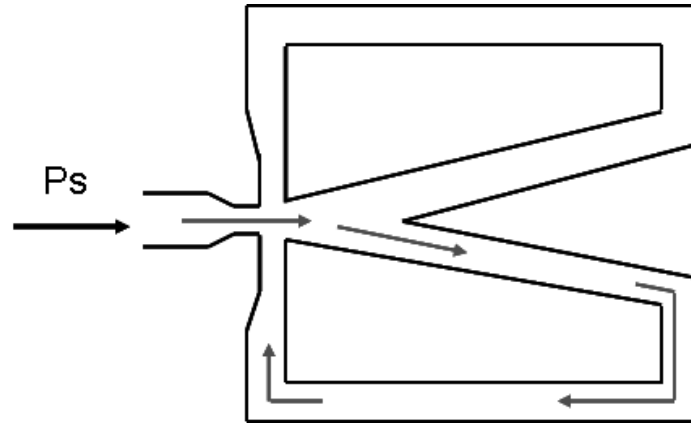


Fig. 4.3. Schematic of a non-vented oscillator.

The schematic of a simple fluidic oscillator is shown in Figure 4.3. The pressurized jet enters the oscillator through the supply port and enters the interaction region. If there is no differential pressure exists across the control ports, the flow will enter the interaction region undisturbed. The feed-back loop connects the exit ports to the control ports, creating a flow path for some of the exit flow to travel back into the control ports causing the main jet to deflect. Initially the majority of the load will exit through the exit ports, making the feed-back loops ineffective. However, when the exit flow becomes restricted (in the case of application of an external load) a back pressure will begin to build up, causing more flow to enter the feed-back loops. Eventually the magnitude of the momentum of the feed-back flow will be sufficient to cause a deflection of the main jet stream, forcing more flow into one of the exit ports. If the left exit port exhibits a higher flow, the increased momentum entering the left control port will causes a deflection of the main jet forcing more flow into the right exit leg. This perturbation in momentum balance between the two control ports will continue to deflect the supply jet, creating a pulsating flow down into the exit ports.

## 5. EXPERIMENTAL SETUP AND RESULTS

This research details the study of a fluidic oscillator for the eventual purpose of water droplet oscillation. The operating environment of the water droplet was reviewed, speed of the sound which travels down the square channel was precisely estimated, and measurement devices were carefully selected. Applicable alternative measurement devices (ear piece or microphone) were considered and its application to pressure wave measurement was considered. Methods for experimental setup and possible approaches were recommended, with some discussion of potential implementation problems provided. Recommendations for further improvements on the experimental setup and data acquisition system will be presented and considered for future implementation.

### *5.1 Experiment 1: GE Oscillator Testing - Single Feed-back Port*

A General Electric (GE) analog fluidic laboratory kit [15] was found in the inventory of Michigan Technological University. The purpose of the GE laboratory kit was to offer those who are unfamiliar with fluidic applications a guide to study the fluidic technology. It contains a variety of components which allows easy assembly of oscillators, frequency doublers, phase discriminators or beat-frequency detectors. Fluidic components are extremely robust and functions entirely on fluid jet interaction principles and consist of no moving parts. With a source of clean dry air and a few pieces of plastic tubing and fittings, one could easily assemble a fluidic device on a laboratory table.

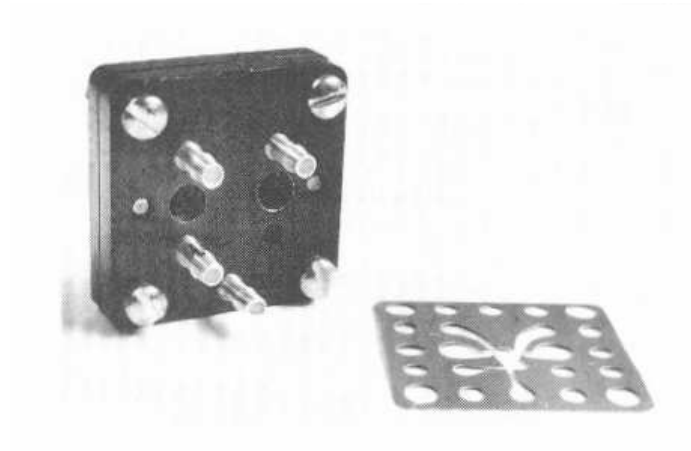


Fig. 5.1. GE proportional amplifier [15].

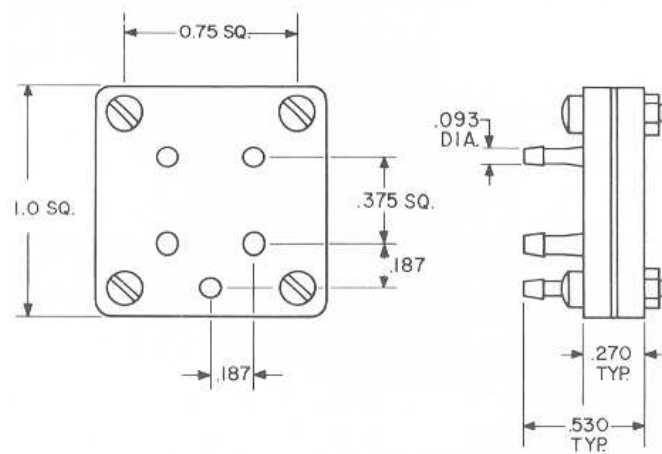


Fig. 5.2. GE proportional amplifier dimensions [15].

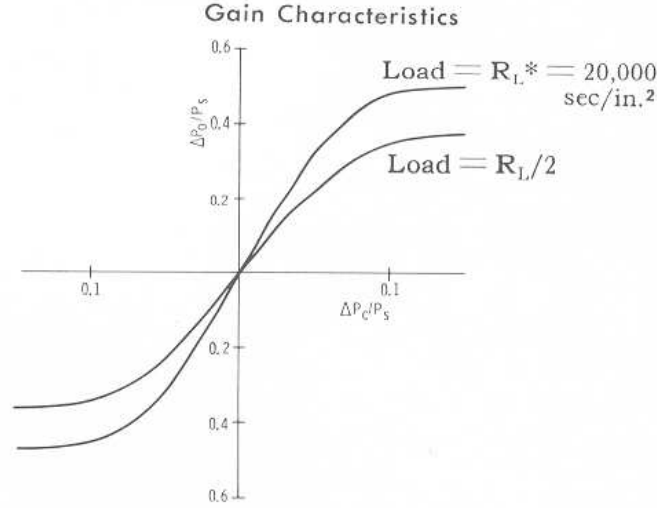


Fig. 5.3. GE proportional amplifier gain curve [15].

The instrument used to capture the frequency generated by the GE oscillator was an electromagnetic ear piece provided in the kit. The signal captured by the ear piece was recorded using an oscilloscope manufactured by Agilent Technologies (model 54621A). The recorded data was saved in a 3.5 inch floppy disk which allowed transfer of the data from the oscilloscope to a personal computer. The data recorded was in the time domain. In order to evaluate the frequency produced by the GE oscillator a code was written using digital signal processing (DSP) technique in Matlab to process the raw data (see Appendix C). The functionality of the GE proportional amplifier was tested to better understand fluidics.

The supply flow in this experiment was controlled by a flow meter manufactured by Gilmont<sup>®</sup> (model 8320) with flow range from 0 to 5 L/min. A GE oscillator was constructed following the setup instruction under Experiment No.5 in the manual [15]. The circuit diagram of the setup is shown in Figure 5.4. Where  $P_s$  indicates the supply pressure and air is used as a working fluid. Circuit oscillation is achieved by connecting the output ports (Line B) back into the input ports (Line A), so that when the jet is diverted to one output it produces an input at the control port on the same side. This deflects the jet to the opposite output port.

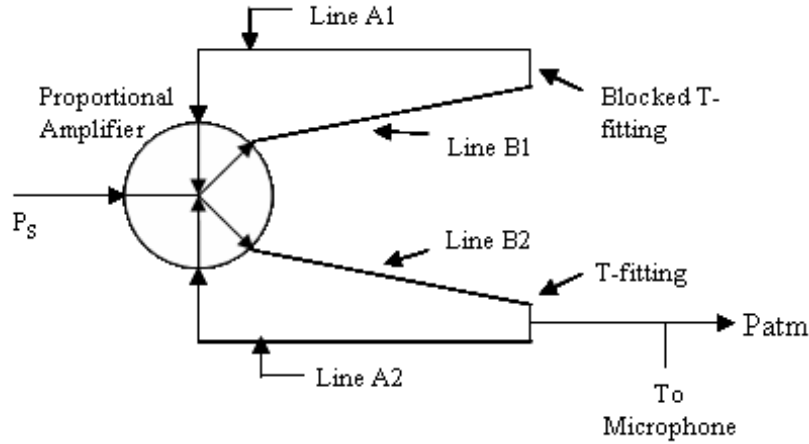


Fig. 5.4. Experimental schematic of a fluidic oscillator construction (using one GE proportional amplifier) following the setup instruction provided by the manufacturer.

Tab. 5.1. Frequencies produced at different feed-back length suggested by the manufacturer [15].

Test No.	Line A (inches)	Line B (inches)	Approximate Frequency (Hz)
1	30	2	180
2	16	2	300
3	8	2	480

Referring to the manual [15], the frequency of oscillation is determined by the propagation time of the pressure wave from the output ports to the input ports plus the delay time for the jet to switch. The frequency will vary with the line length (Line A + Line B) so the longer the feed-back line, the lower the frequency. The calibration chart of the GE oscillator's specification is shown in Table 5.1.

After the experiment was setup as shown in Figure 5.4, a fluid jet with fixed flow rate (5 L/min) enter the oscillator and begin to oscillate at a frequency. One of the feed-back ports was blocked while the other feed-back port was connected to the ear piece and the frequency produced by the oscillator was captured by the oscilloscope via the ear piece. Although a sinusoidal wave form was observed on the display window of the oscilloscope, it appeared noisy. When the air supply was turned off, a consistant 60 Hz frequency was captured by the ear piece. This is due to the poor

shielding of the connecting wire, which made the microphone extremely susceptible to ambient noises. An alternative transducer was necessary.

### 5.1.1 Microphones

Due to the poor shielding of the ear piece included in the GE analog fluidic oscillator kit, a better transducer was needed. A recommendation was made to use the ICP® microphones manufactured by PCB because of their availability. The ICP® microphone is a piezoelectric type of microphone. A piezoelectric microphone uses a quartz or manmade ceramic crystal structure. They produce a high charge output when exposed to external force where they exhibit a permanent polarization. Piezoelectrics exhibit long term stability and are ideal for low-noise measurements [16]. The ICP® microphones are very durable and capable to measure very high amplitude (decibels) pressure ranges. Conversely, the floor noise level on this type of microphone is generally very high but was not considered as an issue in this research. The selection of the right sensitivity range microphone can be carried out with the following calculations:

$$P = \frac{\text{Voltage}}{\text{Sensitivity}(\frac{mV}{Pa})} \quad (5.1)$$

Where P is pressure in Pascals (Pa) and Voltage is the preamps output peak voltage. Once the maximum pressure level that the microphone can sense at its peak voltage is found, it can then be converted to decibels(dB),

$$dB = 20 \log \frac{P}{P_o} \quad (5.2)$$

where P is the pressure in Pascals and  $P_o$  is the reference pressure (Constant = 0.00002 Pa).

Based on calculations above, the suitable microphone selected for the operating range was ICP® Array Microphone Model 130D20. It has a sensitivity range of



45mV per Pa and -26 dB at 1 KHz [16]. The calibration data sheet is attached and can be found in the Appendix. Although the microphones were pre-calibrated, additional calibration must be done before each experiment because the sensitivity of the microphone is a function of temperature and humidity.

### 5.1.2 *Calibration*

Four microphones were involved in the calibration task. The equipment used to calibrate the sensor was a CAL2000 shaker (produced by PCB) which generates a constant excitation of 94 dB at 1000 Hz. The calibration of the microphones were performed with Siglab®, Virtual Network Analyser (VNA) function was used and Bias coupling was selected in the settings, Bias coupling is a setting in Siglab® that provides power for the microphones, eliminating the requirement for additional signal conditioners. For the channels where the microphones were connected, a bandwidth of 2000 Hz (which imply a sampling frequency of 5120 Hz) was used. Also, Siglab® VCAP function was used to record data for longer period of time. Then, as post-processing to calculate the Fast Fourier Transform (FFT) of each signal, 20 flat-top windows with 50% of overlap were applied to data. Figure 5.5 shows the FFT results obtained for each channel. A consistent 1000 Hz frequency was observed, ensuring that the microphones were still calibrated.

### 5.1.3 *Experimental Results*

The connection line used on the GE fluidic devices were Tygon tubing. The Tygon tubing used in the setup has an inner diameter of 1/16 inches and the outer diameter of 1/8 inches, and the wall thickness was 1/32 inches. Polypropylene tubing was also used in the experiment. Quarter inch polypropylene tubing was used to direct the pressurized air from the compressor into the pressure supply port of the fluidic amplifier. The compressed air was filtered prior to entering the amplifier so blockage

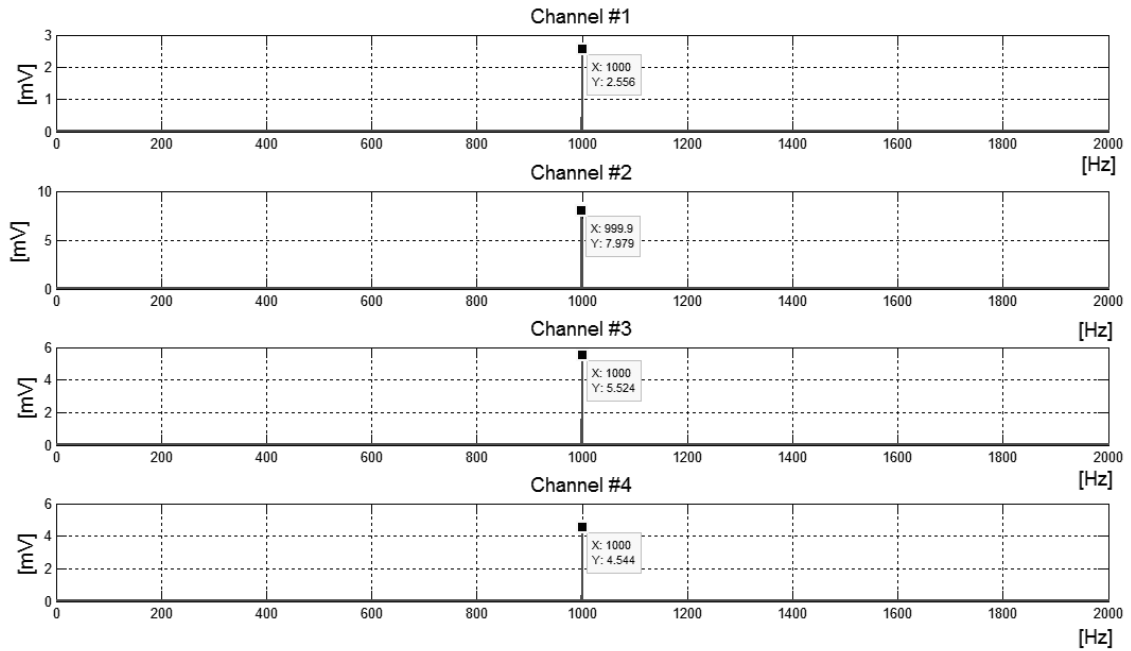


Fig. 5.5. FFT results of the calibration process.

of flow lines by foreign objects would be prevented. Tygon tubing was also used to connect exit ports (Line B) to the control ports (Line A). Tees were included to direct the oscillated flow from the feed-back line into the exit line where the microphone was located to capture the frequency of the pressure wave traveling down the tube.

The first test was performed with a Line A length of 30 inches and a Line B length of 2 inches. A sinusoidal wave form was observed on the oscilloscope and the data was processed with the FFT code written in Matlab. A frequency of 170.3 Hz was recorded. Identical experimental procedures were repeated for Test 2 and 3. The frequency produced when Line A was allowed to vary from 8 to 30 inches was recorded and shown in Figure 5.6. Test 1 indicates the result processed by Siglab® for 30 inches Line A length and Test 2 for 16 inches Line A length and Test 3 for 8 inches Line A length. The comparison of the frequency obtained from the experiment and the manufacturer's data is shown in Table 5.2.

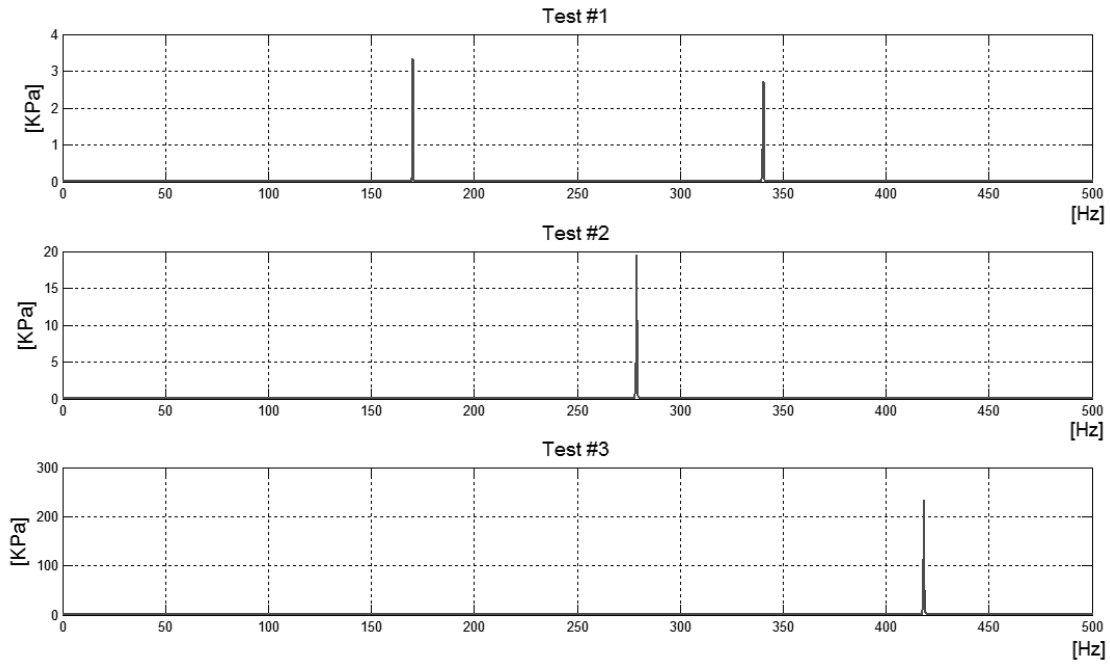


Fig. 5.6. Experimental result showing the frequency produced when Line A was varied from 8 to 30 inches and Line B remained at 2 inches.

Tab. 5.2. Comparison between the results obtained from the experiment and the manufacturer's recommended value.

Test No.	Line A Length (inches)	Suggested (Hz)	Measured (Hz)	Error (%)
1	30	180	170.3	5.3
2	16	300	278.8	7
3	8	480	441	8.1

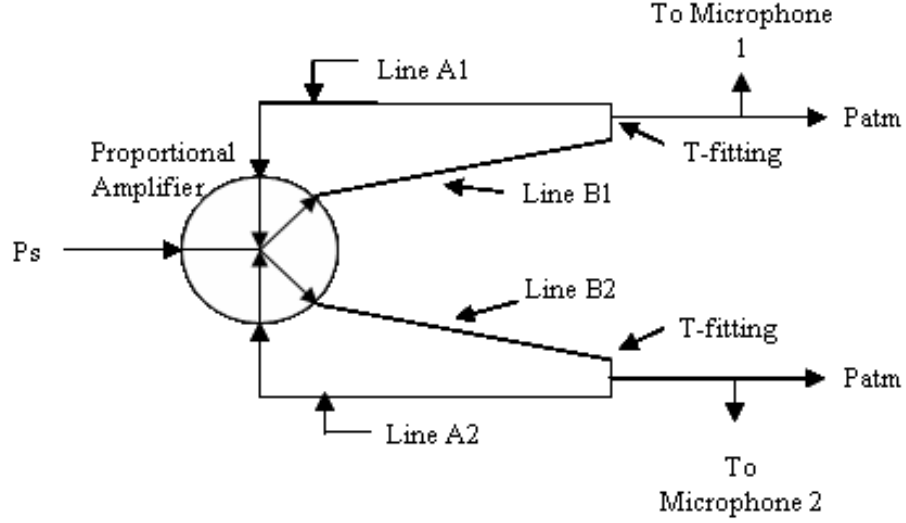


Fig. 5.7. Experimental schematic of a GE fluidic oscillator setup with both output ports exposed to atmospheric.

## 5.2 Single Exit Venting - With Varying Supply Flow Rates

The first sets of experiments studied the effect of feed-back port length on the frequency produced by the GE oscillator and also acted as a pseudo-calibration task for the oscillators. In the setup instruction of Experiment No.5, the manufacturer suggested venting one exit port while the other remained blocked [15]. The second GE oscillator testing was setup by venting both of the feed-back ports to study the frequency produced by the oscillator. In this experiment, an identical parameters were used except both of the T-fittings (Figure 5.7) were connected to two different transducers. Two different Line A length were used, first is 14.5 inches and the second is 16 inches. The supply flow rate was allowed to vary from 1 L/min to 5 L/min.

### 5.2.1 Data Processing

Although Siglab<sup>®</sup> is a very powerful data acquisition tool, it was not compatible with the data acquisition system available. Therefore an alternative data acquisition system was considered. When the PCB microphones were used with Siglab<sup>®</sup>, additional power source was not required due to the 'Bias' function which was embedded in

the Siglab<sup>®</sup> system. The data acquisition system which was compatible with the PC used for data processing was the National Instrument model SC-2345 (Figure 5.8) data acquisition system. The SC-2345 is equipped with configurable connectors which accepts custom I/O connector panellettes for direct signal/sensor connectivity. These enclosures for SCC (Signal Conditioning) modules connect directly to the DAQ devices. This system can connect up to 20 SCC modules which is more than sufficient for these experiments. The NI-DAQ allows the operator to directly communicate with the system via Labview, which was pre-installed and synchronized with the PC to carry out most of the data recording. The ICP<sup>®</sup> microphones connected to the NI-DAQ were powered by two PCB signal conditioners (Model 482A16) which outputs a range of  $2 \sim 20$  mA current which will be received by the data acquisition system. The output of the signal conditioner in the setup was teed thus identical signal can also be processed by the Agilent oscilloscope (Model 54621A) simultaneously.

The oscilloscope converts the signal and displays where the operator can easily identify what is physically happening in the channel immediately without having to process the data with Labview. The oscilloscope also provides the operator with powerful signal manipulating functions. The sampling frequency of the signal can also be modified by altering the time base control on the oscilloscope. The second BNC cables that exit through the tee of the signal conditioner was connected to NI-DAQ. A junction was used between the tee and the NI-DAQ to ensure the quality of the BNC cable. Therefore for compatibility reason, NI-DAQ was used as the primary data acquisition device for data processing.

### 5.2.2 *Experimental Results*

All the data captured was processed with the FFT code written in Matlab. The results obtained from this experiment are shown in Table 5.3 and 5.4 respectively. This test not only studied the effect of feed-back port length on the overall frequency



Fig. 5.8. NI-DAQ, Model SC-2345 [17].

and also the oscillator's response to supply flow rate. Referring to Figure 5.9, one can clearly notice two behaviors. First, at 16.5 inches, the frequency response produced by the oscillator is clearly higher than the frequency response produced when the feed-back length is at 18 inches, proving that frequency increases with increasing feed-back length. Second, as the supply flow rate increases, the frequency was observed to increase as well. This behavior makes sense because increasing the supply flow induces a higher moment flux rate into the control ports. Since only one feed-back port was allowed to vent to the atmosphere, as the rate of input increases, the resultant frequency is expected to increase accordingly.

### 5.3 Experiment 2: GE Oscillator Testing - Both Exit Vented

From the previous tests, the functionality of this 40 year old proportional amplifier was demonstrated. The results obtained were within 10% difference from the manufacturer's data and the frequency of the oscillator with response to different feed-back port length was identified.

The second experiment of single GE amplifier testing was involved with both feed-back loops teed and exposed to atmosphere. Two microphones were used in this case

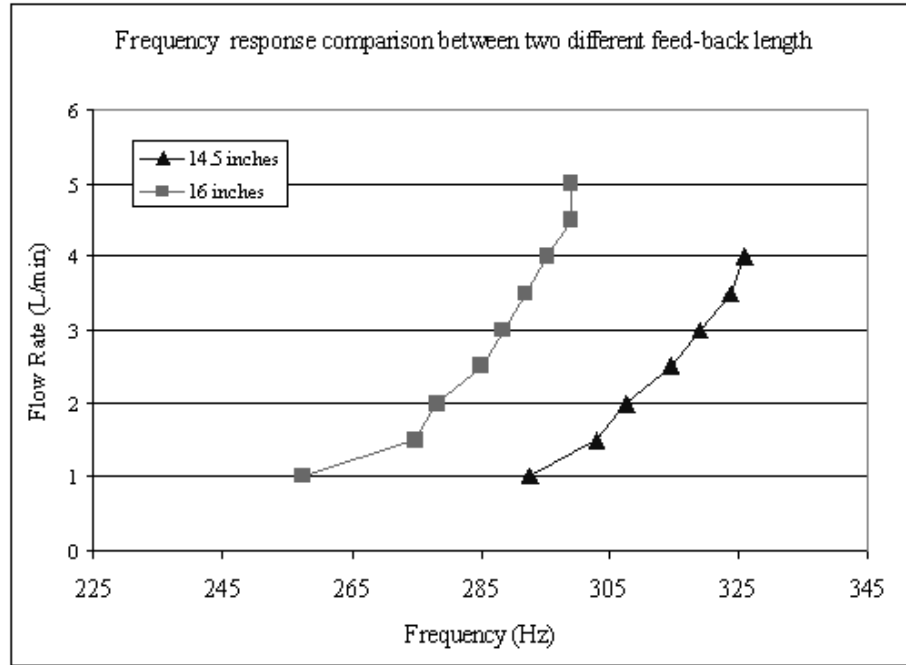


Fig. 5.9. Frequency comparison between 16.5 and 18 inches feed-back length produced by the same oscillator.

Tab. 5.3. Frequencies produced at different supply flow rate with feed-back length fixed at 16.5 inches (one feed-back port blocked).

Flow Rate (L/min)	Frequency (Hz)
1.0	257.4885
1.5	274.7696
2.0	278.2258
2.5	285.1382
3.0	288.5945
3.5	292.0507
4.0	295.5069
4.5	298.9631
5.0	298.9631

Tab. 5.4. Frequencies produced at different supply flow rate with feed-back length fixed at 18 inches (one feed-back port blocked).

Flow Rate (L/min)	Frequency (Hz)
1.0	292.6267
1.5	302.9954
2.0	307.6037
2.5	314.5161
3.0	319.1244
3.5	323.7327
4.0	326.0369

Tab. 5.5. Frequencies produced at different supply flow rate with feed-back length fixed at 18 inches with both ports exhausting.

Flow Rate (L/min)	Frequency of Left loop (Hz)	Frequency of Right loop (Hz)
1.0	247.1198	243.6636
1.5	264.4009	264.4009
2.0	271.3134	271.3134
2.5	274.7696	274.7696
3.0	278.2258	278.2258
3.5	281.682	281.682
4.0	281.682	281.682

to capture the frequency produced at both the feed-back loops. The results were recorded by Labview and processed with the FFT code in Matlab. Table 5.5 to Table 5.8 summarized the results obtained when different feed-back port lengths were used.

From the results, the frequency appeared to be identical between the left feed-back loop and the right feed-back loop (Table 5.5 to Table 5.8). This observation indicates two important clues toward oscillator implementation. First, one of the feed-back ports does not necessarily have to remain blocked in order for the oscillator to function accurately. Second, cascading approach is definitely possible for a single oscillator to control two or more oscillators.

Before approaching the cascading setup, further observations were identified in



Tab. 5.6. Frequencies produced at different supply flow rate with feed-back length fixed at 20 inches with both ports exhausting.

Flow Rate (L/min)	Frequency of Left loop (Hz)	Frequency of Right loop (Hz)
1.0	202.1889	202.1889
1.5	222.9263	222.9263
2.0	229.8387	229.8387
2.5	236.7512	236.7512
3.0	243.6636	243.6636
3.5	243.6636	243.6636
4.0	247.1198	247.1198

Tab. 5.7. Frequencies produced at different supply flow rate with feed-back length fixed at 22 inches with both ports exhausting.

Flow Rate (L/min)	Frequency of Left loop (Hz)	Frequency of Right loop (Hz)
1.0	184.9078	184.9078
1.5	205.6452	205.6452
2.0	212.5576	212.5576
2.5	219.47	219.47
3.0	222.9263	222.9263
3.5	226.3825	226.3825
4.0	226.3825	226.3825

Tab. 5.8. Frequencies produced at different supply flow rate with feed-back length fixed at 32 inches with both ports exhausting.

Flow Rate (L/min)	Frequency of Left loop (Hz)	Frequency of Right loop (Hz)
1.0	143.4332	143.4332
1.5	153.8018	153.8018
2.0	157.2581	157.2581
2.5	160.7143	160.7143
3.0	164.1705	164.1705
3.5	167.6267	167.6267
4.0	167.6267	167.6267

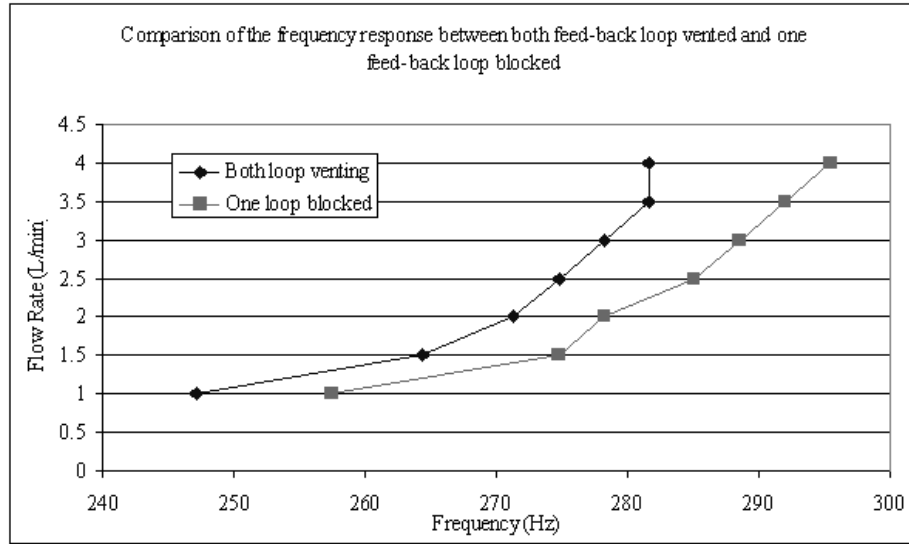


Fig. 5.10. Comparison of the frequency produced by the oscillators, one with both feed-back port oscillating and one with only one feed-back port oscillating.

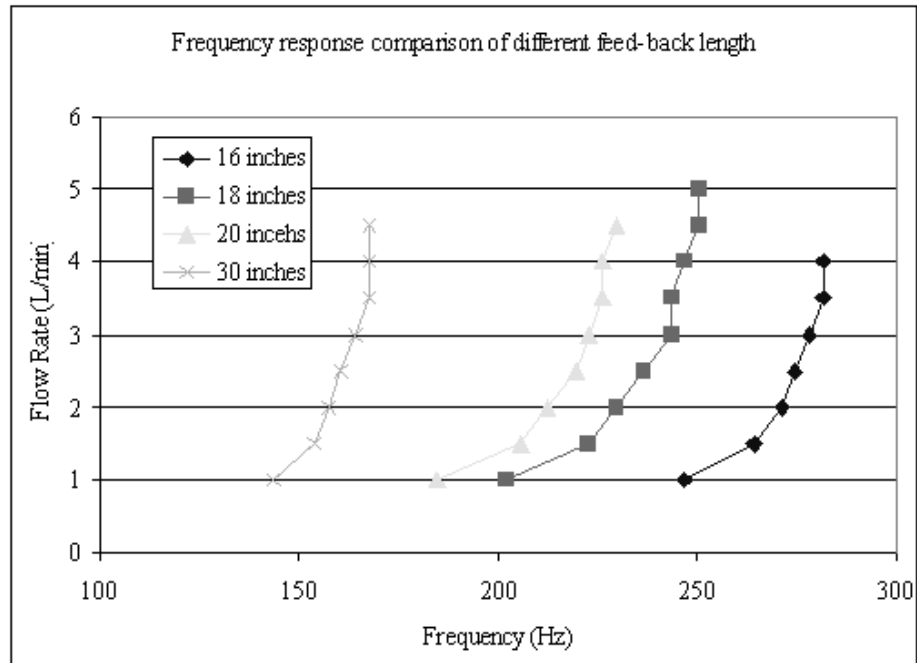


Fig. 5.11. Frequency observation with variable supply flow rate and variable feed-back length (both feed-back ports vented).

the results between single loop oscillation and double loop oscillation. Referring to Figure 5.10, the difference between the two scenarios was presented. The oscillator which was setup with both feed-back loops venting to atmosphere produces a lower frequency compared to the other. With the venting mechanism of the second loop, there is a greater pressure difference between the control ports and the exit ports, more air was allowed to pass into the ambient thus resulting in an increase in pressure recovery at the exit ports. With a greater pressure recovery, the momentum flux at the control ports was expected to increase thus a greater momentum was available to deflect the supply jet, results in a decrease in frequency.

Another similar pattern observed was that as the flow rate increases, the frequency increases accordingly (Figure 5.11) and the longer the feed-back length, the lower the frequency observed. Notice at the flow rate of approximately 4 L/min, the frequency produced by the oscillator began to remain constant. This is because at 4 L/min, the receiver ports has attained the maximum air uptake therefore any increase in supply flow will exit through the side vents. These results matched the behavior observed in the previous setup. Therefore it is safe to conclude that the higher the supply flow, the higher the frequency produced by the oscillator; the longer the feed-back length, the lower the frequency expected.

### 5.4 *Experiment 3: Cascading of GE Oscillators*

This set of experiments used one analog fluidic oscillator (Element 1) to control an identical analog proportional amplifier (Element 2). This network of oscillators is referred to as a cascading orientation. The components used for this setup were:

1. Two Proportional Amplifiers
2. Standard T-fittings
3. Gilmont Flow Meter (0 ~ 5 Liter per Minute)

#### 4. Transducers (2 microphones)

The purpose of this experiment was to test the controllability of the GE oscillators by simultaneously pulsate the flow down two different channels using the first oscillator as a control. The first task in this experiment is to prove that the resultant frequency exiting Element 2 is identical to the frequency produced by Element 1, since the purpose of Element 2 is only amplifying the frequency produced by Element 1 (Element 2 play no part in modulating the frequency produced by Element 1). The experimental schematic is shown in Figure 5.12. Identical flow rates were supplied to both Element 1 and 2.

The purpose of cascading setup is to reduce the load on the control oscillator. In a fuel cell application, each cell stack contains multiple serpentine flow channels on both side of the bipolar plates. If a single oscillator is expected to power the entire fuel cell, the loading effect on the oscillator may be too large to promote any useful oscillation (most of the supply air will pass through the vents). Therefore cascading network of the oscillators became an interest in this research.

The first test was setup using a feed-back length of approximately 16 inches for Element 1 and the left output was connected to the left control port of Element 2 and the right output of Element 1 was connected to the right control port of Element 2. The length of the connecting tubing was 4 inches. Table 5.9 presented the results obtained from this setup. From the results obtained, one can clearly observed the similarity between the frequency recorded by Microphone 1 and Microphone 2 (Table 5.9). A steady increase in frequency (from 271 Hz to 305 Hz) was observed when the supplying flow rate was increased from 1 L/min to 4 L/min. At the exit of Element 2 the exact same frequency was recorded. Note that each of the experiments performed above were repeated three times to demonstrate repeatability and ensure accuracy of the results.

Tab. 5.9. Results of the cascading setup with 16 inches Element 1 feed-back port length.

Flow Rate (L/min)	Microphone 1 (Hz)	Microphone 2 (Hz)
1.0	270.7373	270.7373
1.5	293.7788	293.7788
2.0	301.8433	301.8433
2.5	305.2995	305.2995
3.0	305.2995	305.2995
3.5	305.2995	305.2995
4.0	305.2995	305.2995

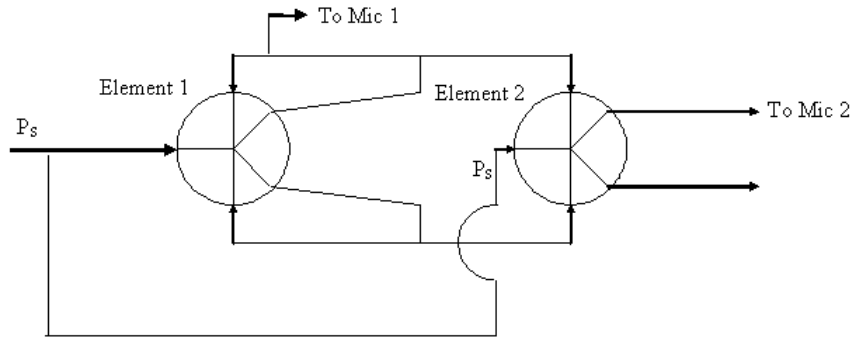


Fig. 5.12. Experimental schematic of two GE fluidic oscillator setup in the cascading orientation.

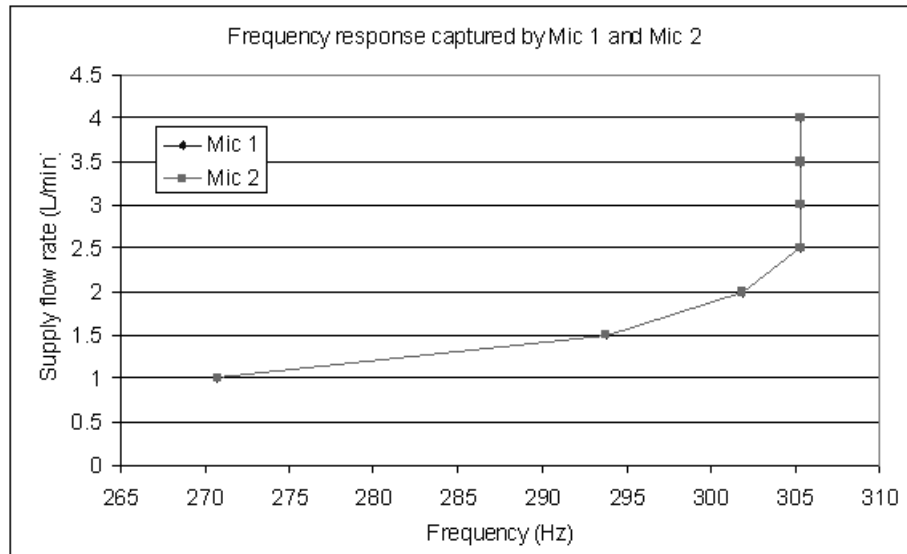


Fig. 5.13. Frequency comparison between Element 1 and Element 2.

The purpose for multiple oscillator control in this research is to reduce the loading on a single oscillator (as mentioned previously). Back-pressure buildup at the exits port may inherently upset the normal oscillating regime of the device. Therefore when a single oscillator was used to control multiple oscillators simultaneously, the loading on the control oscillator was distributed among the amplifiers it is connected to. Also by connecting the fluidic amplifiers in such orientation, simultaneous pulsation down numerous parallel channels can be achieved.

The second task in cascading oscillator network was to use one oscillator to control two other identical oscillators. Unfortunately only two analog proportional amplifiers provided in the GE analog fluidic laboratory kit. Therefore, a third oscillator had to be constructed.

### 5.5 *Analog Fluidic Oscillator Design*

The proportional fluidic amplifiers purchased from General Electric back in the 1960s is no longer available on the market, therefore it is impossible to purchase an identical device. The keys to successfully designed a fluidic device are thorough understanding of the basic principles of the operation, sufficient background in fluid mechanics and experiences gained from GE oscillator testing. The following sections describe the processes and steps taken to achieve the working final model.

In a beam-deflection device such as the proportional amplifier, the directions in which the high-energy jet will travel depend heavily on the resultant momentum flux from the control port jets. The control jets apply pressure forces, momentum flux forces, and sometimes a combination of both. The type of force exerted depends on the position of the control jets and also the size of the control jets.

As the jet leaves the power nozzle, the shape of its velocity profile is approximately Gaussian<sup>1</sup>. At some distance away downstream the flow is divided into two outputs.

---

<sup>1</sup> The profile of the velocity broadens and the velocity in center-line decrease as it moves down-

In most of the proportional amplifiers there are only two output ports symmetrically placed. However the design may differ from one to another. For example, some designers suggested including a center vent between the output legs to reduce the internal noise formation while others do not pursue this approach. Based on the requirement of the design, there is an optimum size and position for the output ports to be placed. The output ports must be placed far enough downstream to receive the deflection of the non-uniform velocity jet and at the same time has to be close enough to recover enough momentum for feed-back deflection.

In order to judge how well a proportional amplifier is designed, four possible gains are usually calculated for fulfill the purpose [14]. They are the flow gain ( $G_Q$ ), pressure gain ( $G_P$ ), momentum gain ( $G_M$ ) and power gain ( $G_{\text{Power}}$ ). Each of these gains represents the change in output relative to the change in control input. The flow gain can be calculated with the equation:

$$G_Q = \frac{\Delta Q_o}{\Delta Q_c} \quad (5.3)$$

Where  $\Delta Q_o$  is the total flow difference between the output ports and  $\Delta Q_c$  is the total flow difference across the control ports. The pressure gain can be calculated in a similiar fashion:

$$G_P = \frac{\Delta P_o}{\Delta P_c} \quad (5.4)$$

Where  $\Delta P_o$  is the total pressure difference between the output ports and  $\Delta P_c$  is the total pressure difference across the control ports. The momentum gain is defined as:

$$G_M = \frac{\Delta M_o}{\Delta M_c} \quad (5.5)$$

Where  $\Delta M_o$  is the total momentum difference between the output ports and  $\Delta M_c$

---

stream

is the total momentum difference across the control ports. Momentum flux can be calculated by  $M = \dot{m}u$ , where  $\dot{m}$  is the mass flow rate and  $u$  is the velocity of the fluid. The power gain is calculated by:

$$G_{\text{Power}} = \frac{\Delta(P_{Lo}Q_{Lo} - P_{Ro}Q_{Ro})}{\Delta(P_{Rc}Q_{Rc} - P_{Lc}Q_{Lc})} \quad (5.6)$$

Where  $P_{Lo}$  is the total pressure recovered at the left output port,  $P_{Ro}$  is the total pressure recovered at the right output port,  $P_{Rc}$  is the total pressure recovered at the right control port,  $P_{Lc}$  is the total pressure recovered at the left control port,  $Q_{Lo}$  is the total flow recovered at the left output port,  $Q_{Ro}$  is the total flow recovered at the right output port,  $Q_{Rc}$  is the total flow recovered at the right control port, and  $Q_{Lc}$  is the total flow recovered at the left control port.

The equations above can be used to characterize the performance of the proportional amplifier. The output flow rate can be specifically designed by selecting an initial mass flow rate with a flow gain predefined. The same approach could be achieved for pressure and momentum flux. In a fluidic oscillator design, the goal is to achieve a maximum pressure or momentum recovery at the exit ports so that the feed-back flow into the control ports is sufficient to cause a deflection in the main fluid jet. Therefore, other than flow gain, pressure gain or momentum gain, additional parameters must also be included in order to optimize the momentum/pressure recovery. Parameter such as the splitter length (length between the exits of the jet nozzle to the position of the splitter), the width of the exit ports, the angle of deflection,  $\theta$ , the pressure profile at the entrance to the exit ports, and the load of the oscillator play an important role in the oscillator design.

### 5.5.1 Deflection Angle

The first oscillator design was inspired by the research done by C.M. Crane [18]. In his work, the geometry and characteristics of a proportional fluidic amplifier was



studied. The first portion of his research involved a trial-and-error approach to obtain an optimum geometry for the amplifier design. The second portion of his research was the study of jet behavior to determine the optimal conditions. Experimental work was done on models of the element and method of converting model data to form a working device was also presented in his research.

The angle of deflection calculation was done by performing a momentum balance between the three impinging jets. First let the momentum of the supply jet stream to be  $M_S u_S$  from the nozzle exit with width  $w_S$ , and let the momentum of one side of the control ports to be  $M_C u_C$  and width of the control ports to be  $w_C$  (identical for both control ports). When this two fluid jet interact with one another, the angle of deflection is represented by:

$$\tan \theta = \frac{M_C u_C}{M_S u_S} \quad (5.7)$$

This equation is a basic equation obtained after simplifying the momentum balance between two impinging jets. In the work performed by E.M. Dexter [19] the simple equation was further expanded to:

$$\tan \theta = \frac{w_C P_C}{w_S P_S} \quad (5.8)$$

Based on the two simple equations suggested by Dexter [19], impinging interaction of three jets (supply, left control port, and right control port) can be presented by:

$$\tan \theta = \frac{w_C (P_{CL} - P_{CR})}{w_S P_S} \quad (5.9)$$

Where  $P_{CL}$  denotes the left control port pressure and  $P_{CR}$  indicates the right control port pressure. A simple control volume analysis was performed and the equations above was varified by hand calculation. Using the equations presented above, the designer will be capable to estimate the angle of deflection  $\theta$  by changing the

magnitude of the supply pressure or the cross sectional area of the control ports.

C.M. Crane [18] also suggested the implementation of a center vent, however by doing so a lower pressure difference will be generated between the exit port and the control port, causing a decrease in pressure recovery at the exit ports. With the implimentation of the center vent, most of the flow will travel through the center vent out to the ambient and the pressure required at the control ports to deflect the jet will have to be much greater. The different between the frequency of the oscillator with and without the center vent will be elaborated further in the Results and Discussion section. For consistency purposes, the center vent was included in the preliminary design.

The selected material for oscillator fabrication was plexiglass, because of its ease of manufacturing and the raw material cost is relatively cheap. Most importantly it is ideal for visualization study because it is transparent, and color dyes can be used to capture the direction of fluid flow if necessary.

After a series of experiments performed by Crane, optimum geometry parameters were developed and it is shown in Table 5.10. These parameters is referred to Figure 5.14 which is the amplifier model designed by Crane. In his drawing the width of the exit nozzle was denoted by  $w_P$  which was identical to  $w_S$  used in the formulas above.

### 5.5.2 *Oscillator Design*

The first design of the oscillator followed the design parameters suggested by Carne [18], the actual design is show in Figure 5.15. However the oscillator did not function as expected; no obvious oscillation of the fluid jet was observed when the output was connected to a transducer, only random noise was observed. The problems with Design 1 were identified as follow:

1. Poor finish. Top and bottom plates of the plexiglass were ‘glued’ together (using acrylic weld), excess glue mass seeped through the gaps and began to fill up the

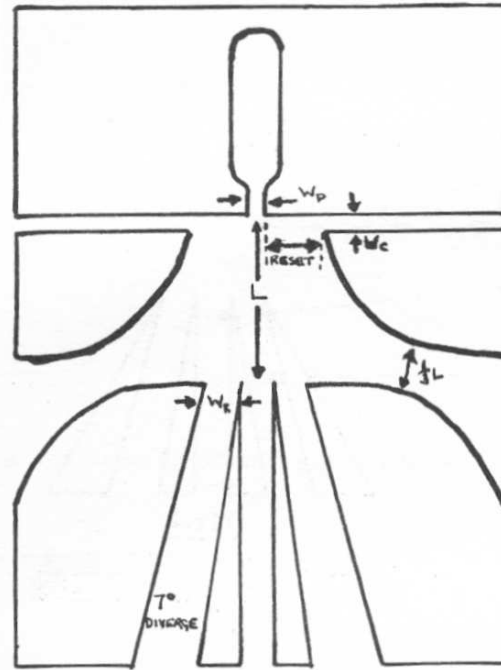


Fig. 5.14. C.M. Crane's Oscillator Design [18].

Tab. 5.10. Model optimal dimensions determined by experiment related to power nozzle width  $w_S$  (Carne [18]).

Detail	Output Port	Output Ports with Center vent included
Width of Control Port ( $w_C$ )	$2.5w_S$	$2.5w_S$
Distance of Splitter from Power Nozzle	$10w_S$	$10w_S$
Width of Output Ports ( $w_O$ )	$2w_S$	$2w_S$
Divergent Angle of the jet ( $\theta$ )	7 degrees	7 degrees
Length of Output Ports	$20w_S$	$20w_S$
Width of Center Vent	0	$2w_S$
Aspect Ratio	3	3
Reset	$0.5w_S$	$0.5w_S$
Length of Orifice Throat	$2w_S$	$2w_S$

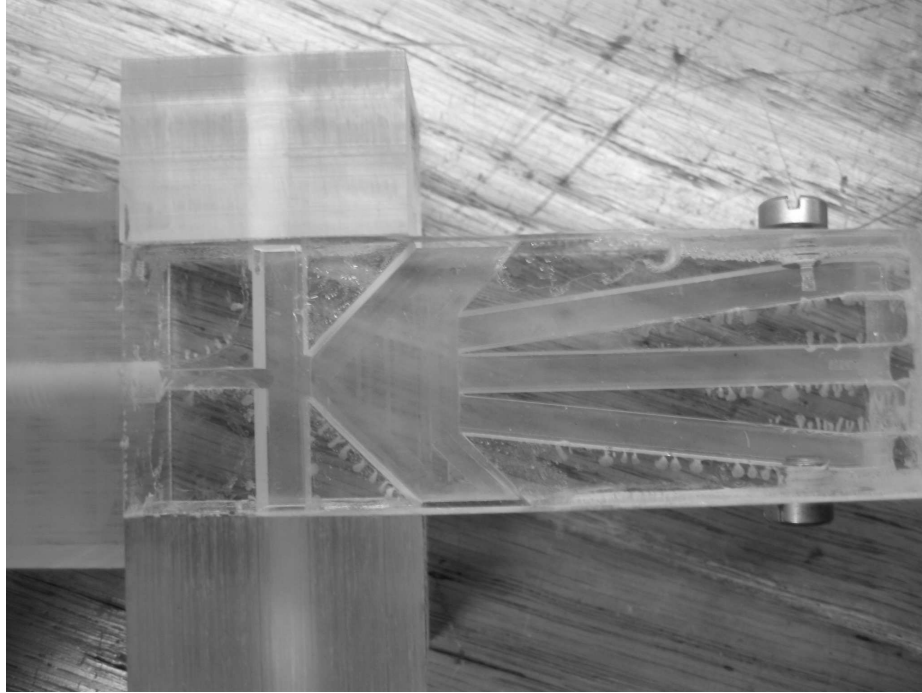


Fig. 5.15. Fluidic oscillator design (Design 1).

corners of the flow passages.

2. Tapping of the connectors were not properly designed prior to fabrication, leaving insufficient room for installation of additional parts (connectors, fittings, etc)
3. Nozzle geometry was not implemented, therefore causing insufficient acceleration of the supplying jet.
4. Majority of the fluid jet exit through the center vent, resulting in insufficient pressure recovery at the exit ports.

After the problems with Design 1 were identified, Design 2 eliminated the possible problems listed above. The inlet geometry was redesigned, the width of the throat  $w_s$  was kept unchanged at 2 mm and a nozzle geometry was implemented. The center vent was shortened to 14 mm instead of 72 mm used in Design 1 and tapped at the exit (so a study of the center venting effect can be performed). The fluid was introduced

vertically (instead of a horizontal inlet shown in Figure 5.15) to eliminate the problem of insufficient space. More room was available for thread tapping so acrylic weld is no longer necessary. The top and the bottom plates were bolted together so the problem with excessive glue blocking the flow channel was successfully removed. The control port geometry was redesigned as well. Instead of a uniform insertion, a nozzle type of control port geometry was implemented. This geometry allows the feed-back momentum to increase as the flow velocity increases. The width of the control port, the distance of the splitter position, the width and length of the output ports were kept untouched except that the aspect ratio<sup>2</sup> was changed from 1:3 to 1:1.

During the test of Design 2, the inlet flow was allowed to increase from 0 to 5 L/min. No apparent oscillation of the jet stream was observed at low flow rates but as the flow rate exceeded 5 L/min (off the scale of the flow meter) a small trace of oscillation was observed. Calculations were carried out based on the geometry of Design 2. In the calculation, venting became a problem because it is difficult to estimate the quantity of air exiting through the vents at a finite amount of time. Therefore an idealized calculation was carried out with non-vented geometry for maximum pressure recovery estimation and a conclusion was made on the control port design. Based on the calculation, greater momentum is required between the control port and the exit ports, therefore the geometry of the control port in Design 2 required to be redesigned.

## 5.6 *Experiment 4: Design 4 Testing*

In Design 4 (Figure 5.16), the control port width was changed from 5 mm to 2 mm. The remaining geometry of the oscillator was remained unchanged. An improved result was observed at higher flow rates but at lower flow rates, oscillation of the jet stream was still not observable. The air supply control method was changed from flow control to pressure controlled (flow meter was replaced with pressure gage) to

---

<sup>2</sup> The ratio of width to depth.

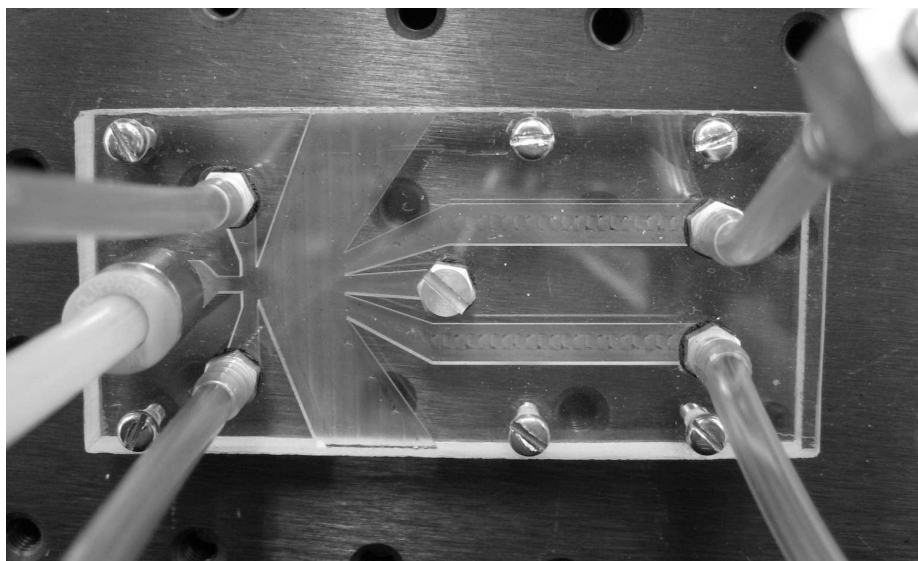


Fig. 5.16. Fluidic oscillator design (Design 4).

allow more flow to pass through the oscillator.

A series of tests were carried out to characterize its frequency. Similar tests which were performed on the GE oscillators were carried out on Design 4. The first experiment performed was a test setup with both feed-back ports vented to atmospheric. A flow meter was used as flow supply and the frequencies were recorded and processed.

The first test was setup identical to the GE oscillator experiment for dual feed-back port oscillation. A flow meter was used as an input for supplying airflow into Design 4, the feed-back length was fixed at 10 inches and the flow rate was allowed to change from 1 to 5 L/min. However, no apparent oscillation was observed after the signal captured was processed with the FFT code. Evaluating the geometry difference between the GE oscillators and Design 4 (feed-back port cross sectional area difference), there was an insufficient momentum flux down the exit ports of Design 4 even when the supply flow was increased to a maximum of 5 L/min. When the flow meter was connected in series with the pressure gage, at 5 L/min flow rate the pressure gage only reads approximately 0.45 psig. Thus the method of flow supply

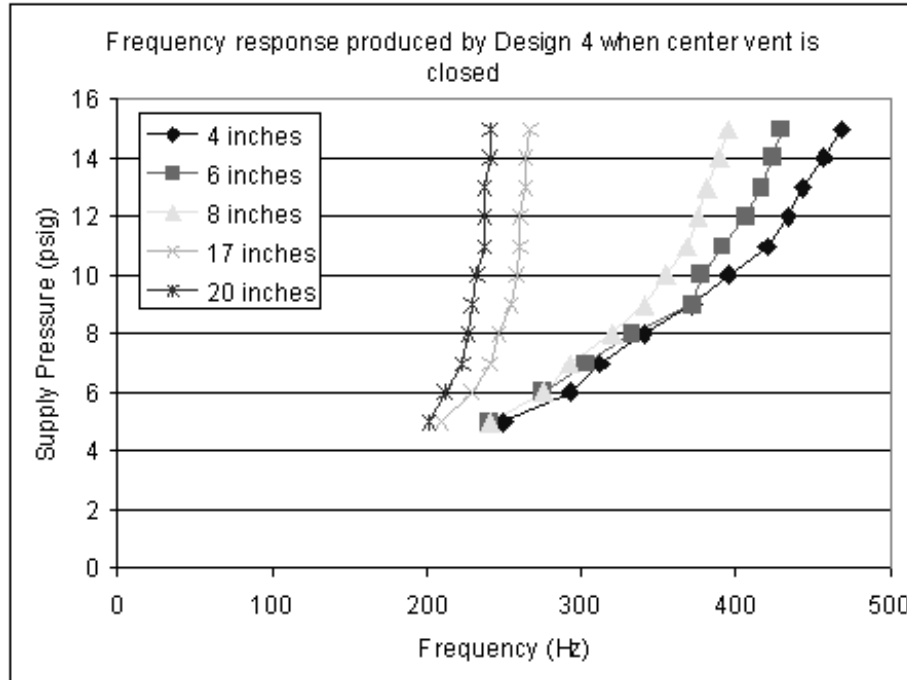


Fig. 5.17. Frequency produced by Design 4 when the feed-back length was varied between 4 to 20 inches and the supply pressure was varied between 5 to 15 psig (center vent closed).

was switched from flow meter to pressure gage. A pressure gage with a needle valve attached was used to regulate the supply pressure from 1 to 15 psig.

An oscillation pattern was observed when the supply pressure was increased to 6 psig. The frequency produced by Design 4 was observed to be at 292 Hz when the feed-back length was fixed at 4 inches and the center vent was closed. The experiment was carried out with varying supply pressure and the results are shown in Table 5.11.

Figure 5.17 shows Design 4 has a similar behavior to that of the GE oscillators. The frequency increases as the input pressure increases and as the feed-back length increases the frequency decreases. The frequency produced when a 20 inches feed-back length was used was significantly lower than the frequency produced when a 4 inches feed-back length was used.

Tab. 5.11. Results of the frequency produced by Design 4 with varying supply pressure and feed-back length (center vent closed).

Supply Pressure (psig)	4 inches	6 inches	8 inches	17 inches	20 inches
5	250.576	240.2074	240.2074	209.1014	202.1889
6	292.0507	274.7696	274.7696	229.8387	212.5576
7	312.788	302.4194	292.0507	240.2074	222.9263
8	340.4378	333.5253	319.7005	247.1198	226.3825
9	371.5438	371.5438	340.4378	254.0323	229.8387
10	395.7373	378.4562	354.2627	257.4885	233.2949
11	419.9309	392.2811	368.0876	260.9447	236.7512
12	433.7558	406.106	375	260.9447	236.7512
13	444.1244	416.4747	381.9124	264.4009	236.7512
14	457.9493	423.3871	388.8249	264.4009	240.2074
15	468.318	430.2995	395.7373	267.8571	240.2074

### 5.6.1 Center Venting Approach

In these tests the center vent was open to the atmosphere and the testing procedure was identical to the previous experiment, where the feed-back length (dual port oscillation) was allowed to change from 4 inches to 20 inches and the supply pressure was allowed to vary from 7 to 15 psig (Table 5.12).

Comparison of the frequency produced with center venting and non-center venting and is presented in Figure 5.19 to Figure 5.23. The non-venting approach produced a higher frequency. Center venting promotes a greater momentum recovery at the exit ports compared to non-center venting because most of the excess air exits through the center vent instead of the side vents. Therefore, there is an increase in momentum recovery at the exit ports which induces a greater momentum flux at the control ports, resulting in a larger angle of deflection.

From the experiments conducted above, the fluid jet behavior of Design 4 exhibits an identical response to feed-back port length and supply pressure as the GE oscillators. An obvious oscillation of the fluid jet was observed on both the oscillo-



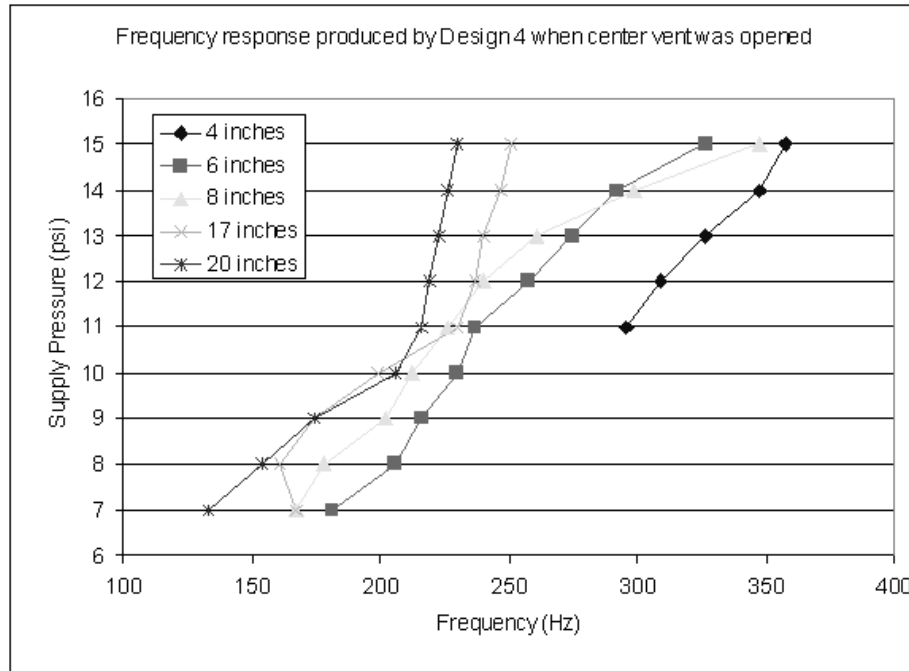


Fig. 5.18. Frequency produced by Design 4 when the feed-back length was varied between 4 to 20 inches and the supply pressure was varied between 5 to 15 psig (center vent opened).

Tab. 5.12. Results of the frequency produced by Design 4 with varying supply pressure and feed-back length (center vent opened to atmosphere).

Supply Pressure (psig)	4 inches	6 inches	8 inches	17 inches	20 inches
7	N/A	181.4616	167.6267	167.6267	133.0645
8	N/A	205.6452	177.9954	160.7143	153.8018
9	N/A	216.0138	202.1889	174.5392	174.5392
10	N/A	229.8387	212.5576	198.7327	205.6452
11	295.5069	236.7512	226.3825	229.8387	216.0138
12	309.3318	257.4885	240.2074	236.7512	219.47
13	326.6129	274.7696	260.9447	240.2074	222.9263
14	347.3502	292.0507	298.9631	247.1198	226.3825
15	357.7159	326.6129	347.3502	250.576	229.8387

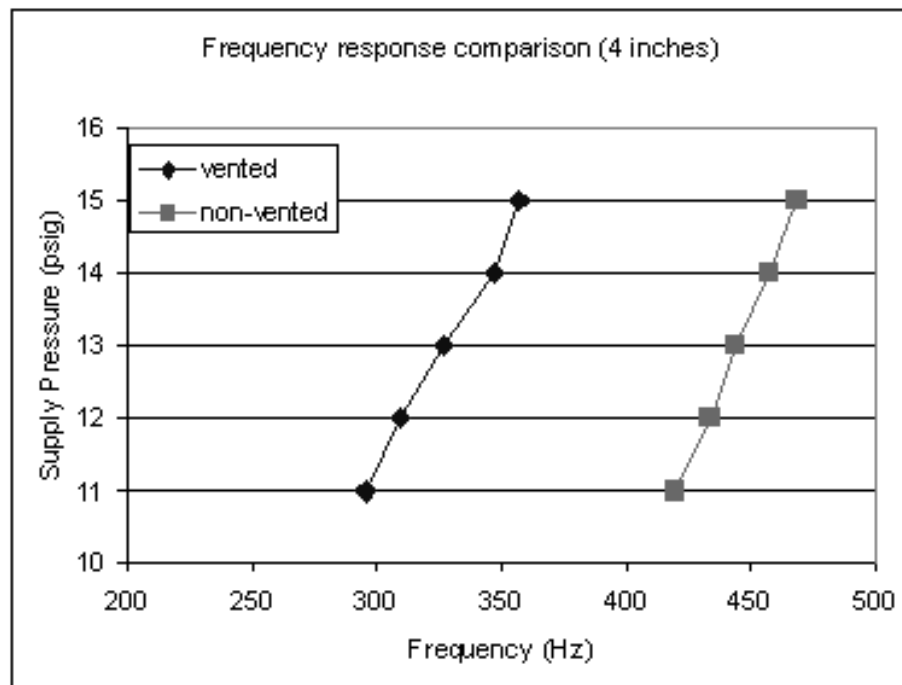


Fig. 5.19. Frequency comparison between center venting and non center venting for a feed-back length fixed at 4 inches.

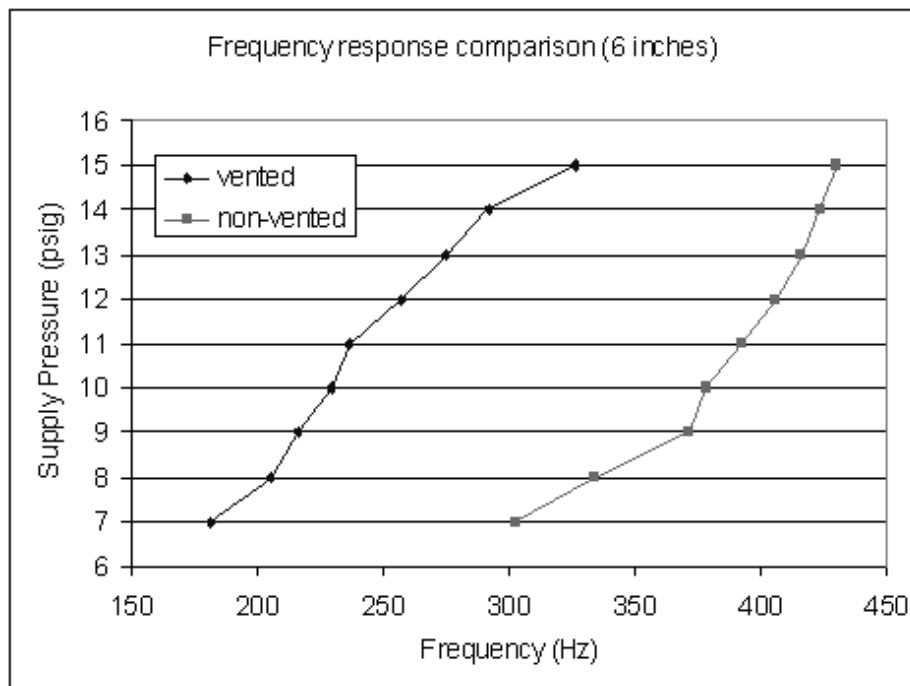


Fig. 5.20. Frequency comparison between center venting and non center venting for a feed-back length fixed at 6 inches.

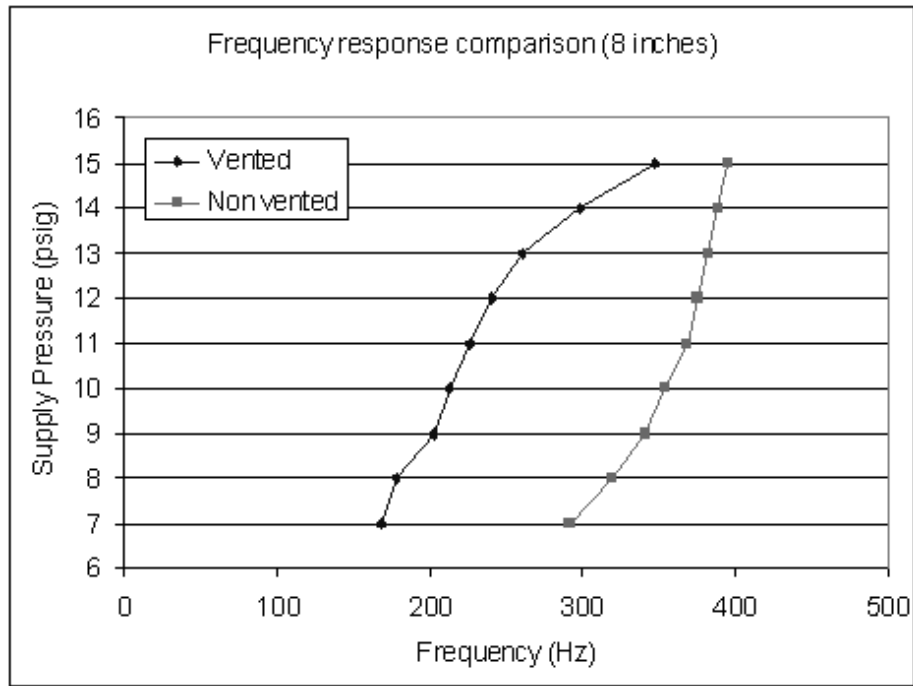


Fig. 5.21. Frequency comparison between center venting and non center venting for a feed-back length fixed at 8 inches.

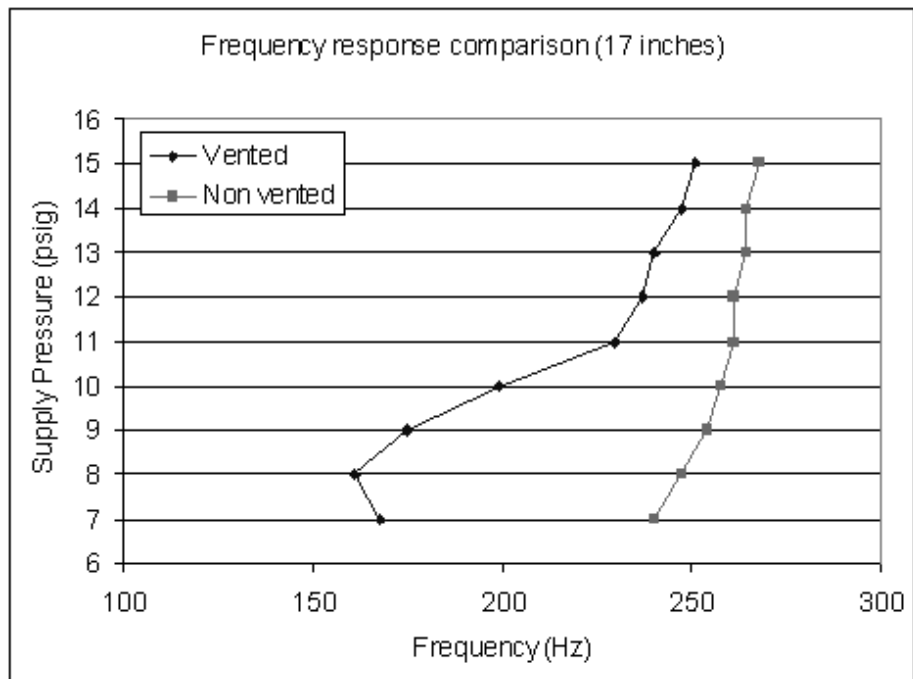


Fig. 5.22. Frequency comparison between center venting and non center venting for a feed-back length fixed at 17 inches.

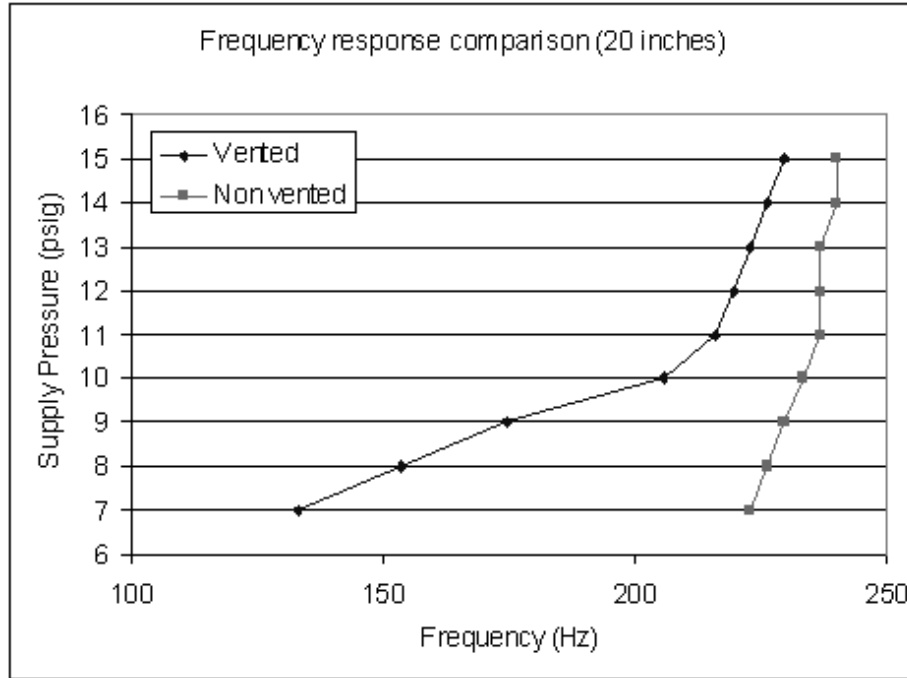


Fig. 5.23. Frequency comparison between center venting and non center venting for a feed-back length fixed at 20 inches.

scope display window and the data processed with Labview. Therefore Design 4 was concluded functional and ready to be tested for cascading setup.

### 5.7 Experiment 5: Cascading Study of Design 4 and GE Oscillators

With the additional oscillator available, the cascading studies between three proportional amplifiers could begin. The cascading of fluidic oscillator network was set up as shown in Figure 5.24. Design 4 was used to control two independent GE proportional amplifiers. The amplifiers are identical to one another and were connected to the outputs of Design 4's feed-back loops. The left output port of Design 4 was connected to the left control ports of the GE amplifiers and the right output port of Design 4 was connected to the right control ports of the GE amplifiers. The feed-back length of Design 4 was fixed at 20 inches and the exit ports of Element 1 and 2 (Channel 1 and 3) were connected to two PCB microphones.

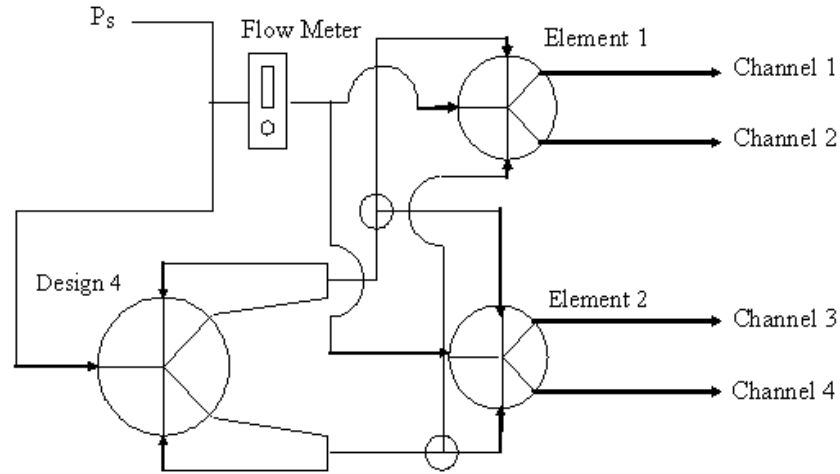


Fig. 5.24. A Cascading network using Design 4 to control two GE proportional amplifiers (Element 1 & 2).

Design 4's pressure supply in this setup was controlled by the pressure regulator (a brass needle valve) and the flow supply into the GE oscillators was controlled by a flow meter. Although the frequency obtained with center venting was lower than center vent blocked, the frequency produced by closing the center vent was much more consistent. Therefore center venting approach for Design 4 was not selected for this experiment. The pressure supply into Design 4 was allowed to vary from 1 to 3 psig while the flow into Element 1 and 2 were kept constant.

### 5.7.1 Experimental Results

Three microphones were used in this setup. Prior to data recording, a test run was performed and the frequency of at the output ports of GE amplifiers were monitored. The results obtained at the output ports of the GE amplifiers showed identical frequency (frequency at left output port of Element 1 is equal to frequency at right output port of Element 1, same for Element 2) therefore only one microphone was used to record the frequency at one of the two output ports of the GE proportional amplifier.

Tab. 5.13. Result of the frequency captured for cascading setup of Design 4 and GE proportional amplifiers with a feed-back length fixed at 20 inches, and no flow into the GE oscillators.

Supply Pressure (psig)	Microphone 1 (Hz)	Microphone 2 (Hz)	Microphone 3 (Hz)
2	198.7327	195.2765	198.7327
3	236.7512	236.7512	236.7512

The experiment was performed with three different supply pressures, 1  $\sim$  3 psig. At 1 psig supply pressure, the frequency of microphone 1 and 2 was not clear enough to support frequency judgment (too noisy). Most likely at 1 psig the fluid jet interaction was going through a transition where there was no consistent oscillation of the fluid jet. The frequency at 2 and 3 psig supply pressure are shown in Table 5.13. Interesting results were obtained from this experiment. First, the oscillation of Design 4 for began at 2 psig, which is significantly lower than the results observed from single element oscillation study of Design 4 (oscillation of 202.2 occurred at 5 psig). This observation was critical because in the functional description section of fluidic oscillator design, a statement was made on the output condition of a fluidic oscillator will directly affect the functionality of the oscillator. In this experiment, the output condition of the oscillator was drastically changed. Instead of venting the feed-back loop to the atmosphere, it was connected to two additional loads. The back pressure built up from the loading effect forced more flow to travel into the exit ports which resulted in a greater momentum flux recovery to deflect the supply jet stream, thus a lower frequency was recorded.

The second interesting observation from the results was the first harmonic of the resultant frequency was amplified (amplitude is significantly greater than the main frequency) by a factor of 5. A possible explanation for this phenomenon is the connector length of the PCB tubing may be approaching the length for standing wave to occur. Also polypropylene tubing was used for some of Design 4's connection

(supply pressure line, Line B1, and Line B2) instead of tygon tubing so less damping of the fluid vibration was available. The following equations were used to estimate the tubing length for a standing wave to occur:

$$\lambda = \frac{c}{f} \quad (5.10)$$

where  $c$  is the speed of sound in m/s and  $f$  is frequency in Hz. The speed of sound can be estimated using equation [20]:

$$c_{air} = 331.5 + 0.6T \quad (5.11)$$

where  $T$  is the temperature of air in Kelvin. At room temperature of 23°C,  $\lambda$  was calculated to be at 22.66 inches, at 600 Hz (amplified frequency). Standing waves will occur at  $\lambda/2$  which is 11.33 inches. Since the polypropylene tubing used was close to 11.33 inches (total connector length was 9 inches to be exact), there is a possibility for standing wave to occur. This calculation therefore explains the amplification of the harmonic waves observed in the results.

The experiment was repeated with different supply flow into the GE amplifiers. Results are shown in the Tables 5.14 and 5.16. As the supply flow into the GE amplifiers increases, the frequency captured at the exit ports increases accordingly. But at a sufficiently high supply flow rate into the GE amplifiers, the frequency begins to decrease. This is because the oscillating pressure wave provided by Design 4 was retarded by the introduction of the third stream of non-oscillating fluid, which induces a damping effect on the frequency. Nevertheless, at no flow into the GE amplifier condition, the frequency captured was identical, concluding the cascading experimentation of the analog fluidic amplifiers successful.

Tab. 5.14. Result of the frequency captured for cascading setup of Design 4 and GE proportional amplifiers (feed-back length fixed at 20 inches, 0.5 L/min flow into the GE oscillators).

Supply Pressure (psig)	Microphone 1 (Hz)	Microphone 2 (Hz)	Microphone 3 (Hz)
2	216.0138	212.5576	198.7327
3	229.8387	229.8387	236.7512

Tab. 5.15. Result of the frequency captured for cascading setup of Design 4 and GE proportional amplifiers (feed-back length fixed at 20 inches, 1.0 L/min flow into the GE oscillators).

Supply Pressure (psig)	Microphone 1 (Hz)	Microphone 2 (Hz)	Microphone 3 (Hz)
2	209.1014	209.1014	198.7327
3	226.3825	226.3825	236.7512

Tab. 5.16. Result of the frequency captured for cascading setup of Design 4 and GE proportional amplifiers (feed-back length fixed at 20 inches, 1.5 L/min flow into the GE oscillators).

Supply Pressure (psig)	Microphone 1 (Hz)	Microphone 2 (Hz)	Microphone 3 (Hz)
2	202.1889	205.6452	198.7327
3	226.3825	226.3825	236.7512



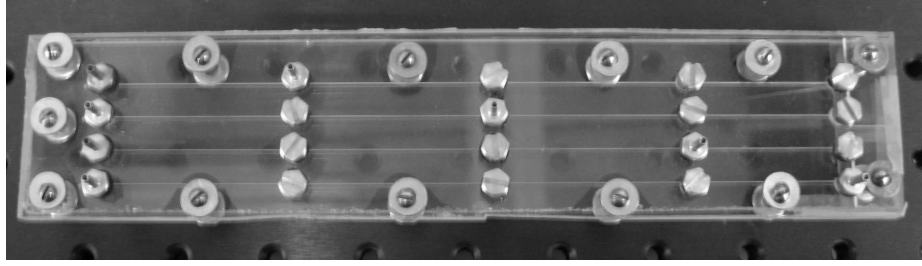


Fig. 5.25. Flow channels fabricated. Its main purpose is to mimic the actual PEMFC flow channels and also to study the effect of position on frequency variation in an air stream.

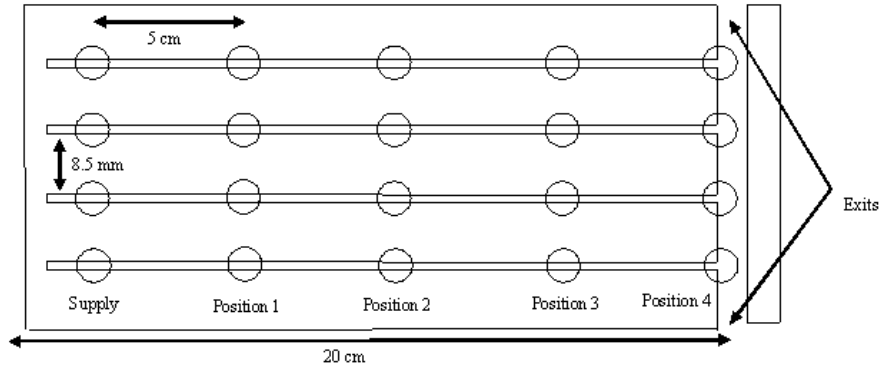


Fig. 5.26. Schematic of the flow channels.

### 5.8 Experiment 6: Frequency Variation in Channel

The progress at this point is closer to the goal of the research, which is to induce an oscillation on the water droplet by pulsating the air stream flowing over it. Thus far, the oscillation of air flow was achieved by fluidic oscillator, the fabrication and design of fluid oscillator was completed. Four 1 mm by 1 mm by 200 mm (width x depth x length) parallel flow channels were machined onto the bottom plate of a plexiglass, four different holes were tapped on the top plate above each channel to study the frequency variation across the channel. The two plates were bolted together and fittings were installed for data collection (Figure 5.25).

The flow rates into the GE amplifiers were fixed while the supply pressure entering Design 4 was allow to vary from 1.5 ~ 3.5 psi. The frequency of the pulsating air stream exiting the GE amplifiers were captured by the microphones and the results

were recorded.

### 5.8.1 *Experimental Results*

A schematic of the flow channels is shown in Figure 5.26. The purpose of these tests was to capture and visualize the pulsating flow down a flow channel and observe if there is an frequency variation between the channels due to feed-back from a common exit manifold.

In the experiment the microphones were located at Position 1 for all four channels. The supply flow into Design 4 was allowed to change from 1.5 to 3.0 psig and the flow rate into the GE amplifiers were varied from 0 to 2.0 L/min. Figure 5.27 to Figure 5.30 show the relationship between flow rate, frequency and supply pressure. The frequency captured at Position 1 decreases as the supply flow rate into the GE amplifiers increases. The frequency captured by the microphones matches exactly from Channel 1 to Channel 4 for most cases, showing the consistency in frequency produced by Design 4.

The experiment was repeated and the microphones were allowed to change from Position 2 to 4. Slight inconsistency may be caused by sudden increase in noise level (human activity in the laboratory or engine noises from neighboring laboratories). The figures also showed a common behavior of the frequency. As the supply pressure into Design 4 increases, the frequency captured at the exit port of the GE amplifiers increases accordingly. Figure 5.31 shows the signal waves captured by four different microphones across 4 different channels. Microphone 1 was fixed at Position 1 and Mic 2 was fixed at Position 2 and so on and so forth. A slight phase difference was observed due to the difference the time taken for the frequency signal to travel from Position 1 to Position 4. Since there is no shift in frequency observed, it is safe to conclude that there is no back pressure between the channels with a common exit manifold.

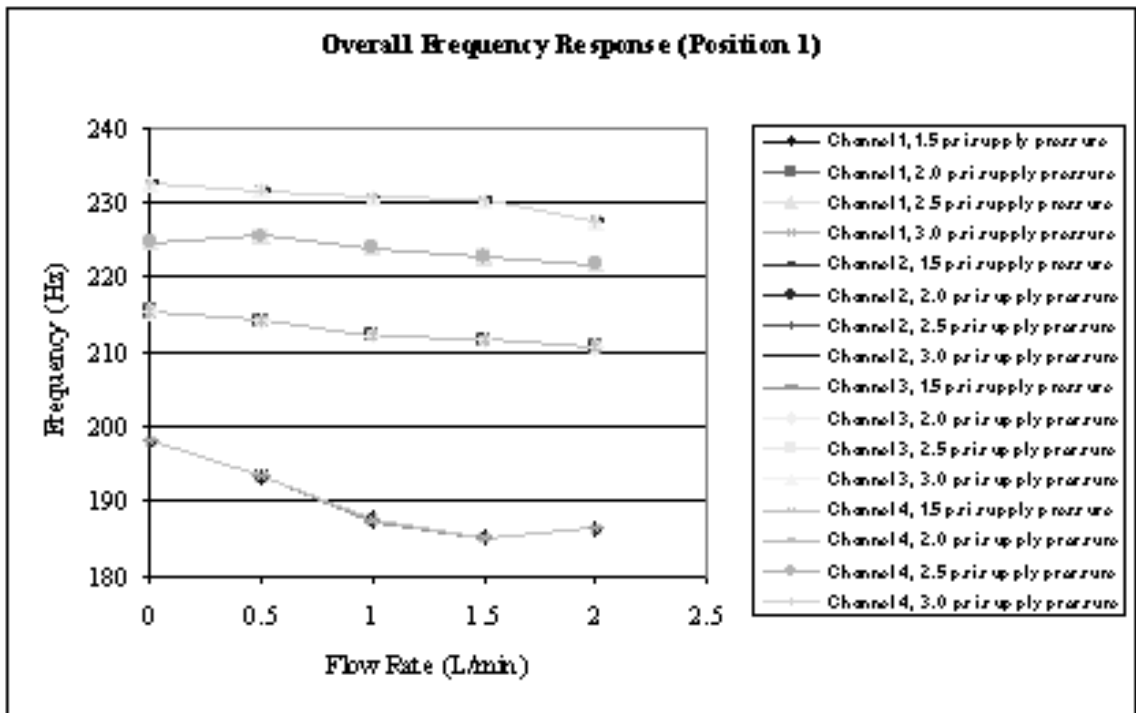


Fig. 5.27. Frequency captured by PCB microphones (mounted at 'Position 1') at different channels when the supply pressure was allowed to vary from 1.5 to 3.0 psig and the supply flow rate into the GE amplifiers were allowed to change from 0 to 2 L/min.

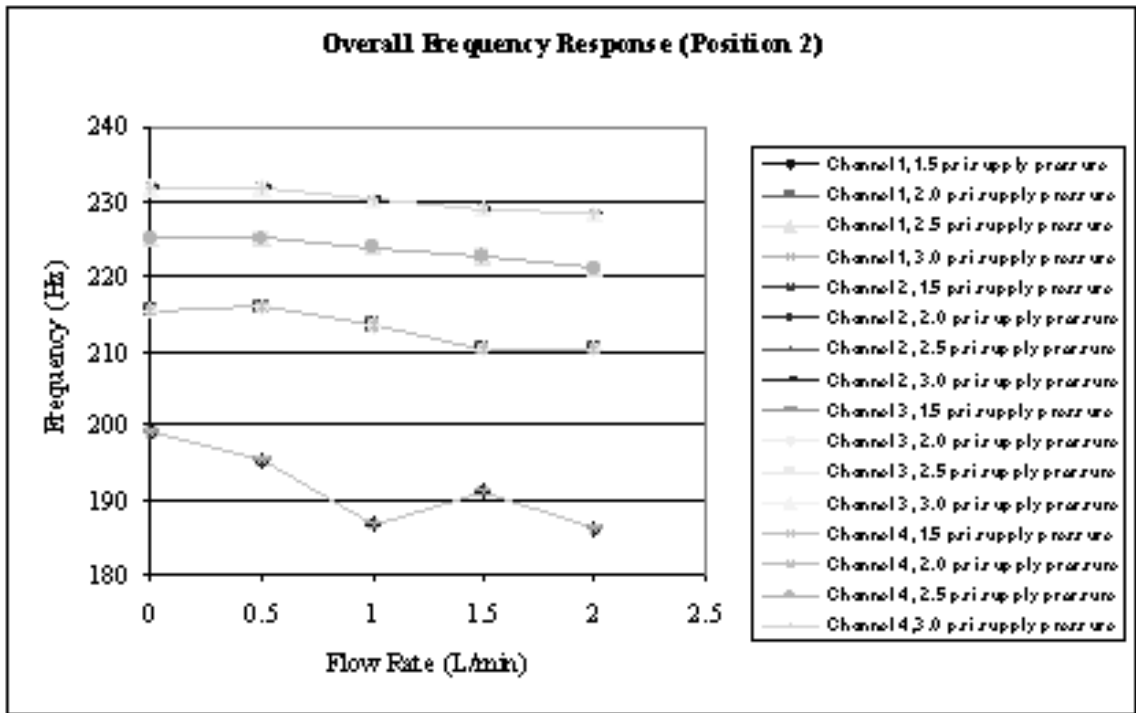


Fig. 5.28. Frequency captured by PCB microphones (mounted at 'Position 2') at different channels when the supply pressure was allowed to vary from 1.5 to 3.0 psig and the supply flow rate into the GE amplifiers were allowed to change from 0 to 2 L/min.

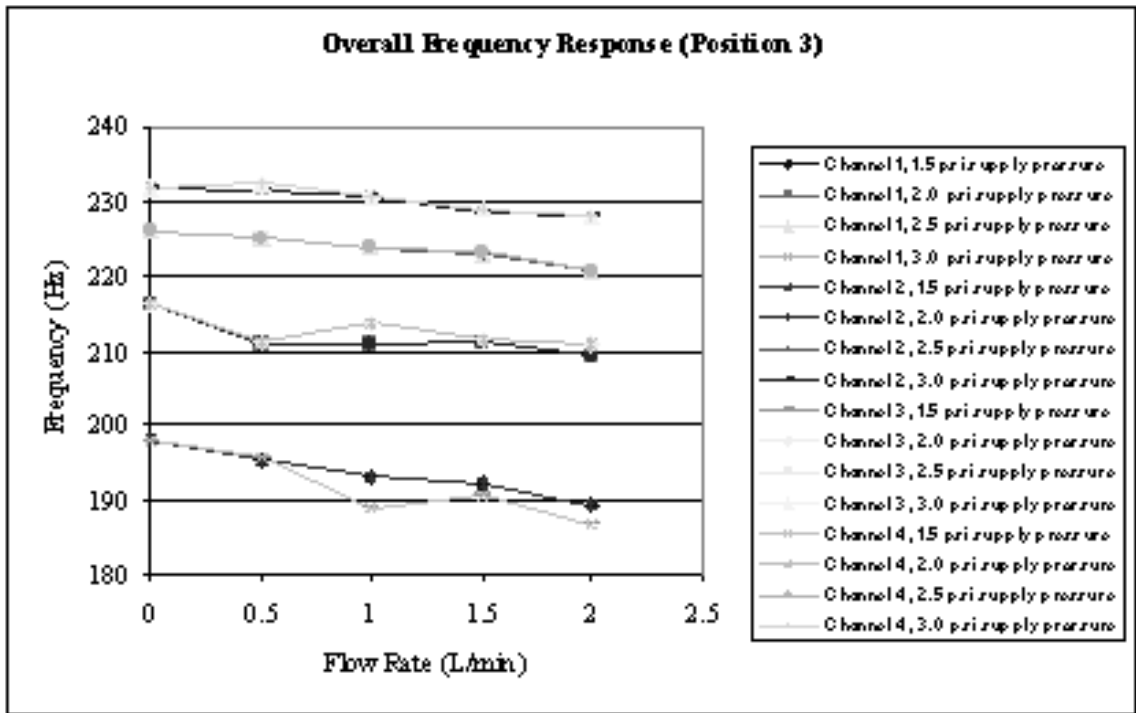


Fig. 5.29. Frequency captured by PCB microphones (mounted at 'Position 3') at different channels when the supply pressure was allowed to vary from 1.5 to 3.0 psig and the supply flow rate into the GE amplifiers were allowed to change from 0 to 2 L/min.

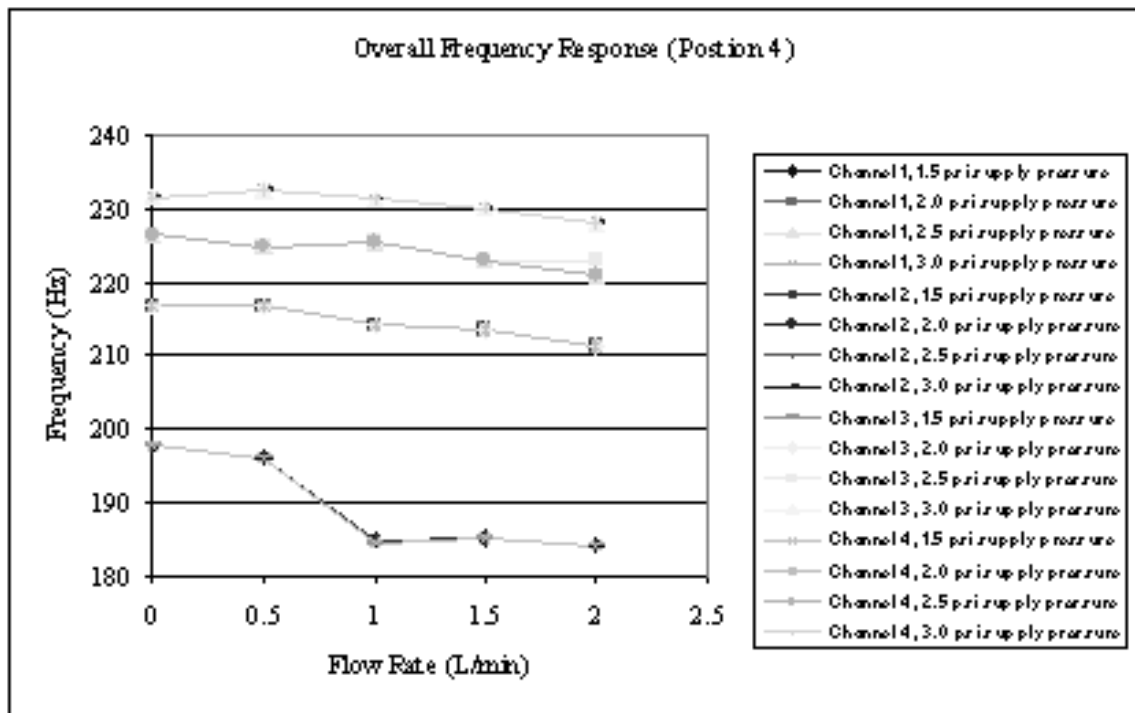


Fig. 5.30. Frequency captured by PCB microphones (mounted at 'Position 4') at different channels when the supply pressure was allowed to vary from 1.5 to 3.0 psig and the supply flow rate into the GE amplifiers were allowed to change from 0 to 2 L/min.

1.5 psig supply pressure into Design 4, no flow into GE amplifiers				
Channel	Position 1	Position 2	Position 3	Position 4
1	197.9	199	198.2	197.9
2	197.9	199	198.2	197.9
3	197.9	199	197.9	197.9
4	197.9	199	197.9	197.9

1.5 psig supply pressure into Design 4, 0.5 L/min flow into GE amplifiers				
Channel	Position 1	Position 2	Position 3	Position 4
1	193.4	195.3	195.2	196.1
2	193.7	195.3	195.2	196.1
3	193.4	195.3	195.5	196.1
4	193.4	195.3	195.6	196.1

1.5 psig supply pressure into Design 4, 1.0 L/min flow into GE amplifiers				
Channel	Position 1	Position 2	Position 3	Position 4
1	187.5	186.6	193.1	184.7
2	187.5	186.6	193.1	184.7
3	187.4	186.6	188.9	184.6
4	187.5	186.6	188.9	184.6

1.5 psig supply pressure into Design 4, 1.5 L/min flow into GE amplifiers				
Channel	Position 1	Position 2	Position 3	Position 4
1	185	191.2	192.1	185.2
2	185	191.2	192.1	185.3
3	185	191.2	190.6	185.3
4	185	191.2	190.6	185.2

1.5 psig supply pressure into Design 4, 2.0 L/min flow into GE amplifiers				
Channel	Position 1	Position 2	Position 3	Position 4
1	186.3	185.9	189.2	184.3
2	186.3	185.9	189.2	184.3
3	186.2	185.9	186.6	184.3
4	186.3	185.9	186.6	184.3

Tab. 5.17. Frequency captured by PCB microphones (in Hz) mounted at 4 different positions on the top of 4 different channels. The supply pressure into Design 4 was fixed at 1.5 psig and the supply flow into the GE amplifiers was allowed to vary from 0 to 2.0 L/min

2.0 psig supply pressure into Design 4, no flow into GE amplifiers				
Channel	Position 1	Position 2	Position 3	Position 4
1	215.5	215.1	216.3	216.8
2	215.5	215.1	216.3	216.8
3	215.5	215.1	216.2	216.8
4	215.5	215.1	216.3	216.8

2.0 psig supply pressure into Design 4, 0.5 L/min flow into GE amplifiers				
Channel	Position 1	Position 2	Position 3	Position 4
1	214	215.8	210.9	216.7
2	214	215.8	210.9	216.7
3	214	215.8	211.1	216.7
4	214	215.8	211.1	216.7

2.0 psig supply pressure into Design 4, 1.0 L/min flow into GE amplifiers				
Channel	Position 1	Position 2	Position 3	Position 4
1	212.3	213.3	210.8	214.3
2	212.3	213.3	210.8	214.3
3	212.3	213.3	213.6	214.3
4	212.3	213.3	213.6	214.3

2.0 psig supply pressure into Design 4, 1.5 L/min flow into GE amplifiers				
Channel	Position 1	Position 2	Position 3	Position 4
1	211.6	210.3	211.2	213.7
2	211.6	210.3	211.2	213.7
3	211.6	210.3	211.5	213.7
4	211.6	210.3	211.5	213.7

2.0 psig supply pressure into Design 4, 2.0 L/min flow into GE amplifiers				
Channel	Position 1	Position 2	Position 3	Position 4
1	210.6	210.2	209.3	211.3
2	210.6	210.2	209.3	211.3
3	210.6	210.2	210.9	211.3
4	210.6	210.2	210.9	211.3

Tab. 5.18. Frequency captured by PCB microphones (in Hz) mounted at 4 different positions on the top of 4 different channels. The supply pressure into Design 4 was fixed at 2.0 psig and the supply flow into the GE amplifiers was allowed to vary from 0 to 2.0 L/min



2.5 psig supply pressure into Design 4, no flow into GE amplifiers				
Channel	Position 1	Position 2	Position 3	Position 4
1	224.6	225.1	226	226.6
2	224.6	225.1	226	226.6
3	224.6	225.1	225.9	226.6
4	224.6	225.1	225.9	226.6

2.5 psig supply pressure into Design 4, 0.5 L/min flow into GE amplifiers				
Channel	Position 1	Position 2	Position 3	Position 4
1	225.4	225.1	225.1	225
2	225.4	225.1	225.1	224.9
3	225.4	225.1	225.1	225
4	225.4	225.1	225.1	225

2.5 psig supply pressure into Design 4, 1.0 L/min flow into GE amplifiers				
Channel	Position 1	Position 2	Position 3	Position 4
1	223.9	223.7	223.7	225.5
2	223.9	223.7	223.9	225.5
3	223.9	223.7	223.7	225.5
4	223.9	223.7	223.7	225.5

2.5 psig supply pressure into Design 4, 1.5 L/min flow into GE amplifiers				
Channel	Position 1	Position 2	Position 3	Position 4
1	222.7	222.6	223	222.9
2	222.7	222.6	223	222.9
3	222.7	222.6	223.3	222.9
4	222.7	222.6	223.3	222.9

2.5 psig supply pressure into Design 4, 2.0 L/min flow into GE amplifiers				
Channel	Position 1	Position 2	Position 3	Position 4
1	221.8	220.9	220.6	221
2	221.8	220.9	220.6	221
3	221.8	220.9	220.6	222.9
4	221.8	220.9	220.6	221

Tab. 5.19. Frequency captured by PCB microphones (in Hz) mounted at 4 different positions on the top of 4 different channels. The supply pressure into Design 4 was fixed at 2.5 psig and the supply flow into the GE amplifiers was allowed to vary from 0 to 2.0 L/min

3.0 psig supply pressure into Design 4, no flow into GE amplifiers				
Channel	Position 1	Position 2	Position 3	Position 4
1	232.3	231.9	231.9	231.6
2	232.3	231.9	231.9	231.5
3	232.4	231.9	231.9	231.5
4	232.4	231.9	231.9	231.5

3.0 psig supply pressure into Design 4, 0.5 L/min flow into GE amplifiers				
Channel	Position 1	Position 2	Position 3	Position 4
1	231.5	231.7	231.4	232.5
2	231.5	231.7	231.4	232.5
3	231.5	231.5	232.4	232.5
4	231.5	231.7	232.4	232.5

3.0 psig supply pressure into Design 4, 1.0 L/min flow into GE amplifiers				
Channel	Position 1	Position 2	Position 3	Position 4
1	230.5	230.3	230.9	231.3
2	230.5	230.3	230.9	231.3
3	230.5	230.3	230.4	231.3
4	230.5	230.3	230.4	231.3

3.0 psig supply pressure into Design 4, 1.5 L/min flow into GE amplifiers				
Channel	Position 1	Position 2	Position 3	Position 4
1	230.1	228.8	228.7	230.1
2	230.1	228.8	228.7	230.1
3	230.1	228.8	229	230.1
4	230.1	228.8	229	230.1

3.0 psig supply pressure into Design 4, 2.0 L/min flow into GE amplifiers				
Channel	Position 1	Position 2	Position 3	Position 4
1	227.5	228.1	227.9	228.2
2	227.5	228.1	227.9	228.2
3	227.5	228.1	227.9	228.2
4	227.5	228.1	227.9	228.2

Tab. 5.20. Frequency captured by PCB microphones (in Hz) mounted at 4 different positions on the top of 4 different channels. The supply pressure into Design 4 was fixed at 3.0 psig and the supply flow into the GE amplifiers was allowed to vary from 0 to 2.0 L/min

Signal Analysis (1.5 psi supply pressure with no flow into the GE oscillators)

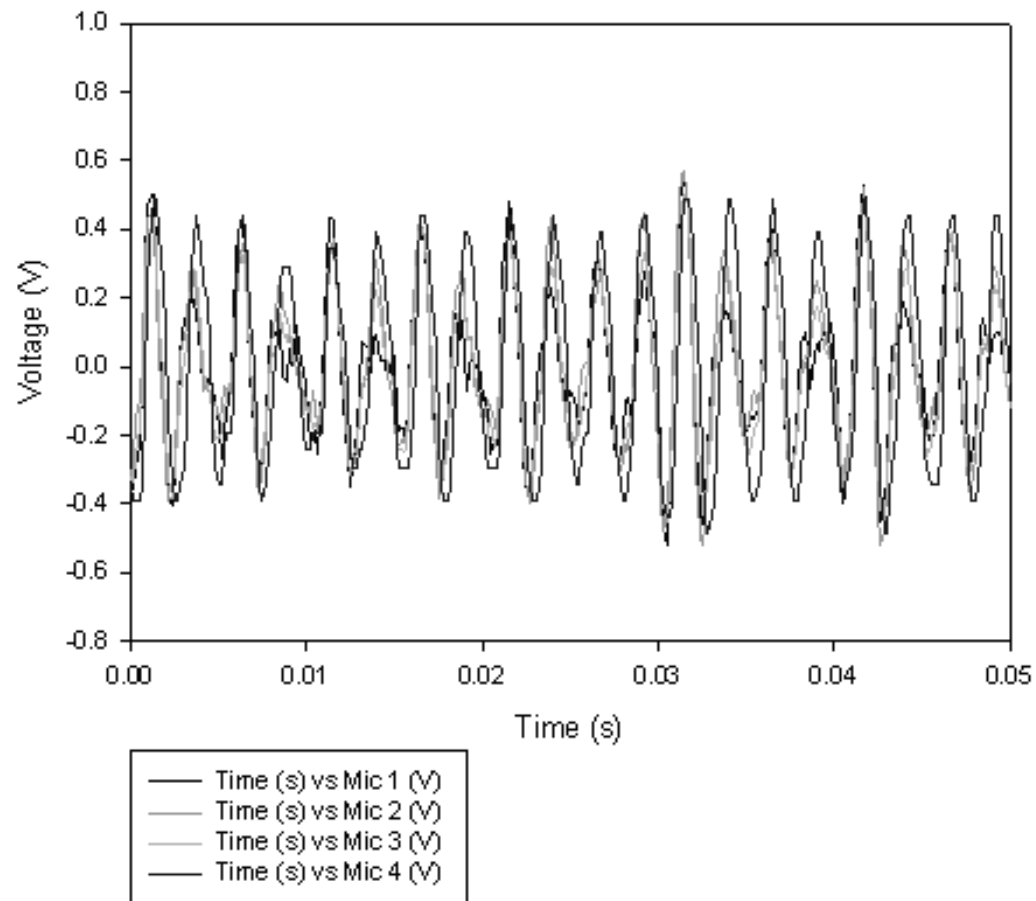


Fig. 5.31. Signal wave captured by four different microphones at four different channels, 1.5 psig supply pressure was introduced into Design 4 and no flow was supplied to the GE amplifiers.

Table 5.17 to 5.20 summarize the results obtained from this setup. Observing the data closely, although there are slight variation among the data collected, the difference in frequency is in the vicinity of  $0 \sim 5$  Hz, which can be still considered as identical. Another observation made was frequency variation across the channel decreases as the supply pressure entering Design 4 increases, which implies that at lower supply pressure the fluid stream was going through a transition scheme therefore a larger variation was captured and the result was not very consistent. At a higher flow rate, the momentum interaction within the oscillation has reached a steady state and the frequency produced was more consistent (more periodic) therefore the frequency variation observed was very small (0.1 to 1 Hz difference).

## 5.9 *Summary*

Experiment 1, introduced fluidic technology by studying the effect of feed-back port length on frequency. Increasing the feed-back port length decreased the frequency produced by the oscillator. Increasing the supply flow rate into the oscillator also directly effect the frequency; as the flow rate increases, the frequency of the oscillator increased. These two observations provided a guide in frequency control of the oscillator. Experiment 2 altered the setup suggested by the operating manual of GE analog laboratory kit. Instead of having one of the exit port closed, both of the exit ports were allowed to vent to atmosphere. The GE oscillator produced a lower frequency compared to single port venting. Experiment 2 provided a clue for cascading network of fluidic oscillators.

The results from the cascading network of GE amplifiers showed identical frequencies captured at Element 1 and 2. The purpose of using the first oscillator to control one or more fluidic device is to simultaneously pulsate the supply flow at a requency down 2 or more parallel channels. Cascading of fluidic devices also reduced the load on the control oscillator. Experiment 3 showed that it is possible to use one oscillator

to control another identical fluidic amplifier.

The frequency produced by Design 4 under different feed-back port length and supply pressure showed a similar trend as the results produced by the GE oscillators. The frequency produced by both of the devices increases as the feed-back port length decreases and the frequency increases and the supply flow rate increased. This result obtained from Experiment 4 demonstrated the functionality of Design 4.

In Experiment 5, Design 4 was used as a control oscillator for two identical GE amplifiers. The loading effect was observed in the results obtained. In Experiment 4, the oscillator began to oscillate only when the supply pressure reached about 6 psig. While in the cascading setup, oscillation was observed when the supply pressure of Design 4 reached 2 psig. However, due to the overloading of the microphones when Design 4's supply pressure reached 3 psig, limited data was available to make any further judgement on the cascading behavior. Investigation on the cascading network behavior remained as future task. Nevertheless, obvious pulsation was observed when the microphones were connect to the exit ports of the GE amplifiers, demonstrated pulsation down four independent parallel channels possible.

In Experiment 6, the cascading network was tested. The objective of the experiment was to observe the existence of back pressure when the pulsating flow travels down a 200 mm channel. From the results obtained, identical frequency was captured at Position 1, 2, 3, and 4. No significant change in frequency was observed between the four channels. Therefore when the flow channels were vented to a common manifold, no frequency modulation was observed, showing the feasibility of cascading network.

## 6. ADDITIONAL WORK

In the previous chapters, the functionality of the proportional amplifiers was validated through a series of experiments. Both the GE proportional amplifiers and Design 4 were proven functional and cascading networks of oscillators were built for feasibility study. The main intention for studying the functionality of fluidic oscillators was to implement this technology into the gas flow channels in PEMFCs. The geometry of the oscillator is simple and can be machined or stamped onto the bipolar plate. The venting of the oscillator is a problem in fuel cell applications because of the hazard associated with the venting of hydrogen. Unless a recovery system is developed to recycle the vented hydrogen, a non-vented oscillator will probably be the best method to pursue.

The main difference between vented and non-vented oscillators is their response to loading. During heavy loading conditions, non-vented oscillator will cease to function due to build up of back pressure at the interaction region. However, the vented oscillator will continue to operate during fully blocked exit condition because any excess back pressure builds up will be exhaust through the vents.

Unlike a vented oscillator, the operation of non-vented oscillator is heavily dependent on geometry. There is limited published materials on non-vented oscillator design. Therefore the chosen method of modeling was using commercial computational fluid dynamic (CFD) software to predict the geometry for a given loading condition.

## 6.1 *Fluent Simulation*

FLUENT is a commercially available CFD software used to simulate fluid flow, heat and mass transfer, and a host of related phenomena involving turbulence, reactions and multiphase flow. In the case of oscillator design, the target is to utilize FLUENT's powerful simulation capability to design the primary geometry of a non-vented fluidic oscillator. Before dwelling into non-vented oscillator design, the current vented oscillator model (Design 4) was analyzed to test the capability of FLUENT to simulate the oscillating fluid stream. The following steps were taken to construct the model in FLUENT.

1. Define the modeling goals
2. Generate model geometry and grid
3. Setup the solver and physical model
4. Compute and monitor the solution
5. Save the results

The first model constructed was Design 4. The goal is to become familiar with the capability of FLUENT and the adjustable parameters and solvers available in the software. Since the purpose of the simulation is not optimization, a simplified 2D model was constructed. To generate the model, Design 4's geometry was first input into GAMBIT. GAMBIT is a software whose main function is to model the geometry and generate a grid for CFD calculations (mesh generation is required for finite element method for numerical computation). The surface of the geometry of interest was partitioned into 'elements' and the element size must be optimized for accurate results. A structured mesh was selected and applied in all of the designs because it is typically easier to compute, which saves some simulation runtime. However

the structured mesh also require more elements compared to unstructured mesh to produce a reliable result. Therefore a decision must be made between accuracy and speed. Since optimization of the model was not the primary concern, the structured mesh was selected.

After the geometry and mesh file were successfully generated by GAMBIT, the next step is to import it into FLUENT. The solver selected to perform the numerical modeling was 2ddp (two dimensional, double precision), a segregated solving approach was used. Segregated approach allowed the user to tackle the governing equation sequentially until the convergence criteria are met. This technique is slightly faster than the coupled solver, where the governing equations of continuity, momentum and energy are solved simultaneously. By selecting the segregated solution approach, each discrete governing equation is linearized implicitly with respect to that equation's dependent variable, therefore explicit solver does not apply here. The turbulent viscous k-epsilon model was selected. The choice of turbulence model depends on the degree of accuracy, computational resources and amount of time the operator have in the hand. Standard k-epsilon was selected because it is the simplest 'complete model' of turbulence, it offers a reasonable accuracy and the computational power required was not as heavy. Air was selected as the working medium under standard temperature and pressure (101325 Pa). Therefore the working material and operating condition was remained unchanged. The boundary was setup as followed and the model was initialized with 'Absolute' reference frame with initial values equal to zero, the convergence criterion was set to 1e-05 for all the residual stresses.

1. Inlet: Pressure Inlet (8 psig or 55158 Pa)
2. Exit 1: Outlet Vent (0 psig or 0 Pa)
3. Exit 2: Outlet Vent (0 psig or 0 Pa)
4. Vent: Outlet Vent (0 psig or 0 Pa)



5. Wall: Stationary wall with No slip boundary condition.

The quality of the mesh must be checked before every simulation in order to avoid problems due to incorrect mesh connectivity. The maximum skewness of the short feed-back length model constructed was 0.35 which is lower than 0.98 (the limit for skewness) and the maximum skewness of the long feed-back length model constructed was 0.70 which is also lower than 0.98. Some calculations were made to ensure the assumption of incompressible flow was valid. This was done by calculating the Mach number.

$$Ma = \frac{U}{C} \quad (6.1)$$

Where U is the flow velocity and C is the speed of the sound. The speed of sound is dependant on the temperature of the fluid and can be estimated by [20]:

$$C = 331.5 + \left(1 + \frac{T}{273.15}\right)^{0.5} \quad (6.2)$$

Where T is the temperature of the fluid in Kelvin.

## 6.2 Simulation Results

The results obtained after the simulation were recorded and displayed in Figure 6.1 through Figure 6.4. The inlet pressure was set to 8 psig and the vents and the exits were exposed to atmospheric pressure (0 psig). The iteration parameters were setup as follow:

1. Time Step Size: 1e-05 seconds
2. Number of Time Steps: 100,000
3. Time Stepping Method: Fixed

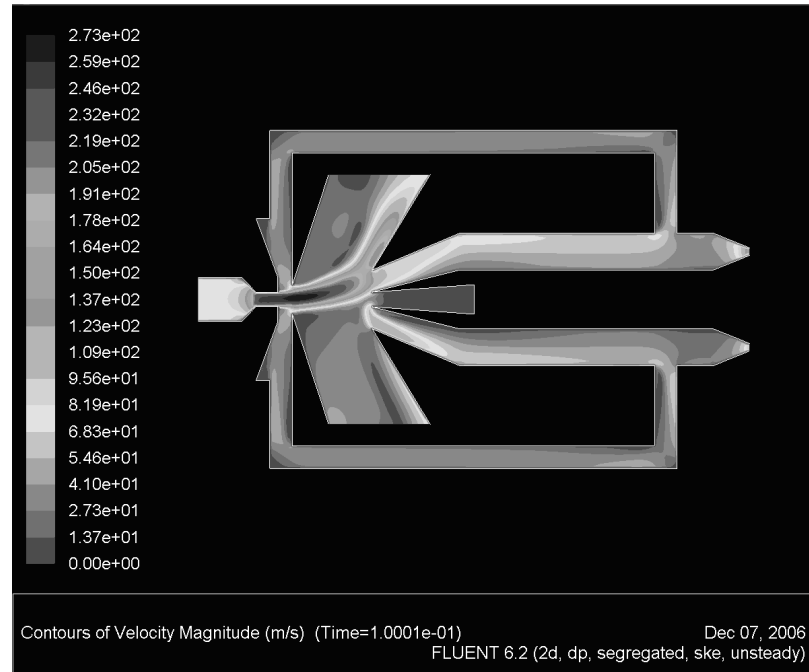


Fig. 6.1. FLUENT result showing the oscillation of fluid jet in the oscillator towards the left feed-back port (short feed-back length).

#### 4. Maximum Iteration per Time Step: 5000

Although FLUENT is a very powerful CFD software, the author was not able to extract the frequency data of the oscillating stream from the simulation. Additional user defined functions must be incorporated into the software in order to fulfill this task. Therefore a crude method was used to obtain the frequency response. The simulation was stopped when the deflected jet reaches a maximum deflection (right) and the time in which the event occurred was noted. The simulation was allowed to resume and was paused when the deflected stream reaches the maximum deflection again (left). The time difference recorded during these two events was calculated for the frequency. The frequency calculated for the long feed-back port was approximately 2420 Hz and the frequency calculated for the short feed-back port was approximately 2437 Hz. The frequency variation was not significant and that is because the feed-back port length difference between the two models was only 10 mm, therefore the variation in frequency response was not noticeable.

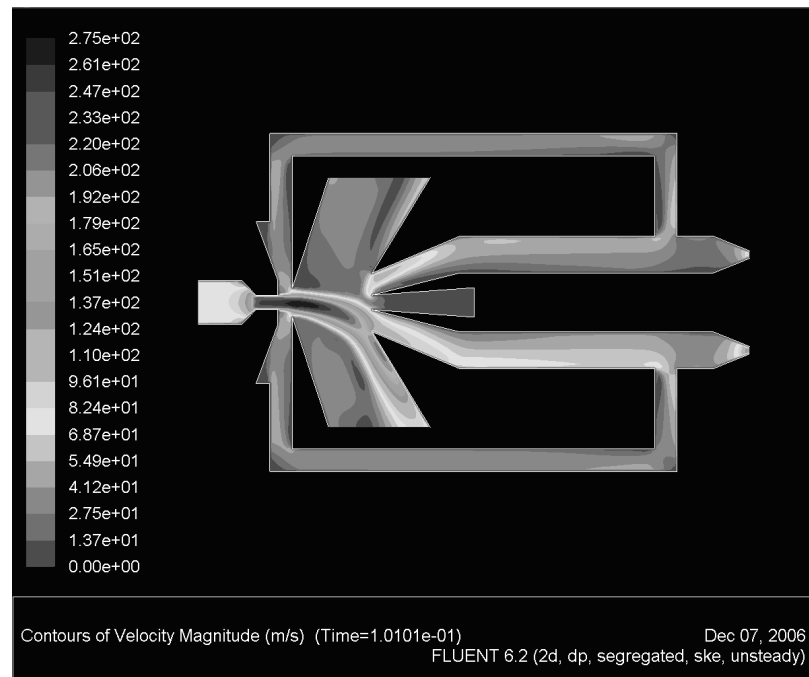


Fig. 6.2. FLUENT result showing the oscillation of fluid jet in the oscillator towards the right feed-back port (short feed-back length).

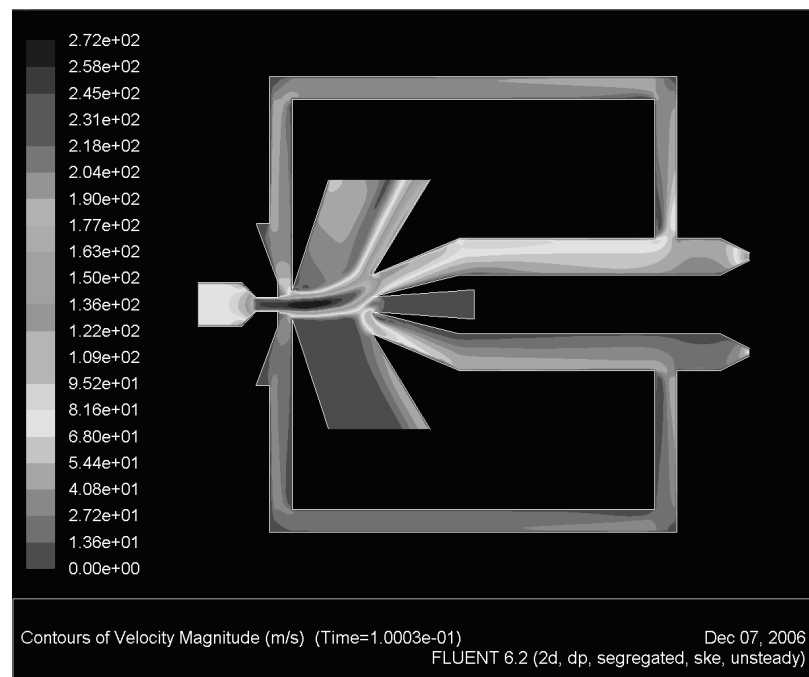


Fig. 6.3. FLUENT result showing the oscillation of fluid jet in the oscillator towards the left feed-back port (long feed-back length).

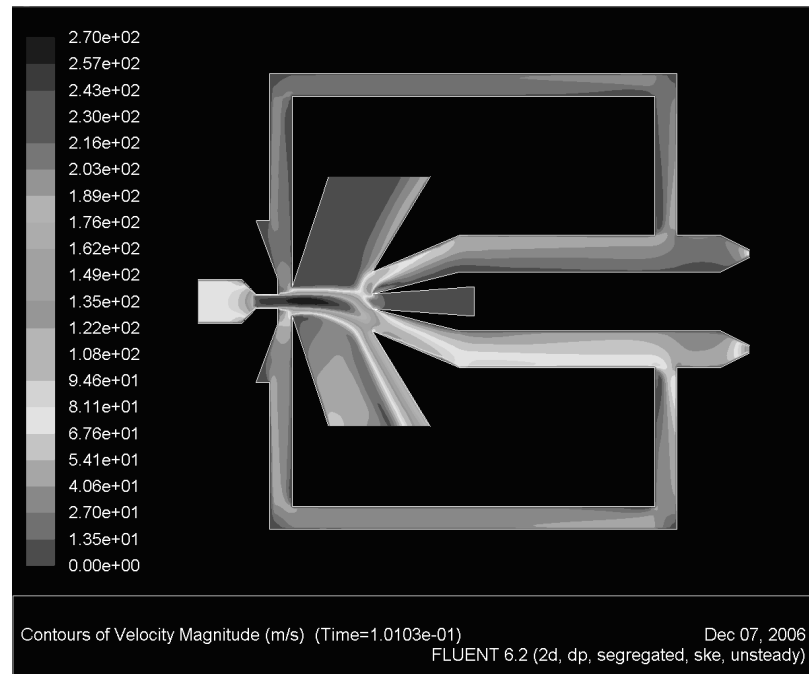


Fig. 6.4. FLUENT result showing the oscillation of fluid jet in the oscillator towards the right feed-back port (long feed-back length).

The rough frequency response simulated by FLUENT was not comparable to the experimental data due to the following reasons. First, the model constructed was in 2D therefore the third component of the momentum and mass equations was not taken into account. Second the Mach number calculated based on the maximum velocity was approximately 0.8, which lies within the transonic region; therefore, incompressible assumption is not valid. However the purpose of this simulation was to evaluate if CFD is capable to simulate the oscillation of fluidic oscillator. Although the results obtained after the simulation did not produce an accurate result, the oscillation of the model was successfully simulated.

### 6.3 Changing Receiver Position

From the previous simulation, the FLUENT results obtained was not identical to the experimental results, but it serves as a great simulation tool which saves a significant amount of experimental time. The time taken to run one case is approximately

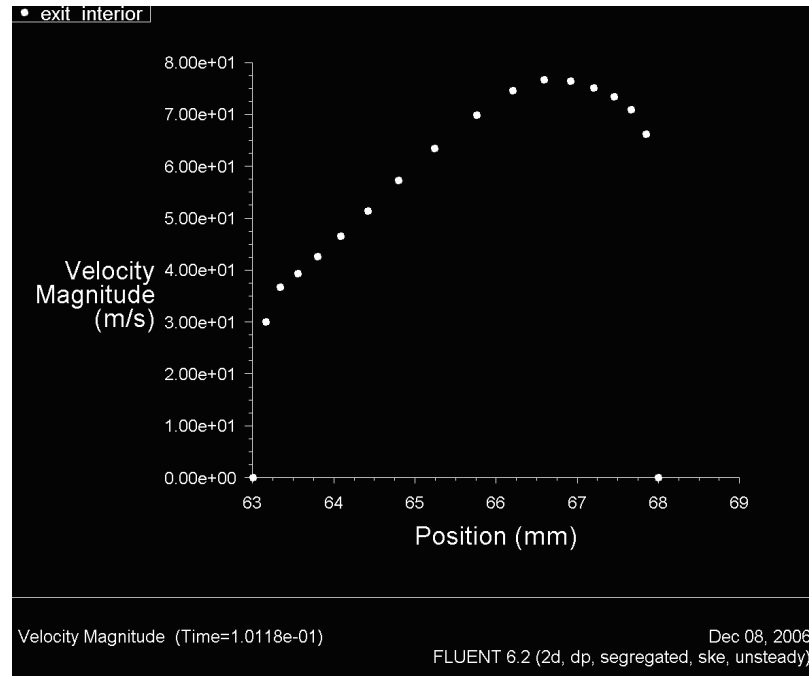


Fig. 6.5. Velocity profile recorded by FLUENT, where the position axis indicate the location (in y-direction) of the interior in the left exit port. The maxima showed a velocity of approximately 76 m/s attained and the velocity at the wall (location 63 and 68) remained at 0 m/s.

six hours for 10000 time steps, and the time required to fabricate a physical model and perform the appropriate data acquisition would easily cost approximately two to three days (under ideal condition), therefore the path chosen for additional modeling remained as simulation approach.

The first simulation of oscillator demonstrated the capability of FLUENT to simulate oscillation in Design 4, both the simulation and experimental results showed that the majority of the fluid exits the system through the side vents. The velocities of the exit ports in the first model after 10,000 iterations were shown in Figure 6.5 and Figure 6.6

The model in FLUENT was re-designed where the splitter distance (distance from the throat to the splitter) was decreased to study the effect of splitter length on overall momentum recovery. A new model was constructed and meshed in GAMBIT under the same approach as the previous simulation. The splitter position in the

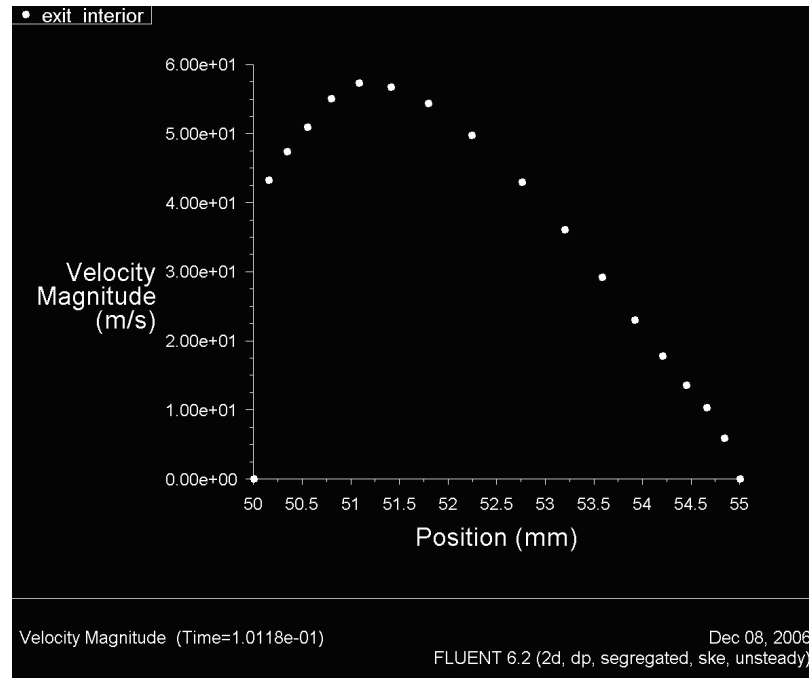


Fig. 6.6. Velocity profile recorded by FLUENT, where the position axis indicate the location (in y-direction) of the interior in the right exit port. The maxima showed a velocity of approximately 58 m/s attained and the velocity at the wall (location 50 and 55) remained at 0 m/s.

new model was decreased by 1mm. When the mesh file was imported into FLUENT, identical parameters used (solver type, boundary condition, time step and size, etc.) in the model before modifying the splitter length was implemented on the new model. Oscillation of the fluid jet was again observed (Figure 6.7 to Figure 6.10).

The velocity profile results were recorded and displayed in Figure 6.11 and Figure 6.12. Comparing the results shown prior to splitter length modification, the velocity extracted at the exit port interior showed a greater flow velocity. The flow velocity result at the left exit port interior was recorded at approximately 76 m/s before the splitter length was modified. A velocity at approximately 80 m/s was recorded at the exit port interior after the splitter length was modified. This implied the pressure variation across the exit ports was evidently higher, demonstrating an improved pressure recovery.

From the simulations performed on vented oscillators (both long and short feed-

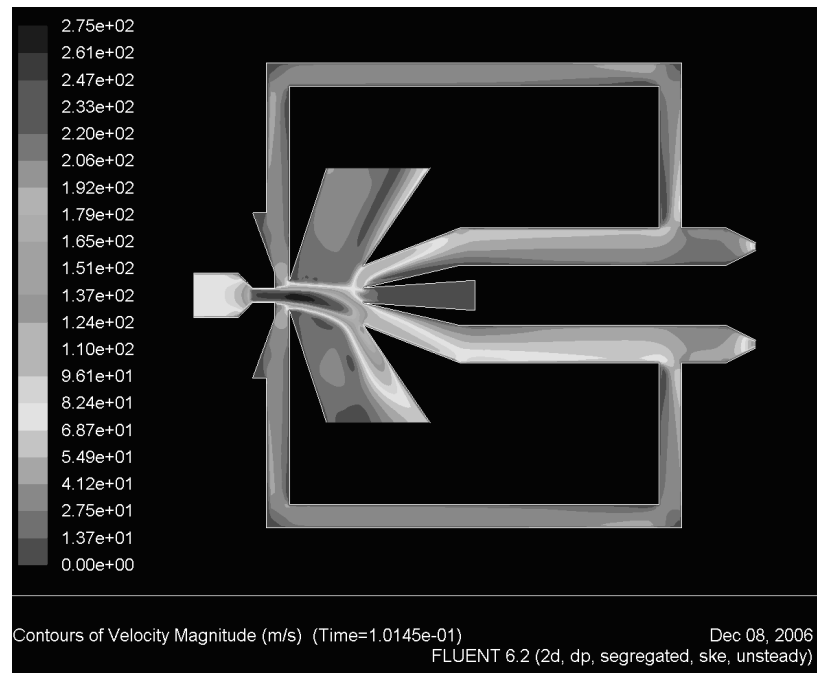


Fig. 6.7. FLUENT result showing the direction of the jet deflection after the splitter position is modified (long feed-back port).

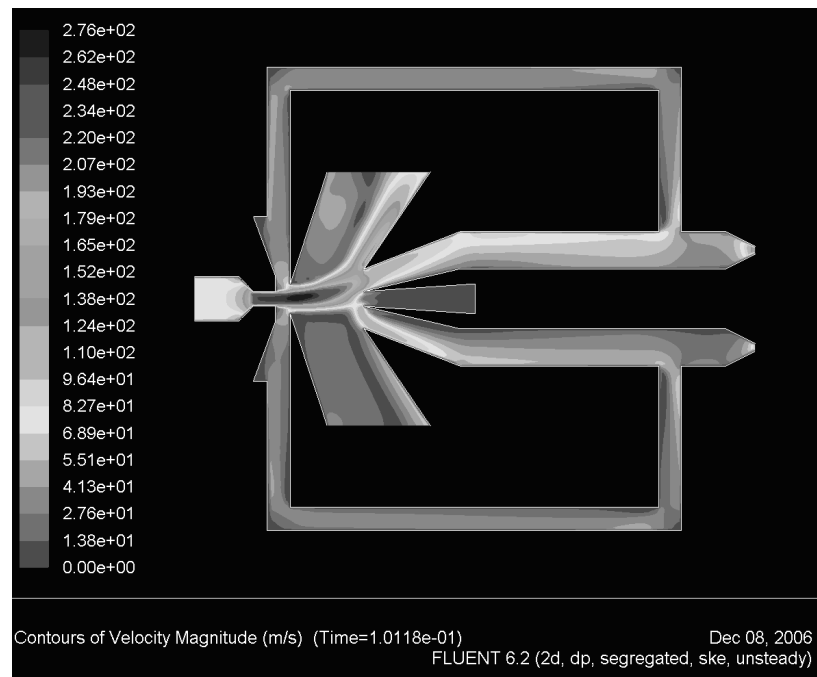


Fig. 6.8. FLUENT result showing the direction of the jet deflection after the splitter position is modified (long feed-back port).

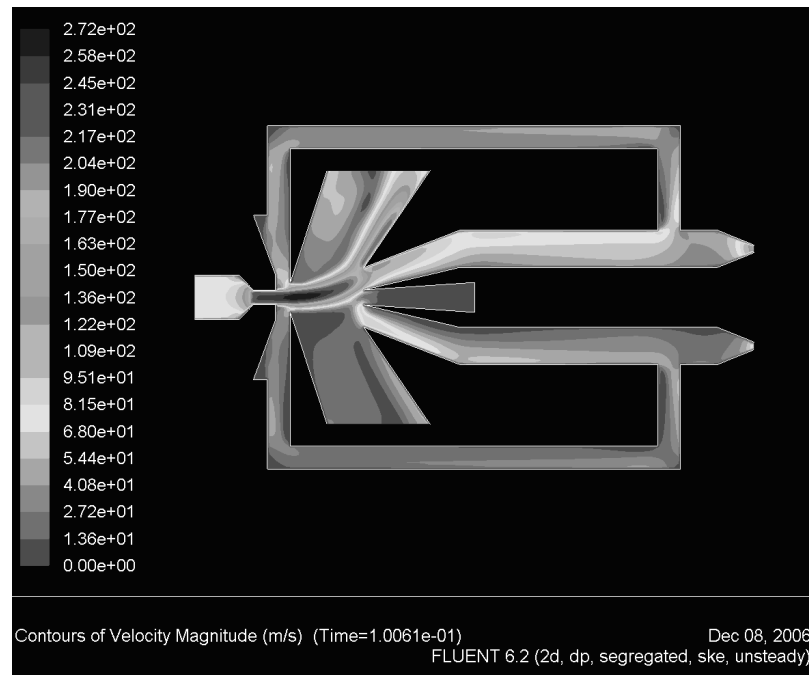


Fig. 6.9. FLUENT result showing the direction of the jet deflection after the splitter position is modified (short feed-back port).

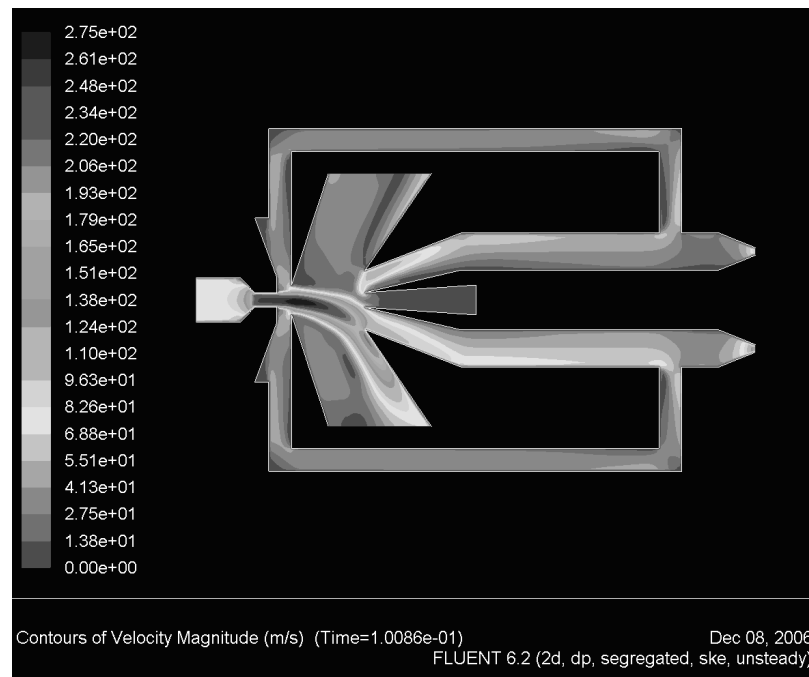


Fig. 6.10. FLUENT result showing the direction of the jet deflection after the splitter position is modified (short feed-back port).



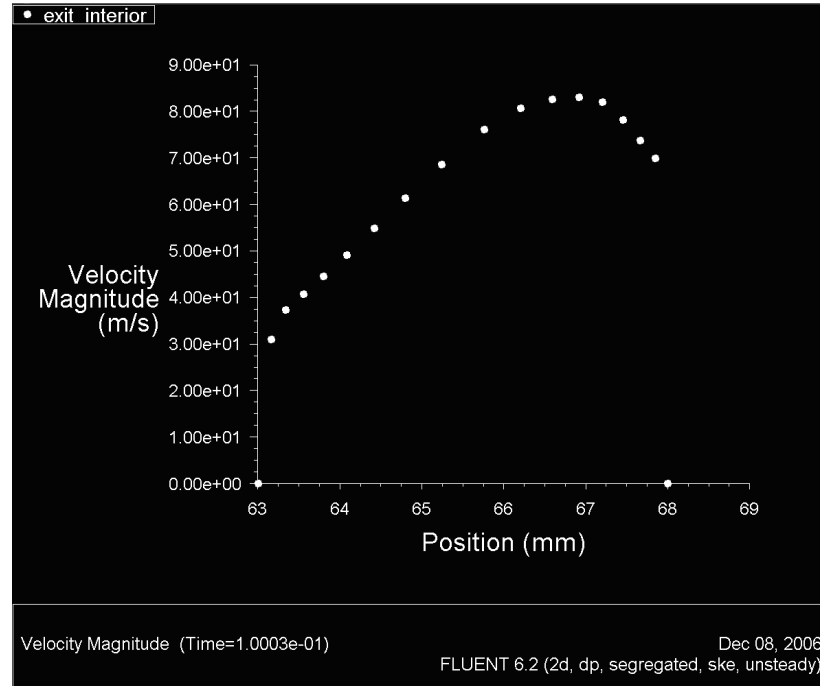


Fig. 6.11. Velocity profile recorded by FLUENT, where the position axis indicate the location (in y-direction) of the interior in the left exit port. The maxima showed a velocity of approximately 80 m/s attained and the velocity at the wall (location 63 and 68) remained at 0 m/s.

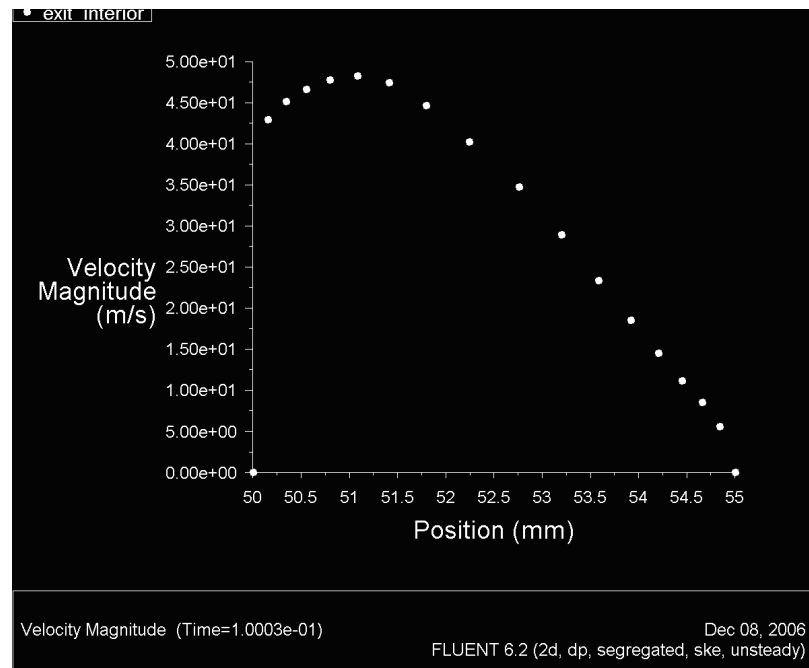


Fig. 6.12. Velocity profile recorded by FLUENT, where the position axis indicate the location (in y-direction) of the interior in the right exit port. The maxima showed a velocity of approximately 48 m/s attained and the velocity at the wall (location 50 and 55) remained at 0 m/s.

back length), obvious oscillation of the fluid jet was observed. These results fulfilled the primary target of FLUENT simulation which is to utilize CFD to approach fluidic oscillator design. Although the simulation results do not match with the experimental results, an approach in fluidic oscillator design using commercial CFD software is feasible. The second simulation on splitter position modification showed an improved momentum recovery. This result provided the evidence which commercially available CFD software can be used as a tool for design and modelling of fluidic oscillator. Through these series of tests, some confidence was gained towards FLUENT operation. The next target was to initialize non-vented oscillator design.

#### 6.4 *Non-Vented Oscillator Design*

The geometry of the non-vented oscillator was constructed in GAMBIT and proper meshing parameters were selected. The mesh file was imported to FLUENT and the appropriate solver type and boundary conditions were defined. 5 psig supply pressure was used to ensure incompressible flow assumption sustains, step size of 1e-05 second was chosen and number of steps were set to 10,000.

Convergence was achieved after 10,000 iterations, no obvious oscillation of the fluid jet was observed for both long and short feed-back loop length. The iteration was allowed to continue for additional 10,000 iterations and yet the simulated results did not show any sign of fluid oscillation. Based on this result, one would be able to conclude that the momentum recovery at the exit port was insufficient to cause a deflection at the control port.

Since the oscillation of the non-vented oscillator relies heavily on interaction chamber geometry, addition effort must be made to the modification of the current geometry. New mathematical model must be built in order to perform the necessary impact momentum estimation to more effectively predict the pressure difference across the control and the exit ports. Therefore additional tasks must be performed before

---

successful oscillation can be achieved.

## 7. CONCLUSION

Inspired by the water management problem occurred within the fuel cell, a fluidic oscillator was proposed to enhance the removal of water hold up. The main achievement in this research is to design and construct a fluidic amplifier and carry out a number of tests to ensure its functionality.

The test results were compared to the frequency response produced by the oscillators constructed using the General Electric analog fluidic laboratory kit. The first experiment was performed as a pseudo-calibration process for the GE oscillators. The difference between the results obtained and the manufacturer's data were less than ten percent for both of the GE oscillators, proving the functionality of the oscillators. A study on the feed-back loop length on the overall frequency response produced was also performed. The frequency response of the oscillator was observed to increase when the feed-back port length was decreased, matching the predicted behavior of the oscillator.

The goal of the second experiment was to visualize the effect when both of the feed-back loops were allowed to vent to the atmosphere. A clear oscillation was observed from the frequency response captured by the microphones. This result demonstrated that dual feed-back port oscillation is a possibility and the frequency response produced by dual port oscillation is significantly lower than single feed-back loop oscillation.

The second experiment demonstrated the possibility to use a single oscillator to control other identical devices. This connection of two or more oscillators is called a 'cascading' network. The advantage in setting up a cascading network is to reduce

the load on the control oscillator. Results from Experiment 3 showed this hypothesis accurate by using a single oscillator (Element 1) to control another identical proportional amplifier (Element 2) connected in series with common supply flow rate. The results showed an intimate similarity between the frequency response captured at Element 1 and Element 2. The behavior of increasing feed-back loop length was observed to have a direct effect on frequency response.

Since cascading between two identical amplifiers demonstrated a promising result, an idea of utilizing one control oscillator to power two identical proportional amplifiers became the next target. Due to the lack of existing oscillators, fabricating an additional amplifier became a necessity. From the results, Design 4 was found to produce a similar response to feed back length and supply pressure. Cascading between three fluidic elements demonstrated no phase shift which shows no back pressure built up. Identical frequency response was recorded by the PCB microphones across all four channels which concluded cascading using Design 4 to control two identical GE proportional amplifiers a successful approach.

Some CFD was performed on Design 4. Although the simulation result does not show an identical frequency response, it provided the author a clue in which CFD could be utilized as a design tool which will save both time and effort. Non-vented oscillator design will be the next target in this research and hopefully a successful model can be achieved and implemented on a serpentine flow field of the PEMFC.

## REFERENCES

- [1] US Department of Energy. 2005 Annual Energy Review, DOE/EIA-0384 (2005), <http://www.eia.doe.gov/aer>, last accessed 1/16/2007.
- [2] US Department of Energy Office of Fossil Energy. *Fuel Cell Handbook*. National Energy Technology Laboratory, Morgantown, 6 edition, Nov 2002.
- [3] U.S. Department of Energy, Energy Efficiency and Renewable Energy - Fuel Cells, [http://www.eere.energy.gov/hydrogenandfuelcells/fuelcells/fc\\_types.html](http://www.eere.energy.gov/hydrogenandfuelcells/fuelcells/fc_types.html), last accessed 1/15/2007 .
- [4] Fluent 6.2 User Guide, January 11, 2005, Lebanon, NH.
- [5] B. Bahar, A.R. Hobson, and J.A. Kolde, patent #5,599,614, 1997.
- [6] R.F. Louh and H. Huang, *Electrophoretic Deposition of Pt/C Nanocatalysts on Carbon Electrodes of PEMFC*, MS Thesis, Feng Chia University, 2004.
- [7] F. Lufrano, E. Passalacqua, G. Squadrito, A. Patti, and L. Giorgi, *J. Appl. Electrochem.*, **29** 445, 1999.
- [8] M. Mathias, J. Roth, J. Fleming, and W. Lehnert, Handbook of Fuel Cells - Fundamentals, Technology and Applications, **3**, 2003.
- [9] E. Wikes and O. A. Basaran, Forced oscillations of pendant (sessile) drops, *Phy. Fluids*, **9**, 1512, 1997.
- [10] Susan Daniel, Manoj K. Chaundhury, and P. G. de Gennes, Vibration-actuated drop motion on surfaces for batch microfluidic processes, *Langmuir*, **21**, 4540–4248, 2005.
- [11] J. H. Moon and B. H. Kang, The lowest oscillation mode of a pendant drop, *Phy. Fluids*, **18**(2), 4, 2006.
- [12] Xu Yong, Yang Shuxing, and Zhou Ziguang, The Research and Application Survey of Fluidic Amplifiers, Fifth International Conference on Fluid Power Transmission and Control (ICFP2001), Beijing Institute of Technology, Hangzhou, China, April 3-5, 2001.
- [13] C. A. Belsterling, *Fluidic System Design*, John Wiley and Sons, NY, 1971.
- [14] A. Conway, *A Guide to Fluidics*, Macdonald and Co. Ltd, N.Y., 1971.

- 
- [15] General Electric Company, *Analog Fluidic Laboratory Instructions Manual*, GEK-5024, N.Y., 1967.
  - [16] PCB Piezotronics, Inc., [pcb.com](http://pcb.com), last accessed 12/16/2006.
  - [17] National Instruments, [www.ni.com](http://www.ni.com), last accessed 1/15/2007.
  - [18] C. M. Carne. Experiments using the momentum interaction principle to produce a proportional fluidic amplifier, *Second Cranfield Fluidics Conference*, C1, Cranfield, England, 1967.
  - [19] E. M. Dexter, An Analogue Pure Fluid Amplifier, In *Symposium on Fluid Jet Control Devices*, NY, 1962.
  - [20] George Walter Stewart, *Introductory Acoustics*, Van Nostrand, New York, 1933.

## APPENDIX



## A. TYPES OF FUEL CELLS

Ever since the 1950s, fuel cell scientists around the globe have achieved tremendous success in design and development of numerous types of fuel cells [2]. Each of them was designed for different scale of electricity production, powering from small automobiles to larger scales such as full size power plants. In general fuel cells can be categorized by the type of fuel used, electrolyte, operating temperatures, or fuel processing methods. There are five common types of fuel cells categorized by electrolyte:

1. Polymer Electrolyte Fuel Cell (PEMFC)
2. Alkaline Fuel Cell (AFC)
3. Phosphoric Acid Fuel Cell (PAFC)
4. Molten Carbonate Fuel Cell (MCFC)
5. Solid Oxide Fuel Cell (SOFC).

Each of these fuel cells has their distinct characteristics and the following sections will illustrate some main functionalities and differences between them.

### **(A) PEMFC:**

PEMFC is a low operating temperature fuel cell that utilizes a polymer based membrane as its electrolyte, hence the name “Polymer Electrolyte Membrane Fuel Cell”. PEMFC is also commonly known as “Proton Exchange Membrane Fuel Cell” because the electrolyte in PEMFC is an excellent proton conductor

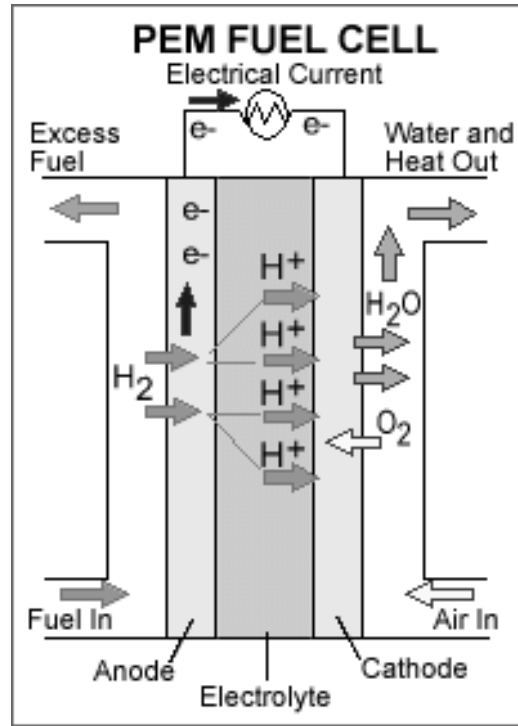


Fig. A.1. Operating schematic of PEMFC [3].

when it is at the fully saturated state. Due to the low operating temperature of PEMFC (less than  $120^{\circ}\text{C}$ ), internal reforming is not possible. Hence the typical fuel used is pure hydrogen and air. Using pure hydrogen as fuel has a significant advantage to PEMFC because the poisoning effect of platinum catalyst is eliminated. Platinum is used in PEMFC as a catalyst which is used to speed up the chemical half reaction of hydrogen and oxygen. Platinum is highly sensitive to carbon monoxide (CO); therefore for fuel cell that uses hydrocarbon fuel, an expensive and tedious CO removal process must be implemented to ensure the proper functionality of the cell.

The by-product of the chemical reaction between hydrogen and oxygen is water and heat. The excess water produced must be removed from the system to prevent flooding of the cell but at the same time the evaporation rate of the moisture content in the polymer membrane. This is a delicate process and is also one of the major problem faced by PEMFC, this section will be revisited

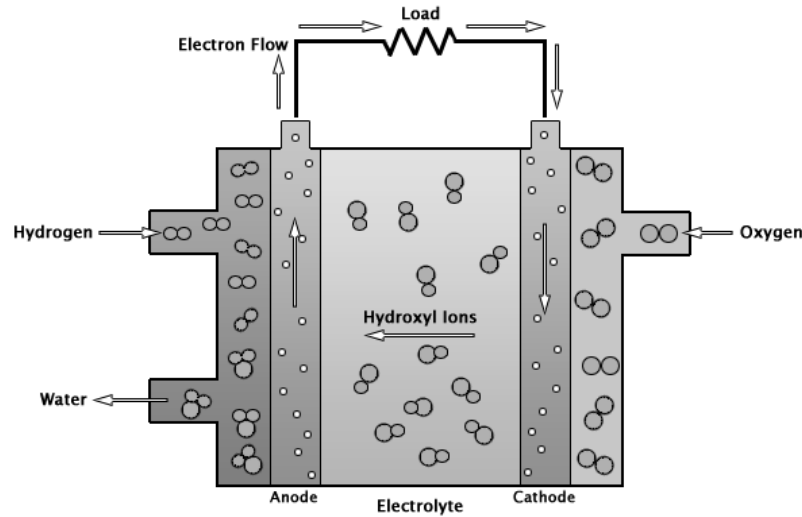


Fig. A.2. Operating schematic of AFC [3].

and further discussed in more depth under 'Water Management' section of this report.

#### (B) AFC:

Among the five different types of fuel cells, the alkaline fuel cell is probably the most developed. NASA used AFC in their Apollo series missions on the space shuttle in the mid 1960s because of its high electrochemical efficiency (approximately 70%) and its ability to operate in mid and low temperatures [2]. The typical electrolyte used in AFCs is concentrated Potassium Hydroxide (KOH). High concentration KOH is used ( $\sim 85\%$  wt) for high temperature operation and lower concentration KOH ( $\sim 50\%$  wt) when low operating temperature is required [2]. There is one disadvantage with AFC, the fuel of choice is limited to pure hydrogen and oxygen because KOH will react with CO and CO<sub>2</sub> to form K<sub>2</sub>CO<sub>3</sub>, which destroys the purity of the electrolyte and eventually results in failure of the fuel cell.

#### (C) PAFC:

The phosphoric acid fuel cell is generally expected to operate up to 200°C and

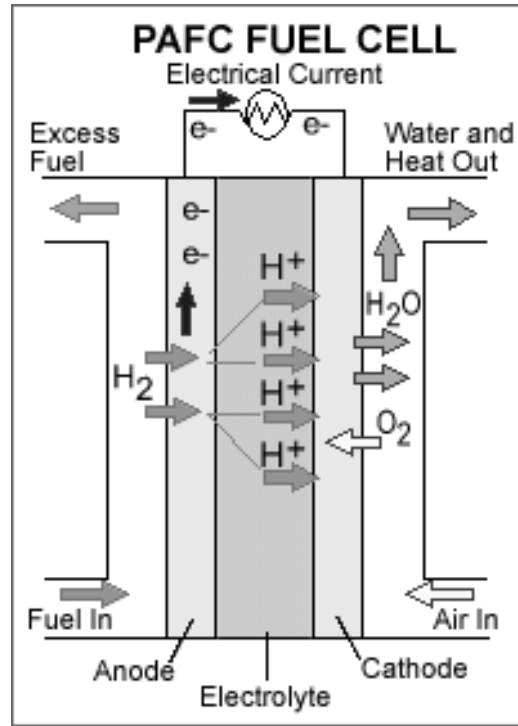


Fig. A.3. Operating schematic of PAFC [3].

it is the first fuel cell to be commercialized. In general, PAFCs have lower overall cell efficiency (37% ~ 48%) and are still very sensitive to CO content [2]. But disregarding its disadvantages, PAFCs have several interesting advantages. First it does not require solid electrolyte, which eliminates the unnecessary attendant pressure drop. Second the water management is simple because when 100% wt phosphoric acid concentration is used, it reduces the water vapor pressure to the minimum [2]. Third, due to the high operating temperature of the cell, scrubbing of CO<sub>2</sub> from the system is no longer required and the excess heat produced is high enough to be put to other useful applications (air and water heating). Most of the recent efforts being done in the United States is concentrated on the improvement of stationary, dispersed power plant and on-site cogeneration power plants. The fuel cell uses platinum or platinum alloys as catalysts dispersed in both electrodes (polytetrafluoroethylene). Over the last two decades, the platinum loading on the electrodes has successfully decreased.

Experiments have shown that when the PAFC is operating at 8 atm instead of 1 atm, an increase in power efficiency can be achieved [2]. But there are a lot of issues on whether to operate the cell at 1 atm or 8 atm because if the cell would to operate at higher pressure level, the manufacturing cost for the cell will increase accordingly. Therefore due to the unbalance in improvement and cost, the market still favors the atmospheric operating PAFCs.

Another issue why higher pressure operation should be avoided is that pressurization of the system will promote corrosion. However the major breakthrough in PAFC technology is the development of carbon black and graphite for cell construction materials. These two materials successfully replace the former material for cell structure due to its stability, corrosion resistance and significant decrease in noble metal utilization. Therefore, PAFC has demonstrated many advantages and provided a great deal of contributions to stationary power generation. The research should focus on bringing the cell efficiency to a higher level and make PAFC a more beneficial investment for the public.

### (C) MCFC:

Molten Carbonate Fuel Cells operate approximately up to 650°C therefore it is considered as a high temperature fuel cell. The main purpose to operate at such high operating temperature is to achieve sufficient ionic conductivity (at this temperature the alkali electrolyte forms a highly conductive molten carbonate salt) and allows the usage of cheaper cell components such as graphite and ceramics. The biggest advantage to operate at such high temperature is the elimination of expensive noble metals, Ni and NiO can be used as electrodes for this fuel cell. The basic idea is to oxidize the oxygen into its carbonate ions using carbon dioxide, and this ion will react with the hydrogen to produce water and carbon dioxide and release electrons.

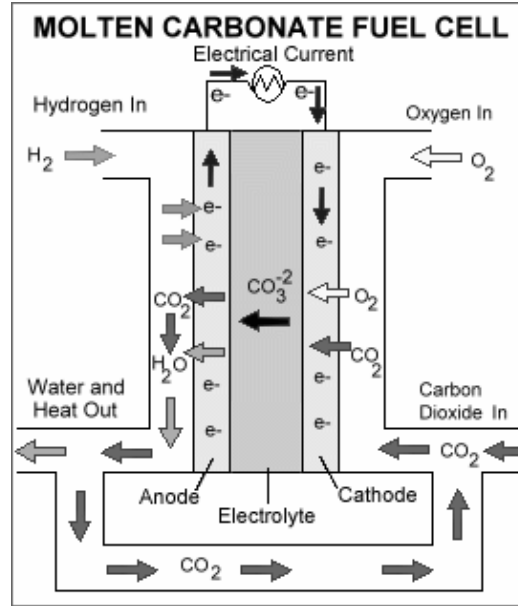


Fig. A.4. Operating schematic of MCFC [3].

The high operating temperature of the cell allowed the system to achieve an overall higher efficiency (approximately 60%)[2]. However this high operating temperature has certain drawback such as the corrosion issues. Another difference of MCFC compared to other types of fuel cells is its method of electrolyte management. Previously described fuel cell types have a binder and wet proofing agent to stabilize the gas and electrolyte interface. But in MCFC, the existence of wet proofing agent which will operate at such high temperature was not available. Therefore in MCFC, the only way to separate the gas and electrolyte interface is by relying on the balancing of capillary pressure [2]. This method establishes the electrolyte interfacial boundaries in the porous electrodes. Thus electrolyte balancing plays an important role in MCFC because it is critical for achieving the high cell performance.

In the pass 28 years, concentration of MCFC has been primarily focused on the fabrication of electrolyte. The conventional method to fabricate electrolyte up till 1980 was by hot pressing the mixtures of  $\text{Li AlO}_2$ , but the electrolyte

structures were relatively thick and difficult to produce in large size because large tooling and press are required [2]. To overcome this difficulty, a new manufacturing process called tape casting was introduced. The reason for a thin electrolyte is to reduce ohmic losses, which is proportional to electrolyte thickness. Experiments have showed that a structure that is 0.25cm thick would require 35mV more than a same material that is 0.18cm thick [2].

Another advantage with this high operating temperature is that the reforming can occur within the cell when a reforming catalyst is provided. And the rejected heat is high enough to run another gas or steam turbine. MCFC are not opened to carbon monoxide or carbon dioxide “poisoning” the carbon oxides produced can even be used as fuels. The primary disadvantage of current MCFC technology is durability. The high temperatures at which these cells operate and the corrosive electrolyte used accelerate component breakdown and corrosion, decreasing cell life. Scientists are currently exploring corrosion-resistant materials for components as well as fuel cell designs that increase cell life without decreasing performance.

#### **(E) SOFC:**

Solid Oxide fuel cell operates at about 600-1000 degrees Celsius which allows internal reforming, promote rapid kinetic reactions with non-noble metals and produce high quality by-product heat for cogeneration or use in a bottoming cycle<sup>1</sup>. This high temperature operating fuel cell is mainly implemented for stationary applications producing useful power ranged from 1 kW to 2 MW [2]. Overall efficiency of this family of fuel cell can reach as high as 70% and the usage of expensive catalyst material is no longer necessary. Solid oxide fuel cells can operate on methane, propane, butane, fermentation gas, gasified biomass

---

<sup>1</sup> Bottoming Cycle is a form of energy cogeneration where useful heat and electricity are generated simultaneously by heat engines or power station.

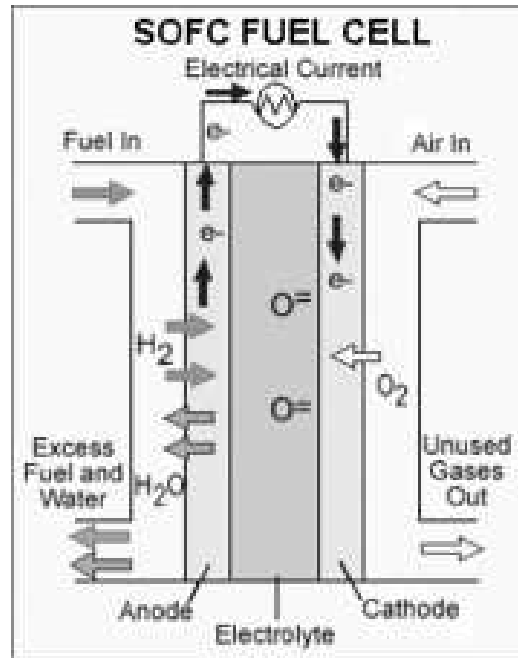


Fig. A.5. Operating schematic of SOFC [3].

and paint fumes as long as sulfur components present in the fuel is removed before entering the cell. This can easily be done by an active coal bed or a zinc absorbent.

The key challenge faced by the SOFC is the material structure and the fabrication process of cheap materials such as ceramics that is suitable for such a high temperature operation. Due to the fact that the electrolyte is solid, it could be manufactured into a variety of shapes. There are basically two types of SOFC structures; the planar and tubular orientations. The nature of the ceramic material used also eliminated the problem of corrosion encountered by the fuel cells that uses liquid electrolyte and it also has the advantage which gas cross over between the electrodes is prevented. There is no problem with the flooding because the electrolyte is immobilized.

However there are drawbacks associate with the high operating temperature, first there are thermal expansion mismatch between the materials and the seal-



ing between the cells is difficult in the planar configuration. Second, the high operation temperature limits the material selection available for cell construction which results in difficult fabrication processes. Third the SOFC is likely to experience great deal of difficulties in high resistivity of the electrolytes. High resistivity of the electrolyte will result in an overall decrease in performance, therefore research is now focused on the development of the cell operating at a lower temperature (typically around 650°C) [2]. However, using low temperature electrolyte material will cause an increase in electrical resistance, so a delicate balance between the temperature and electrical resistance must be maintained to achieve the optimum operating condition.

### *A.1 Advantages and Disadvantages of PEMFC*

Referring to the report written by the Department of Energy, the functionality of PEMFC operating under ambient pressure has been validated by more than 25,000 hours (almost 3 years) with a six-cell stack without forced air flow, humidification, or active cooling [2]. There are currently wide areas of fuel cell application in the market which include public transportation, hybrid fuel cell vehicles, and residential power generator. They all demonstrated a tremendous success in this upraising technology.

The most obvious advantage of PEMFC is the utilization of the solid electrolyte, providing the fuel cell with excellent conductivity and preventing the reactant gases from crossing-over. The corrosion effect of the liquid electrolyte is avoided when pure hydrogen and air (oxygen) is used as fuel. The fuel cell operated at about 80°C which provides a very short amount of time to bring the whole system to its stable operating temperature, this feature is suitable for fast startup application such as automobiles. The fuel cell can also operate at high current

density compared to other candidates.

The major disadvantage of the PEMFC is the problem of water management. Due to the low operating temperature, water is produced as liquid and if it is not removed efficiently, flooding of the fuel cell will occur, which will eventually upset the performance of the fuel cell. Other problems associated with PEMFC is that if hydrocarbon is used as fuel, the problem of CO poisoning becomes significant. The area of focus in the state of the art PEMFC also includes the reduction in cost of high-volume manufacture for the catalyst, electrolytes, and alternate material for bipolar plate constructions. Once an advance problem solving technique is developed, fuel cell will be a possible answer for many of the energy crises our society is currently facing.

## B. SINGLE OSCILLATOR TESTING, SINGLE FEED-BACK PORT VENTING

In the setup instruction of Experiment No.5, the manufacturer suggested venting one exit port while the other remained blocked [15]. The second GE oscillator testing was setup by venting both of the feed-back ports to study the frequency produced by the oscillator. In this experiment, an identical parameters were used except both of the T-fittings (Figure 5.7) were connected to two different transducers. Two different Line A length were used, first is 14.5 inches and the second is 16 inches. The supply flow rate was allowed to vary from 1 L/min to 5 L/min.

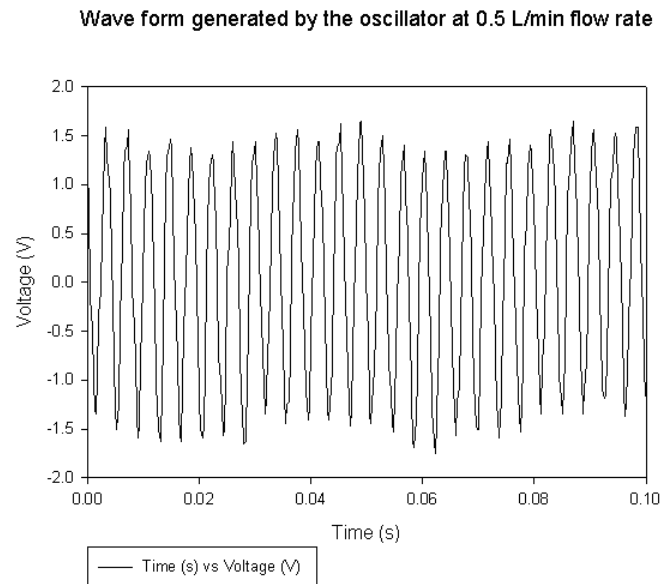
*B.0.1 16 inches Line A length*

Fig. B.1. Experimental result showing the frequency response produced when Line A was set at 16 inches and Line B remained at 2 inches and the supply flow rate was set at 0.5 L/min.

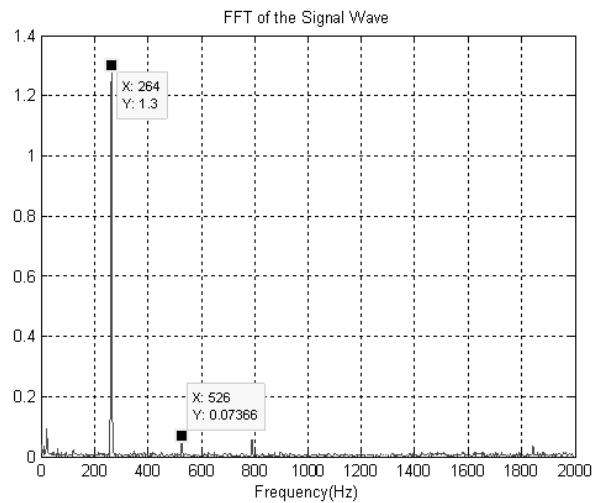


Fig. B.2. Frequency of the wave form (generated at 0.5 L/min supply pressure) estimated using FFT codes.

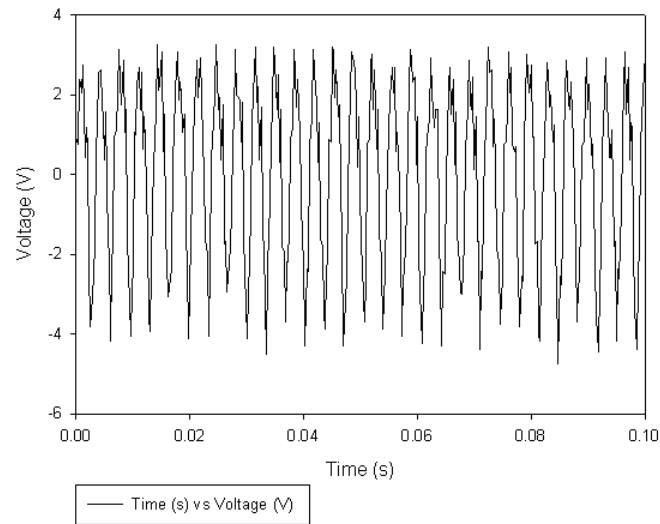


Fig. B.3. Experimental result showing the frequency response produced when Line A was set at 16 inches and Line B remained at 2 inches and the supply flow rate was set at 1.0 L/min.

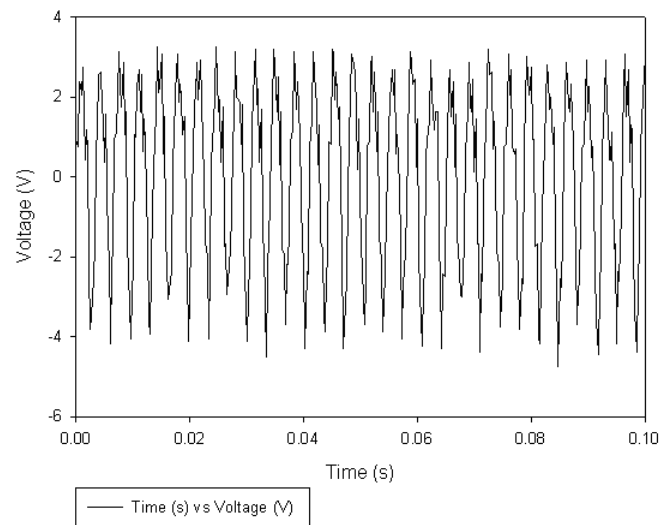


Fig. B.4. Frequency of the wave form (generated at 1.0 L/min supply pressure) estimated using FFT codes.

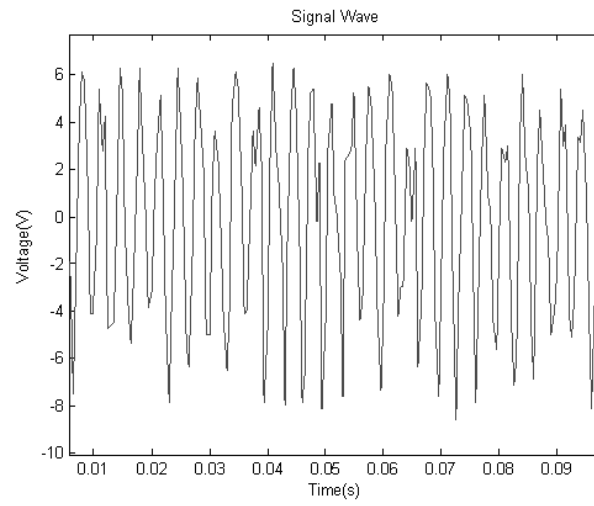


Fig. B.5. Experimental result showing the frequency response produced when Line A was set at 16 inches and Line B remained at 2 inches and the supply flow rate was set at 1.5 L/min.

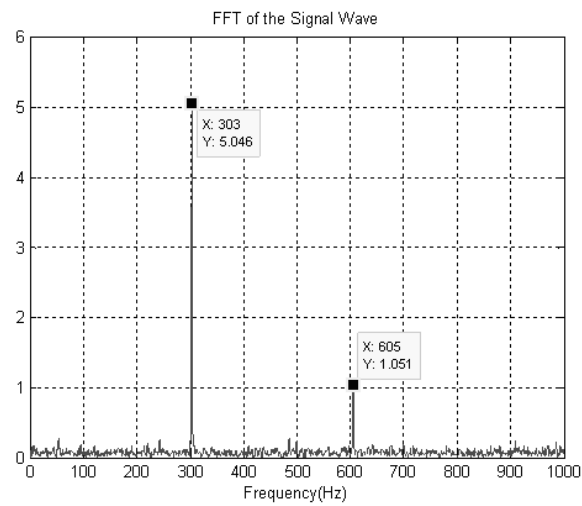


Fig. B.6. Frequency of the wave form (generated at 1.5 L/min supply pressure) estimated using FFT codes.

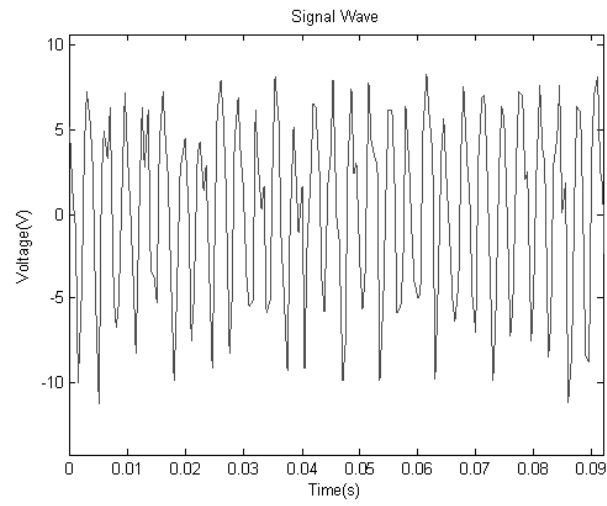


Fig. B.7. Experimental result showing the frequency response produced when Line A was set at 16 inches and Line B remained at 2 inches and the supply flow rate was set at 2.0 L/min.

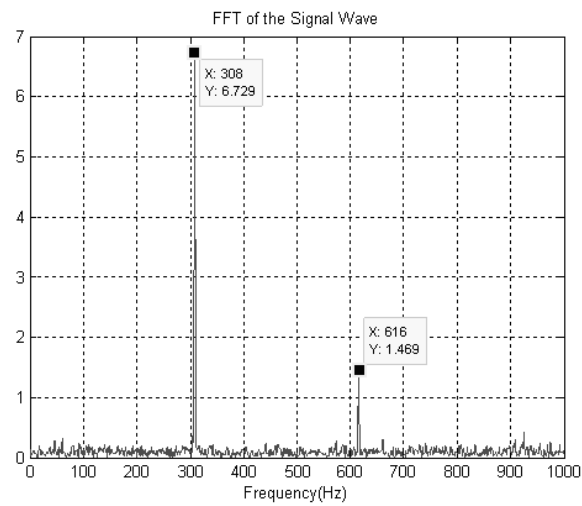


Fig. B.8. Frequency of the wave form (generated at 2.0 L/min supply pressure) estimated using FFT codes.

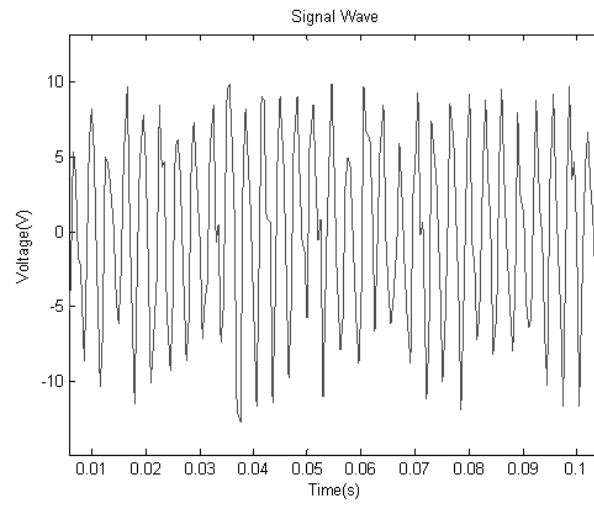


Fig. B.9. Experimental result showing the frequency response produced when Line A was set at 16 inches and Line B remained at 2 inches and the supply flow rate was set at 2.5 L/min.

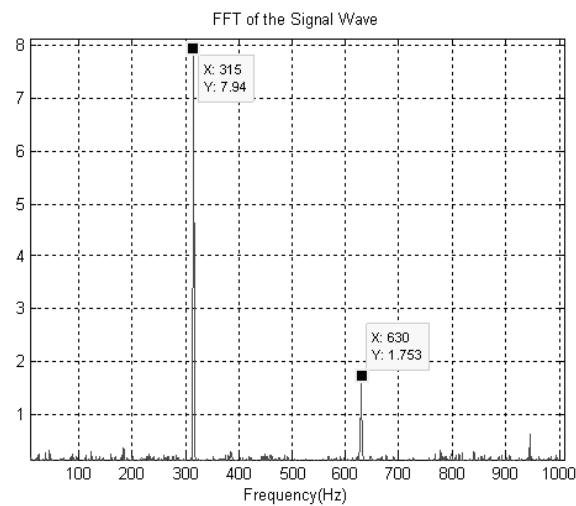


Fig. B.10. Frequency of the wave form (generated at 2.5 L/min supply pressure) estimated using FFT codes.



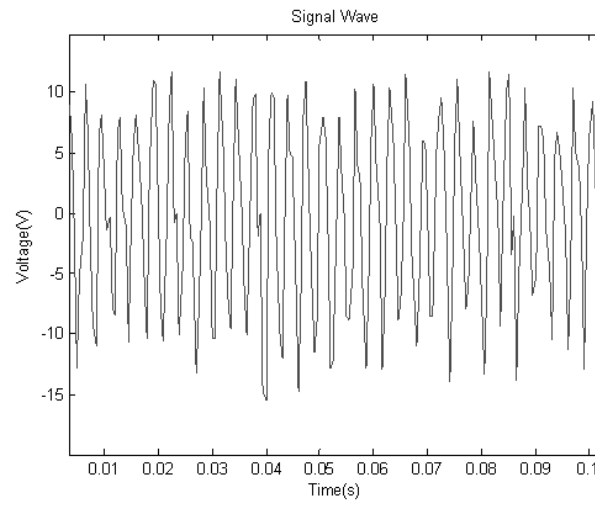


Fig. B.11. Experimental result showing the frequency response produced when Line A was set at 16 inches and Line B remained at 2 inches and the supply flow rate was set at 3.0 L/min.

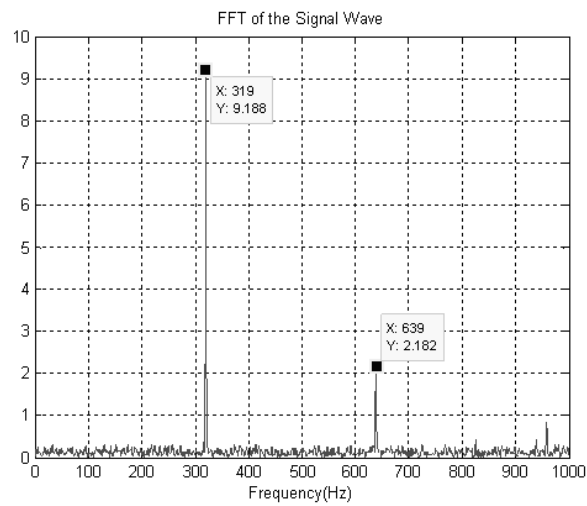


Fig. B.12. Frequency of the wave form (generated at 3.0 L/min supply pressure) estimated using FFT codes.

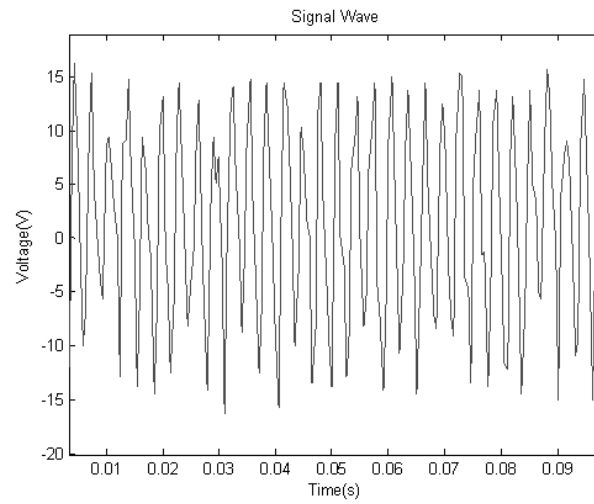


Fig. B.13. Experimental result showing the frequency response produced when Line A was set at 16 inches and Line B remained at 2 inches and the supply flow rate was set at 3.5 L/min.

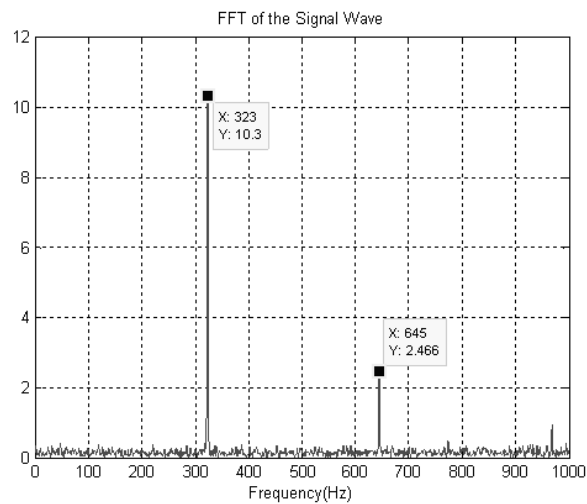


Fig. B.14. Frequency of the wave form (generated at 3.5 L/min supply pressure) estimated using FFT codes.

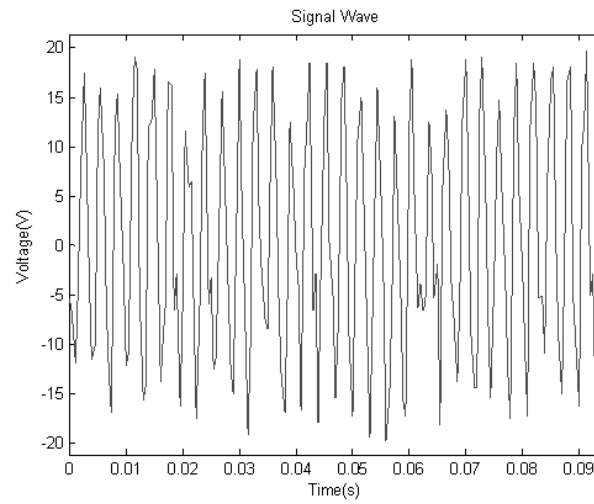


Fig. B.15. Experimental result showing the frequency response produced when Line A was set at 16 inches and Line B remained at 2 inches and the supply flow rate was set at 4.0 L/min.

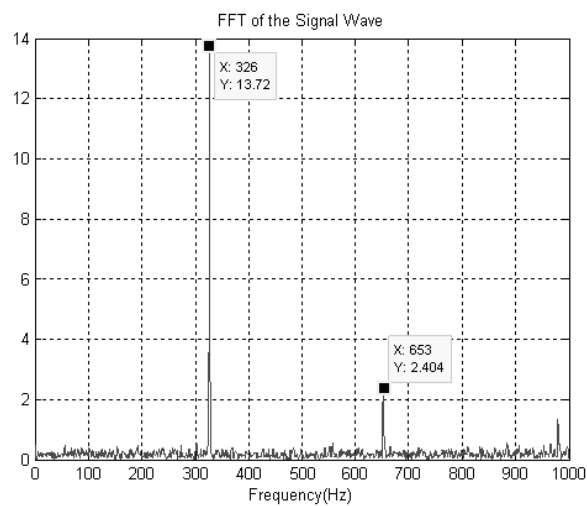


Fig. B.16. Frequency of the wave form (generated at 4.0 L/min supply pressure) estimated using FFT codes.

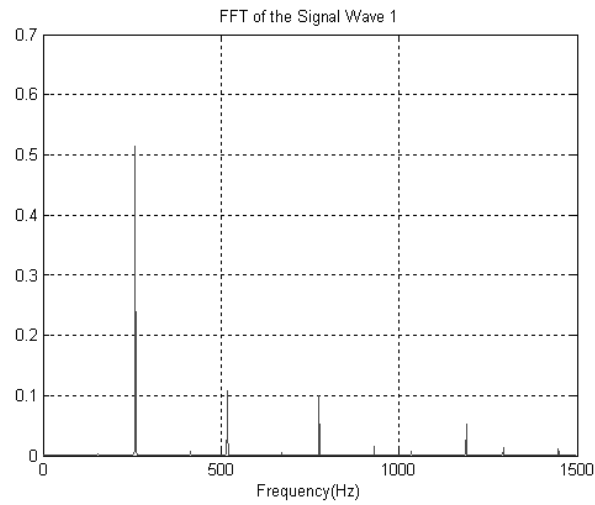
*B.0.2 14.5 inches Line A length*

Fig. B.17. Frequency of the wave form (generated at 1.0 L/min supply pressure) estimated using FFT codes. The main frequency was calculated to be at 257.4885 Hz

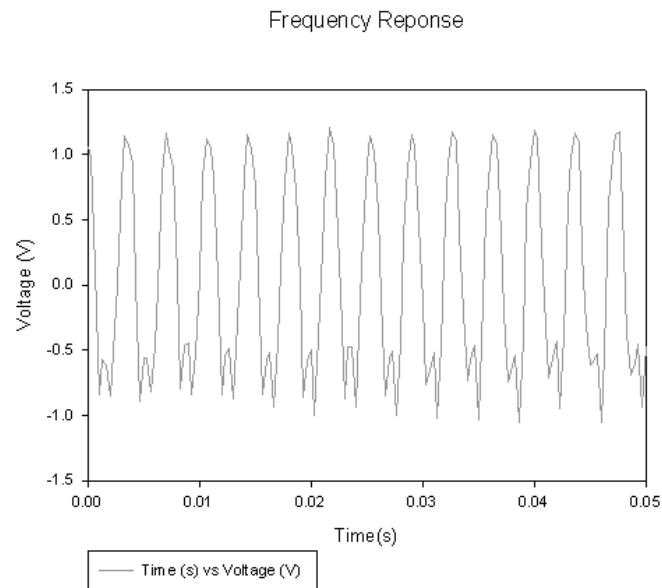


Fig. B.18. Experimental result showing the frequency response produced when Line A was set at 14.5 inches and Line B remained at 2 inches and the supply flow rate was set at 1.5 L/min.

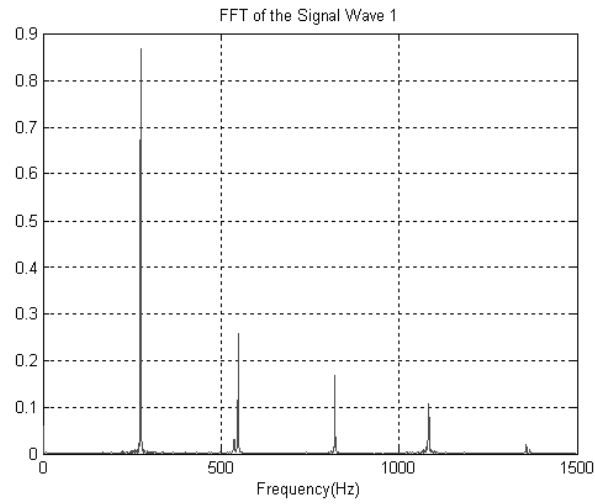


Fig. B.19. Frequency of the wave form (generated at 1.5 L/min supply pressure) estimated using FFT codes. The main frequency was calculated to be at 274.7696 Hz

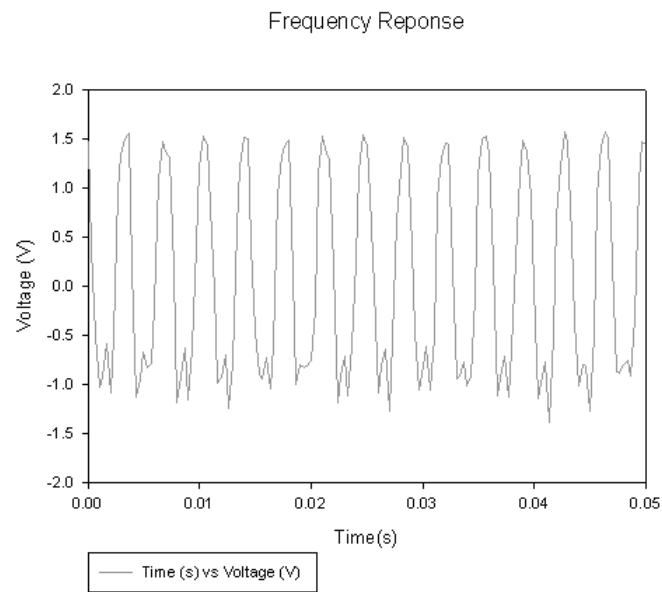


Fig. B.20. Experimental result showing the frequency response produced when Line A was set at 14.5 inches and Line B remained at 2 inches and the supply flow rate was set at 2.0 L/min.

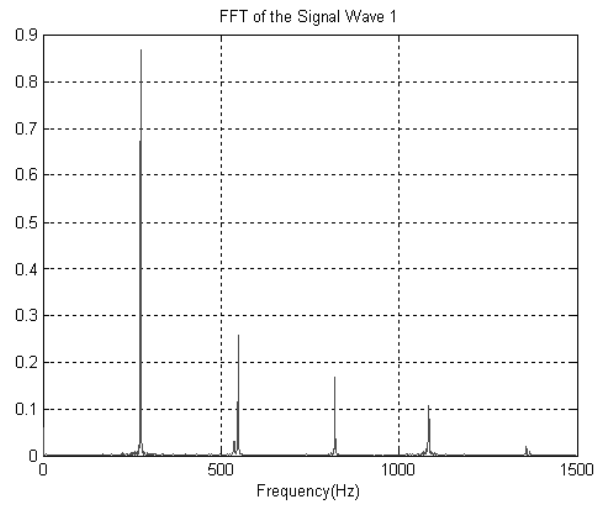


Fig. B.21. Frequency of the wave form (generated at 2.0 L/min supply pressure) estimated using FFT codes. The main frequency was calculated to be at 278.2258 Hz

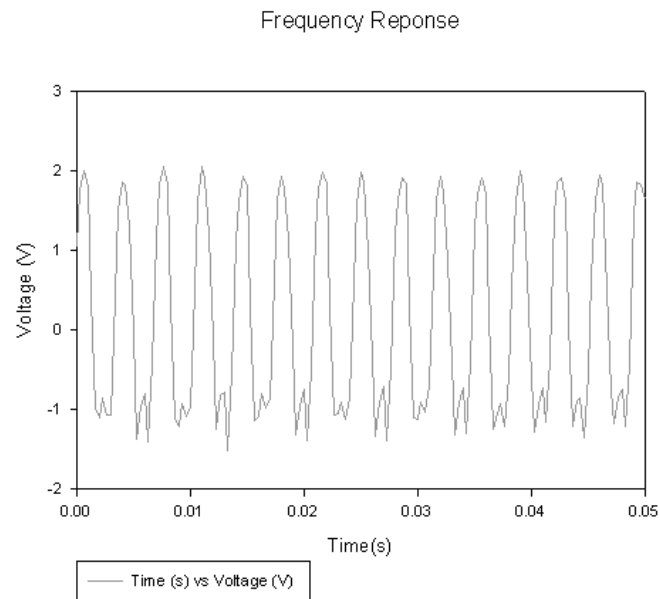


Fig. B.22. Experimental result showing the frequency response produced when Line A was set at 14.5 inches and Line B remained at 2 inches and the supply flow rate was set at 2.5 L/min.

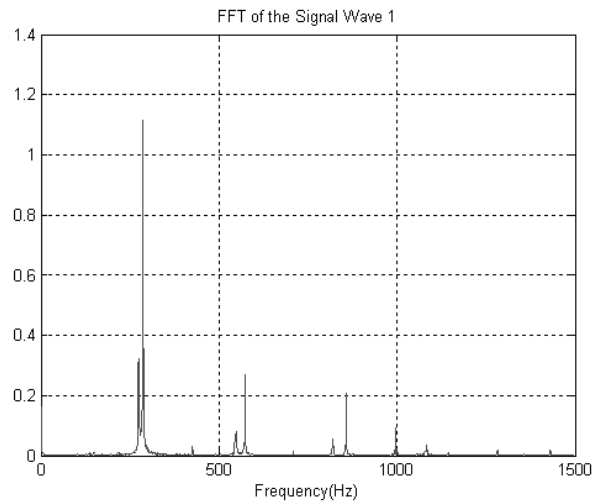


Fig. B.23. Frequency of the wave form (generated at 2.5 L/min supply pressure) estimated using FFT codes. The main frequency was calculated to be at 285.1382 Hz

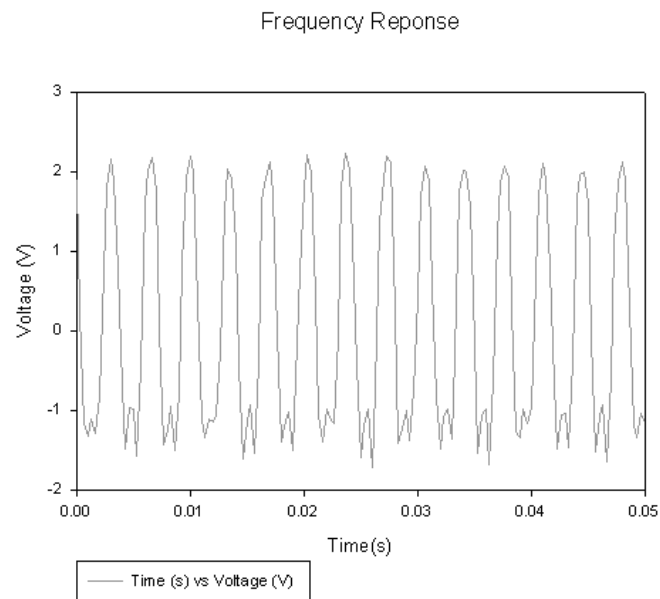


Fig. B.24. Experimental result showing the frequency response produced when Line A was set at 14.5 inches and Line B remained at 2 inches and the supply flow rate was set at 3.0 L/min.

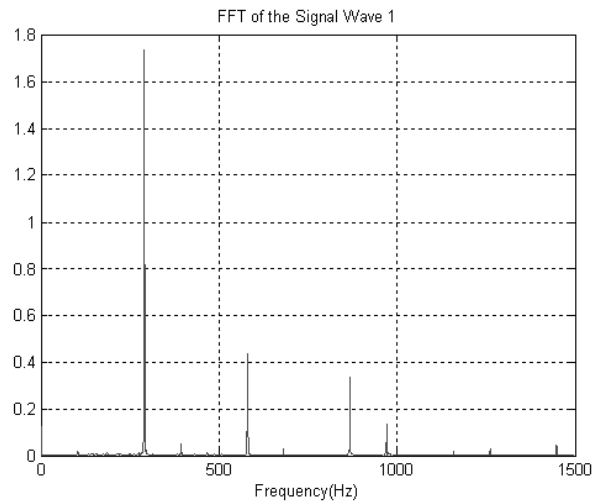


Fig. B.25. Frequency of the wave form (generated at 3.0 L/min supply pressure) estimated using FFT codes. The main frequency was calculated to be at 288.5945 Hz

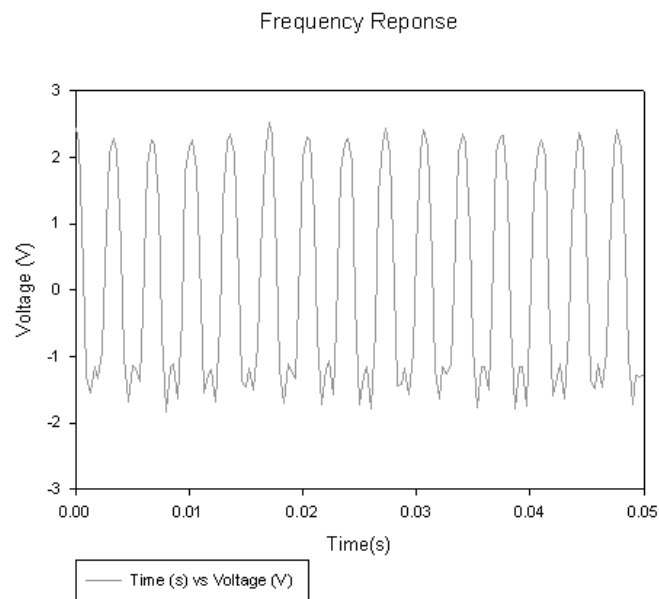


Fig. B.26. Experimental result showing the frequency response produced when Line A was set at 14.5 inches and Line B remained at 2 inches and the supply flow rate was set at 3.5 L/min.



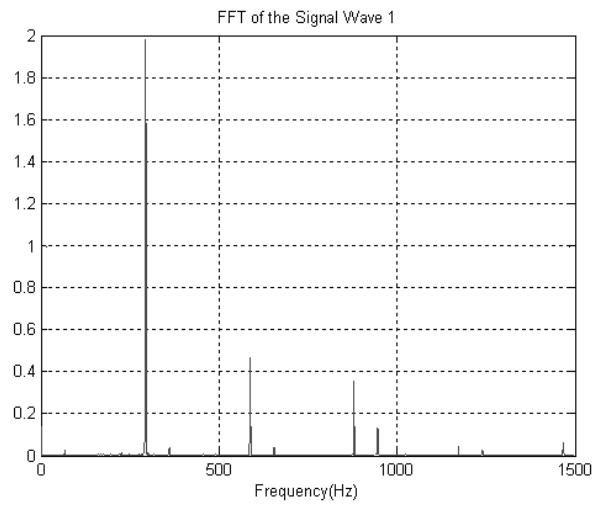


Fig. B.27. Frequency of the wave form (generated at 3.5 L/min supply pressure) estimated using FFT codes. The main frequency was calculated to be at 292.0507 Hz

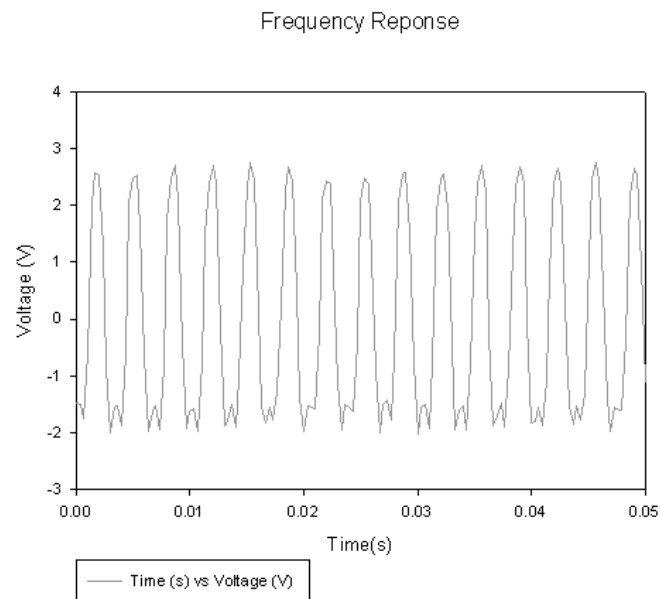


Fig. B.28. Experimental result showing the frequency response produced when Line A was set at 14.5 inches and Line B remained at 2 inches and the supply flow rate was set at 4.0 L/min.

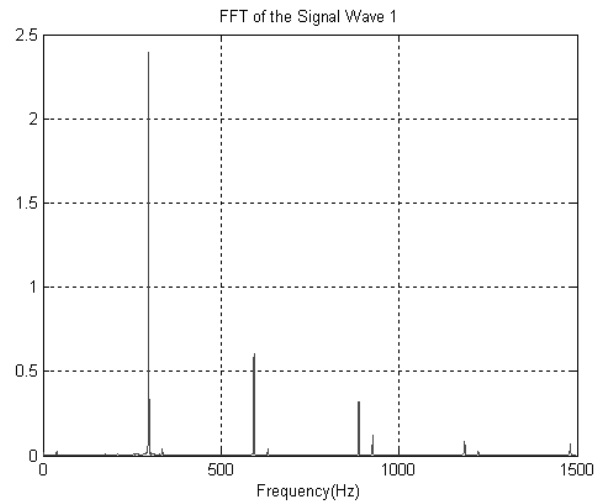


Fig. B.29. Frequency of the wave form (generated at 4.0 L/min supply pressure) estimated using FFT codes. The main frequency was calculated to be at 295.5069 Hz

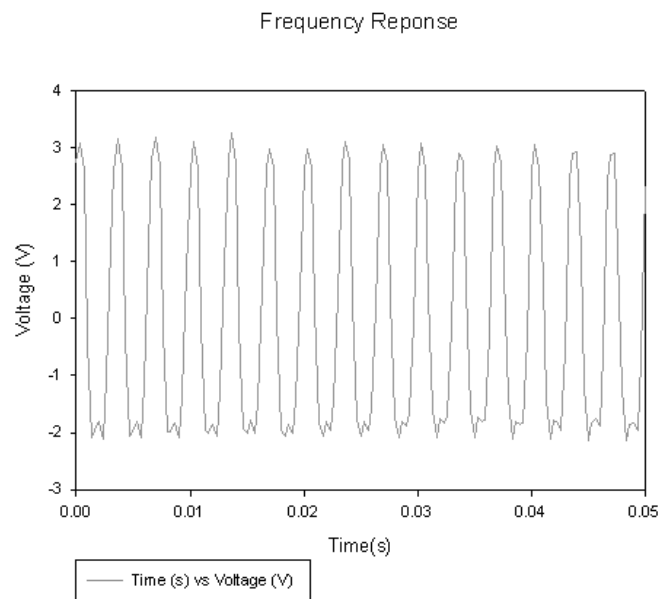


Fig. B.30. Experimental result showing the frequency response produced when Line A was set at 14.5 inches and Line B remained at 2 inches and the supply flow rate was set at 4.0 L/min.

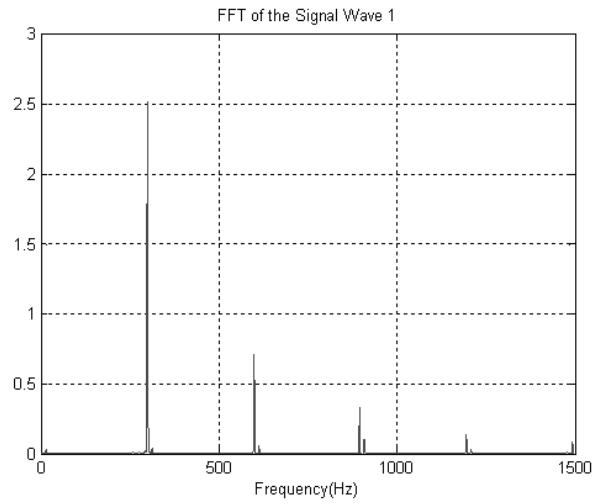


Fig. B.31. Frequency of the wave form (generated at 4.0 L/min supply pressure) estimated using FFT codes. The main frequency was calculated to be at 298.9631 Hz

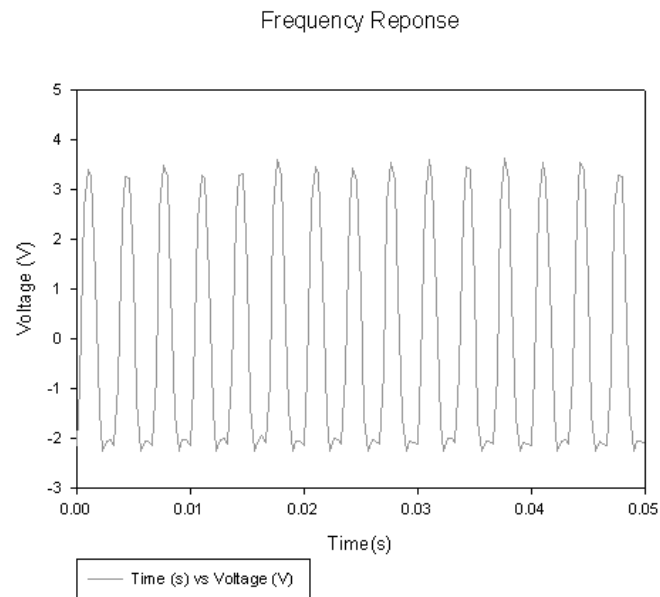


Fig. B.32. Experimental result showing the frequency response produced when Line A was set at 14.5 inches and Line B remained at 2 inches and the supply flow rate was set at 4.0 L/min.

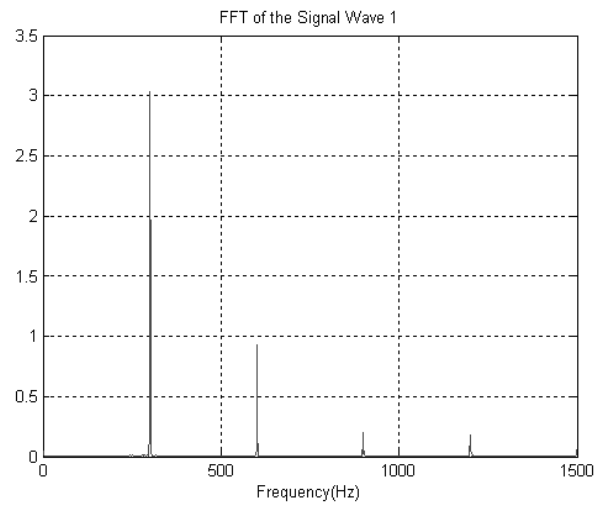


Fig. B.33. Frequency of the wave form (generated at 4.0 L/min supply pressure) estimated using FFT codes. The main frequency was calculated to be at 298.9631 Hz

## C. MATLAB CODE

```
function out=mydft(in,num_ave,delta_t,wintype)
% digital fourier transfer a time history
% [freq dfts]=mydft(vector,num_ave,delta_t,wintype)
% 1 Rectangular
% 2 Flat Top window
% 3 Hanning Window (default)
vec = in;
sz_vec = size(vec);
if sz_vec(1)==1
disp('WARNING: Input vector must be Column Vector');
disp(' ')
end
vec_blk = blk(vec,num_ave);
sz_data = size(vec_blk);
data_wf = pwindow(wintype,sz_data(1));
% 1 Rectangular
% 2 Flat Top window
% 3 Hanning Window (default)
% Windows Amplitude Correction Factor
win_corr_a=sum(data_wf)/length(data_wf);
vec_dft=[];
for ct=1:num_ave
```

---

```
vec_dft(:,ct) = dft( vec_blk(:,ct).*data_wf ) ./win_corr_a;
end
% freq vector generation
N = sz_data(1)*2;
data_T = delta_t*N;
delta_f = 1/data_T;
fmax = N*delta_f / 2;
freq=0:delta_f*2:fmax-delta_f*2;
out=([freq' vec_dft]);
nave = n;
nrow = floor(length(vec)/nave);
high=0;
output=[];
for ct=0:nave-1
    low=high+1;
    high=low+nrow-1;
    output(:,ct+1)=vec(low:high,1);
end
function [w]=pwindow(W,N);
switch W
case 1
    w=ones(N,1);
case 2
    w=flattopwin(N);
case 3
    w=hanning(N);
otherwise
```

---

```
w=hanning(N);  
end  
  
function output=dft(input)  
% Discrete Fourier Transform of the input vector  
if mod(length(input),2)==1  
disp('vector evaluated has length = length-1')  
input=input(1:length(input)-1);  
end  
x=fft(input);  
x=x/length(input);  
x=x(1:length(x)/2);  
x=x*2;  
x(1)=x(1)/2;  
output=x;
```

## D. CONTROL VOLUME ANALYSIS

Momentum Balance:

$$\sum \vec{F} = \frac{d}{dt} \int_{CV} \vec{u} \rho dV + \sum \dot{m}_e \vec{u}_e - \sum \dot{m}_i \vec{u}_i \quad (D.1)$$

Considering the momentum balance in the x-direction:

$$P_1 A_1 + P_3 A_3 \cos \theta = \dot{m}_3 \vec{u}_3 \cos \theta - \dot{m}_1 \vec{u}_1 \quad (D.2)$$

Considering the momentum balance in the y-direction:

$$P_2 A_2 + P_3 A_3 \sin \theta = \dot{m}_3 \vec{u}_3 \sin \theta - \dot{m}_2 \vec{u}_2 \quad (D.3)$$

From conservation of mass (incompressible flow assumption),

$$\dot{m}_{in} = \dot{m}_{out} \quad (D.4)$$

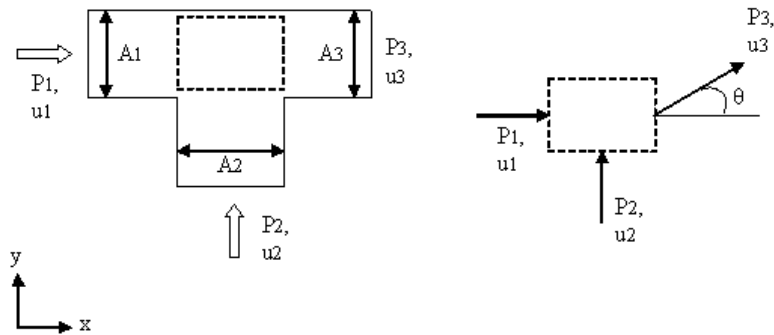


Fig. D.1. Free body diagram of the control volume analysis.



$$\dot{m}_1 + \dot{m}_2 = \dot{m}_3 \quad (\text{D.5})$$

$$A_1 \vec{u}_1 + A_2 \vec{u}_2 = A_3 \vec{u}_3 \quad (\text{D.6})$$

Rearranging Equation 11.2 and 11.3,

$$P_3 = \rho \vec{u}_3 - \frac{\rho A_1 \vec{u}_1^2 - P_1 A_1}{A_3 \cos \theta} \quad (\text{D.7})$$

$$P_3 = \rho \vec{u}_3 - \frac{\rho A_2 \vec{u}_2^2 - P_2 A_2}{A_3 \sin \theta} \quad (\text{D.8})$$

Equating eq. 11.7 and 11.8,

$$\tan \theta = \frac{\dot{m}_2 \vec{u}_2 - P_2 A_2}{\dot{m}_1 \vec{u}_1 - P_1 A_1} \quad (\text{D.9})$$